LYAPUNOV-BASED CONTROL METHODS FOR NEUROMUSCULAR ELECTRICAL STIMULATION

By

NITIN SHARMA

A DISSERTATION PRESENTED TO THE GRADUATE SCHOOL
OF THE UNIVERSITY OF FLORIDA IN PARTIAL FULFILLMENT
OF THE REQUIREMENTS FOR THE DEGREE OF
DOCTOR OF PHILOSOPHY

UNIVERSITY OF FLORIDA

2010

To my loving wife, *Deepti*, my dear parents, *Neena* and *Balwinder Sharma*, and my affectionate sister, *Nitika* for their unwavering support

LIST OF TABLES

LIST OF FIGURES

Abstract of Dissertation Presented to the Graduate School
of the University of Florida in Partial Fulfillment of the
Requirements for the Degree of Doctor of Philosophy

LYAPUNOV-BASED CONTROL METHODS FOR NEUROMUSCULAR ELECTRICAL
STIMULATION

By

Nitin Sharma

August 2010

Chair: Warren E. Dixon
Major: Mechanical Engineering

Neuromuscular electrical stimulation (NMES) is the application of a potential field
across a muscle in order to produce a desired muscle contraction. NMES is a promising
treatment that has the potential to restore functional tasks in persons with movement
disorders. Towards this goal, the research objective in the dissertation is to develop NMES
controllers that will enable a person's lower shank to track a continuous desired trajectory
(or constant setpoint).

A nonlinear musculoskeletal model is developed in Chapter 2 which describes muscle
activation and contraction dynamics and body segmental dynamics during NMES. The
definitions of various components in the musculoskeletal dynamics are provided but are
not required for control implementation. Instead, the structure of the relationships is used
to define properties and make assumptions for control development.

A nonlinear control method is developed in Chapter 3 to control the human
quadriceps femoris muscle undergoing non-isometric contractions. The developed
controller does not require a muscle model and can be proven to yield asymptotic stability
for a nonlinear muscle model in the presence of bounded nonlinear disturbances. The
performance of the controller is demonstrated through a series of closed-loop experiments
on healthy normal volunteers. The experiments illustrate the ability of the controller to
enable the shank to follow trajectories with different periods and ranges of motion, and
also track desired step changes with changing loads.

The most promising and popular control methods for NMES are neural network (NN)-based methods since these methods can be used to learn nonlinear muscle force to length and velocity relationship, and the inherent unstructured and time-varying uncertainties in available models. Further efforts in Chapter 3 focus on the use of a NN feedforward controller that is augmented with a continuous robust feedback term to yield an asymptotic result (in lieu of typical uniformly ultimately bounded (UUB) stability). Specifically, a NN-based controller and Lyapunov-based stability analysis are provided to enable semi-global asymptotic tracking of a desired time-varying limb trajectory (i.e., non-isometric contractions). The added value of incorporating a NN feedforward term is illustrated through experiments on healthy normal volunteers that compare the developed controller with the pure RISE-based feedback controller.

A pervasive problem with current NMES technology is the rapid onset of the unavoidable muscle fatigue during NMES. In closed-loop NMES control, disturbances such as muscle fatigue are often tackled through high-gain feedback which can overstimulate the muscle which further intensifies the fatigue onset. In Chapter 4, a NMES controller is developed that incorporates the effects of muscle fatigue through an uncertain function of the calcium dynamics. A NN-based estimate of the fatigue model mismatch is incorporated in a nonlinear controller through a backstepping method to control the human quadriceps femoris muscle undergoing non-isometric contractions. The developed controller is proven to yield UUB stability for an uncertain nonlinear muscle model in the presence of bounded nonlinear disturbances (e.g., spasticity, delays, changing load dynamics). Simulations are provided to illustrate the performance of the proposed controller. Continued efforts will focus on achieving asymptotic tracking versus the UUB result, and on validating the controller through experiments.

Another impediment in NMES control is the presence of input or actuator delay. Control of nonlinear systems with actuator delay is a challenging problem because of the need to develop some form of prediction of the nonlinear dynamics. The problem

becomes more difficult for systems with uncertain dynamics. Motivated to address the input delay problem in NMES control and the absence of non-model based controllers for a nonlinear system with input delay in the literature, tracking controllers are developed in Chapter 5 for an Euler-Lagrange system with time-delayed actuation, parametric uncertainty, and additive bounded disturbances. One controller is developed under the assumption that the inertia is known, and a second controller is developed when the inertia is unknown. For each case a predictor-like method is developed to address the time delay in the control input. Lyapunov-Krasovskii functionals are used within a Lyapunov-based stability analysis to prove semi-global UUB tracking. Extensive experiments show better performance compared to traditional PD/PID controller as well as robustness to uncertainty in the inertia matrix and time delay value. Experiments are performed on healthy normal individuals to show the feasibility, performance, and robustness of the developed controller.

In addition to efforts focussed on input delayed nonlinear systems, a parallel motivation exists to address another class of time delayed systems which consist of nonlinear systems with unknown state delays. A continuous robust adaptive control method is designed in Chapter 6 for a class of uncertain nonlinear systems with unknown constant time-delays in the states. Specifically, the robust adaptive control method, a gradient-based desired compensation adaptation law (DCAL), and a Lyapunov-Kravoskii (LK) functional-based delay control term are utilized to compensate for unknown time-delays, linearly parameterizable uncertainties, and additive bounded disturbances for a general nonlinear system. Despite these disturbances, a Lyapunov-based analysis is used to conclude that the system output asymptotically tracks a desired time varying bounded trajectory.

Chapter 7 concludes the dissertation with a discussion of the developed contributions and future efforts.

CHAPTER 1
INTRODUCTION

1.1   Motivation and Problem Statement

Neuromuscular electrical stimulation (NMES) is the application of a potential field across a muscle to produce a desired muscle contraction (for functional tasks, NMES is described as functional electrical stimulation (FES)). Efforts in NMES facilitate improved limb control and functionality for patients with stroke, spinal cord injuries, and other neurological impairments [1, 2]. Although most NMES procedures in physical therapy clinics consist of tabulated open-loop application of electrical stimulation, a significant market exists for the development of noninvasive closed-loop methods. However, the application and development of NMES control have been stymied by several technical challenges. Specifically, due to a variety of uncertainties in muscle physiology (e.g., temperature, pH, and architecture), predicting the exact contraction force exerted by the muscle is difficult. One cause of this difficulty is that there is an unknown mapping between the generated muscle force and stimulation parameters. There are additional problems with delivering consistent stimulation energy to the muscle due to a variety of factors including: muscle fatigue, input delay, electrode placement, hyperactive somatosensory reflexes, inter- and intra-subject variability in muscle properties, changing muscle geometry under the electrodes in non-isometric conditions, percentage of subcutaneous body fat, overall body hydration, etc.

Given the uncertainties in the structure of the muscle model and the parametric uncertainty for specific muscles, some investigators have explored various linear PID-based methods (cf. [3–8] and the references therein). Typically, these approaches have only been empirically investigated and no analytical stability analysis has been developed that provides an indication of the performance, robustness or stability of these control methods. The development of a stability analysis for previous PID-based NMES controllers has been evasive because of the fact that the governing equations for a muscle contraction/limb

motion are nonlinear with unstructured uncertainties. Some efforts have focused on analytical control development for linear controllers (e.g., [6, 9, 10]); however, the governing equations are typically linearized to accommodate a gain scheduling or linear optimal controller approach.

Motivated to develop effective NMES control in light of these challenges, the first result in Chapter 3 develops an open-loop error system for a general uncertain nonlinear muscle model based on available analytical and empirical data [11, 12]) that facilitates the development of a new continuous feedback method (coined RISE for Robust Integral of the Sign of the Error). Through this error-system development, the continuous RISE controller is proven (through a Lyapunov-based stability analysis) to yield an asymptotic stability result despite the uncertain nonlinear muscle model and the presence of additive bounded disturbances (e.g., muscle spasticity, fatigue, changing loads in functional tasks, and unmodeled muscle behavior).

Seminal work in [13–18] continue to inspire new investigations (cf. [19–26] and the references therein) in neural network (NN)-based NMES control development. One motivation for NN-based controllers is the desire to augment feedback methods with an adaptive element that can adjust to the uncertain muscle model, rather than only relying on feedback to dominate the uncertainty based on worse case scenarios. NN-based control methods have attracted more attention in NMES than other adaptive feedforward methods because of the nature of the unstructured uncertainty and the universal approximation property of NNs. However, since NNs can only approximate a function within some residual approximation error, all previous NN-based controllers yield uniformly ultimately bounded stability (i.e., the errors converge to a region of bounded steady-state error).

The result in the third section of Chapter 3 focuses on the development of a RISE-based NMES controller and the associated analytical stability analysis that yields asymptotic tracking in the presence of a nonlinear uncertain muscle model with

nonvanishing additive disturbances. This result uses feedback and an implicit learning mechanism to dominate uncertainty and disturbances. However, the RISE method as well as the previous linear feedback methods inherently rely on high gains or high frequency to dominate the model uncertainty, potentially resulting in overstimulation. Recent results from general control systems literature [27] indicate that the RISE-based feedback structure can be augmented with a NN feedforward term to yield asymptotic tracking for some classes of systems. Based on these general results, an extension is provided in the fourth section of Chapter 3 where the RISE-based method is modified with a NN to develop a new NMES controller for the uncertain muscle model.

While efforts in Chapter 3, provide an inroad to the development of analytical NMES controllers for the nonlinear muscle model, these results do not account for muscle fatigue, which is a primary factor to consider to yield some functional results in many rehabilitation applications. Heuristically, muscle fatigue is a decrease in the muscle force output for a given input and is a complex, multifactorial phenomenon [28–30]. In general, some of the factors associated with the onset of fatigue are failure of excitation of motor neurons, impairment of action potential propagation in the muscle membrane and conductivity of sarcoplasmic reticulum to Ca^{2+} ion concentration, and the change in concentration of catabolites and metabolites [31]. Factors such as the stimulation method, muscle fibre composition, state of training of the muscle, and the duration and task to be performed have been noticed to affect fatigue during NMES. Given the impact of fatigue effects during NMES, researchers have proposed different stimulation strategies [30, 32, 33] to delay the onset of fatigue such as choosing different stimulation patterns and parameters, improving fatigue resistance through muscle retraining, sequential stimulation, and size order recruitment.

Controllers can be designed with some feedforward knowledge to approximate the fatigue onset or employ some assumed mathematical model of the fatigue in the control design. Researchers in [34–38] developed various mathematical models for fatigue. In

[34], a musculotendon model for a quadriceps muscle undergoing isometric contractions during functional electrical stimulation (FES) was proposed. The model incorporated fatigue based on the intracellular pH level where the fatigue parameters for a typical subject were found through metabolic information, experimentation and curve fitting. A more general mathematical model for dynamic fatigue defined as a function of normalized muscle activation variable (Ca^{2+} dynamics) was proposed in [35, 36]. The fatigue was introduced as a fitness function that varies according to the increase or decrease in muscle activation during electrical stimulation. The fatigue time parameters were estimated from stimulation experiments. Models in [37] and [38] predict force due to the effect of stimulation patterns and resting times with changing physiological conditions, where model parameterization required investigating experimental forces generated from a standardized stimulation protocol. Although these mathematical models for fatigue prediction are present in literature, few researchers have utilized these assumed fatigue models in closed-loop NMES control. Results in [36] and [39] use the fatigue model proposed in [35] and [36] for a FES controller, where patient specific parameters (e.g. fatigue time constants) are assumed to be known along with exact model knowledge of the calcium dynamics. The difficulty involved in the control design using calcium dynamics or intracellular pH level is that these states cannot be measured easily for real-time control. Therefore, these states (calcium dynamics or pH level) are modeled as a first or second order ordinary differential equation (cf., [34, 36, 39]) and the parameters in the equations are estimated from experimentation or are based on data from past studies.

The focus of Chapter 4 is to address muscle fatigue by incorporating an uncertain fatigue model (i.e., the model developed in [35]) in the NMES controller. The uncertain fatigue model is defined as a function of a normalized muscle activation variable. The normalized muscle activation variable denotes the calcium (Ca^{2+} ion) dynamics which act as an intermediate variable between contractile machinery and external stimulus. The calcium dynamics are modeled as a first order differential equation based on [6] and

17

[39]. A backstepping approach is utilized to design virtual control input that consists of NN-based feedforward signal and feedback signal. The developed controller yields a uniformly ultimately bounded stability result given an unknown nonlinear muscle model with uncertain fatigue and calcium dynamics.

Another technical challenge that hampers the satisfactory NMES control performance is electromechanical delay in muscle force generation which is defined as the difference in time from the arrival of action potential at the neuromuscular junction to the development of tension in the muscle [8]. In NMES control, the electromechanical delay is modeled as an input delay in the musculoskeletal dynamics [6] and occurs due to finite conduction velocities of the chemical ions in the muscle in response to the external electrical input [36]. Input delay can cause performance degradation as was observed during NMES experimental trials on volunteer subjects with RISE and NN+RISE controllers and has also been reported to potentially cause instability during human stance experiments with NMES [40]. Time delay in the control input (also known as dead time, or input delay) is a pervasive problem in control applications other than NMES control. Chemical and combustion processes, telerobotic systems, vehicle platoons, and communication networks [41–44] often encounter delays in the control input. Such delays are often attributed to sensor measurement delay, transport lags, communication delays, or task prioritization, and can lead to poor performance and potential instability.

Motivated by performance and stability problems, various methods have been developed for linear systems with input delays (cf. [45–57] and the references therein). As discussed in [45, 46], an outcome of these results is the development and use of prediction techniques such as Artstein model reduction [48], finite spectrum assignment [51], and continuous pole placement [58]. The concept of predictive control originated from classic Smith predictor methods [59]. The Smith predictor requires a plant model for output prediction and has been widely studied and modified for control purposes (cf. [60–67] and references therein). However, the Smith predictor does not provide good closed-loop

performance in the presence of model mismatch and can only be applied for stable plants [42, 46]. Contrary to the Smith predictor, finite spectrum assignment or Artstein model reduction techniques and their extensions [47–53, 68–71] can be applied to unstable or multivariable linear plants. These predictor-based methods utilize finite integrals over past control values to reduce the delayed system to a delay free system.

Another approach to develop predictive controllers is based on the fact that input delay systems can be represented by hyperbolic partial differential equations (cf. [45, 46] and references therein). This fact is exploited in [54–57] to design controllers for actuator delayed linear systems. These novel methods model the time delayed system as an ordinary differential equation (ODE)-partial differential equation (PDE) cascade where the non-delayed input acts at the PDE boundary. The controller is then designed by employing a backstepping type approach for PDE control [72].

Predictor techniques have also been extended to adaptive control of unknown linear plants in [41, 56, 73]. In [41, 73] the controller utilizes a modified Smith predictor type structure to achieve a semi-global result. In [56] (and the companion paper [55]), a global adaptive controller is developed that compensates for uncertain plant parameters and a possibly large unknown delay.

In comparison to input delayed linear systems, fewer results are available for nonlinear systems. Approaches for input delayed nonlinear systems such as [74, 75] utilize a Smith predictor-based globally linearizing control method and require a known nonlinear plant model for time delay compensation. In [42], a specific technique is developed for a telerobotic system with constant input and feedback delays where a Smith predictor for a locally linearized subsystem is used in combination with a neural network controller for a remotely located uncertain nonlinear plant. In [76], an approach to construct Lyapunov-Krasovskii (LK) functionals for input delayed nonlinear system in feedback form is provided, and the control method in [77] utilizes a composite Lyapunov function containing an integral cross term and LK functional for stabilizing nonlinear cascade

systems, where time delay can be either in the input or the states. The robustness of input to state stabilizability is proven in [78] for nonlinear finite-dimensional control systems in presence of small input delays by utilizing a Razumikhin-type theorem. In [79], the backstepping approach that utilizes ODE-PDE cascade transformation for input delayed systems is extended to a scalar nonlinear system with actuator delay of unrestricted length. However, to the best of our knowledge, no attempt has been made towards stabilizing an input delayed nonlinear system with parametric uncertainty and/or additive bounded disturbances.

Motivated by the lack of NMES controllers that compensate for input delay and the desire to develop non-model based controllers for nonlinear systems with input delay Chapter 5 focuses on the development of a tracking controller for an uncertain nonlinear Euler-Lagrange system with input delay. The input time delay is assumed to be a known constant and can be arbitrary large. The dynamics are assumed to contain parametric uncertainty and additive bounded disturbances. The first developed controller is based on the assumption that the mass inertia is known, whereas the second controller is based on the assumption that the mass inertia is unknown. The key contributions of this effort is the design of a delay compensating auxiliary signal to obtain a time delay free open-loop error system and the construction of LK functionals to cancel time delayed terms. The auxiliary signal leads to the development of a predictor-based controller that contains a finite integral of past control values. This delayed state to delay free transformation is analogous to the Artstein model reduction approach, where a similar predictor-based control is obtained. LK functionals containing finite integrals of control input values are used in a Lyapunov-based analysis that proves the tracking errors are semi-global uniformly ultimately bounded.

Another class of time-delayed systems which are also endemic to engineering systems and can cause degraded control performance and make closed-loop stabilization difficult are systems with state delays. In time-delayed systems, the dynamics not only depends

on the current system states but also depends on the past state values. These systems occur in many industrial and manufacturing systems (e.g., metal cutting process, rolling mill, and chemical processes [46, 80].) A desire parallel to NMES research existed to address this class of time delay systems. Various controllers have been developed to address time-delay induced performance and stability issues as described in the survey papers [45, 46] and in recent results that target control of uncertain systems with state delays (cf. [80–86] and references therein). Control synthesis and stability analysis methods for nonlinear time-delayed systems are often based on Lyapunov techniques in conjunction with a Lyapunov-Kravoskii (LK) functional (cf. [82, 83, 85, 87]). For example, in [82], an iterative procedure utilizing LK functionals for robust stabilization of a class of nonlinear systems with triangular structure is developed. However, as stated in [88], the controller cannot be constructed from the given iterative procedure. Semi-global uniformly ultimately bounded (SUUB) results have been developed for time-delayed nonlinear systems [83, 85] by utilizing neural network-based control, where appropriate LK functionals are utilized to remove time delayed states. A discontinuous adaptive controller was recently developed in [87] for a nonlinear system with an unknown time delay to achieve a UUB result with the aid of LK functionals. However, controllers designed in [83, 87] can become singular when the controlled state reaches zero and an *ad hoc* control strategy is proposed to overcome the problem. Moreover, as stated in [89] and [90], the control design procedure described in [85] cannot be generalized for nth order nonlinear systems.

Sliding mode control (SMC) has also been utilized for time delayed systems in [80, 91–94]. However, utilizing SMC still poses a challenging design and computation problem when delays are present in states [45, 46]. Moreover, the discontinuous sign function present in SMC controller often gives rise to the undesirable chattering phenomenon during practical applications. To overcome the limitations of discontinuity in SMC, a continuous adaptive sliding mode strategy is designed in [95] for nonlinear plants with

unknown state delays, where an LK functional along with a discontinuous Lyapunov function is proposed for the stability analysis.

The development in Chapter 6 is motivated by the lack of continuous robust controllers that can achieve asymptotic stability for a class of uncertain time-delayed nonlinear systems with additive bounded disturbances. The approach described in the current effort uses a continuous implicit learning [96] based Robust Integral of the Sign of the Error (RISE) structure [11, 27]. Due to the added benefit of reduced control effort and improved control performance, an adaptive controller in conjunction with RISE feedback structure is designed. However, since the time delay value is not always known, it becomes challenging to design a delay free adaptive control law. Through the use of a desired compensation adaptive law (DCAL) based technique and segregating the appropriate terms in the open loop error system, the dependence of parameter estimate laws on the time delayed unknown regression matrix is removed. Contrary to previous results, there is no singularity in the developed controller. A Lyapunov-based stability analysis is provided that uses an LK functional along with Young's inequality to remove time delayed terms and achieves asymptotic tracking.

1.2 Contributions

This dissertation focuses on developing nonlinear controllers for a musculoskeletal system excited by NMES. The controllers are developed to account for various technical challenges hampering an effective NMES control performance such as unknown nonlinear muscle model, muscle fatigue, input and measurement delay. The contributions of Chapters 3-6 are as follows.

1. Chapter 3, *Nonlinear Neuromuscular Electrical Stimulation Tracking Control of a Human Limb*: The contribution of this chapter is to illustrate how a recently developed continuous feedback method called robust integral of signum of the error (coined as RISE) can be applied for NMES systems. The muscle model developed in Chapter 2 is rewritten in a form that adheres to RISE-based Lyapunov stability analysis. Through this error-system development, the continuous RISE controller is proven (through a Lyapunov-based stability analysis) to yield an asymptotic stability result despite the uncertain nonlinear muscle model and the presence

of additive bounded disturbances (e.g., muscle spasticity, fatigue, changing loads in functional tasks, and delays). The performance of the nonlinear controller is experimentally verified for a human leg tracking on a leg extension machine by applying the controller as a voltage potential across external electrodes attached to the distal-medial and proximal-lateral portion of the quadriceps femoris muscle group. The RISE controller is implemented by a voltage modulation scheme with a fixed frequency and a fixed pulse width. Other modulation strategies (e.g., frequency or pulse-width modulation) could have also been implemented (and applied to other skeletal muscle groups) without loss of generality. The experiments illustrate the ability of the controller to enable the shank to track single and multiple period trajectories with different ranges of motion, and also track desired step changes with changing loads.

The second result in the chapter focusses on blending NN-based feedforward technique with RISE based feedback method which was shown to yield asymptotic tracking in the presence of a nonlinear uncertain muscle model with nonvanishing additive disturbances. The first result uses feedback and an implicit learning mechanism to dominate uncertainty and disturbances. Recent results from general control systems literature [27] indicate that the RISE-based feedback structure can be augmented with a NN feedforward term to yield asymptotic tracking for some classes of systems. Based on these general results, the RISE-based method is modified with a multi layered NN to develop a new NMES controller for the uncertain muscle model. The experimental results indicate that the addition of the NN reduces the root mean squared (RMS) tracking error for similar stimulation effort when compared to the first method developed in the chapter(RISE method without the NN feedforward component). Additional experiments were conducted to depict that the NN-based feedforward technique holds promise in clinical-type tasks. Specifically, a preliminary sit-to-stand experiment was performed to show controller's feasibility for any functional task.

2. Chapter 4, *Nonlinear Control of NMES: Incorporating Fatigue and Calcium Dynamics* An open-loop error system for an uncertain nonlinear muscle model is developed that includes the fatigue and calcium dynamics. A virtual control input is designed using nonlinear backstepping technique which is composed of a NN based feedforward signal and an error based feedback signal. The NN based control structure is exploited not only to feedforward muscle dynamics but also to approximate the error generated due to parametric uncertainties in the assumed fatigue model. The actual external control input (applied voltage) is designed based on the backstepping error. Through this error-system development, the continuous NN based controller is proven (through a Lyapunov-based stability analysis) to yield an uniformly ultimately bounded stability result despite the uncertain nonlinear muscle model and the presence of additive bounded disturbances (e.g., muscle spasticity, changing loads in functional tasks, and delays).

3. Chapter 5, *Predictor-Based Control for an Uncertain Euler-Lagrange System with Input Delay* This chapter focuses on the development of a tracking controller for

an uncertain nonlinear Euler-Lagrange system with input delay. The input time delay is assumed to be a known constant and can be arbitrary large. The dynamics are assumed to contain parametric uncertainty and additive bounded disturbances. The first developed controller is based on the assumption that the mass inertia is known, whereas the second controller is based on the assumption that the mass inertia is unknown. The key contributions of this effort is the design of a delay compensating auxiliary signal to obtain a time delay free open-loop error system and the construction of LK functionals to cancel time delayed terms. The auxiliary signal leads to the development of a predictor-based controller that contains a finite integral of past control values. This delayed state to delay free transformation is analogous to the Artstein model reduction approach, where a similar predictor-based control is obtained. LK functionals containing finite integrals of control input values are used in a Lyapunov-based analysis that proves the tracking errors are semi-global uniformly ultimately bounded. Extensive experiments were performed to show the controller's better performance in comparison to traditional PID/PD controllers and robustness to uncertainty in time delay and inertia matrix. Additional experiments show that the developed controller can be applied to compensate input delay in NMES.

4. Chapter 6, *RISE-Based Adaptive Control of an Uncertain Nonlinear System with Unknown State Delays* The development in this chapter is motivated by the lack of continuous robust controllers that can achieve asymptotic stability for a class of uncertain time-delayed nonlinear systems with additive bounded disturbances. The approach described in the current effort uses a continuous implicit learning [96] based Robust Integral of the Sign of the Error (RISE) structure [11, 27]. Due to the added benefit of reduced control effort and improved control performance, an adaptive controller in conjunction with RISE feedback structure is designed. However, since the time delay value is not always known, it becomes challenging to design a delay free adaptive control law. Through the use of a desired compensation adaptive law (DCAL) based technique and segregating the appropriate terms in the open loop error system, the dependence of parameter estimate laws on the time delayed unknown regression matrix is removed. Contrary to previous results, there is no singularity in the developed controller. A Lyapunov-based stability analysis is provided that uses an LK functional along with Young's inequality to remove time delayed terms and achieves asymptotic tracking.

CHAPTER 2
MUSCLE ACTIVATION AND LIMB MODEL

The following model development represents the musculoskeletal dynamics during neuromuscular electrical stimulation performed on human quadriceps muscle. The model simulates limb dynamics when external voltage is applied on the muscle. The total muscle knee joint model can be categorized into body segmental dynamics and muscle activation and contraction dynamics. The muscle activation and contraction dynamics explains the force generation in the muscle while the body segmental dynamics considers the active moment and passive joint moments.

The total knee-joint dynamics can be modeled as [6]

$$M_I + M_e + M_g + M_v + \tau_d = \tau. \tag{2–1}$$

In (2–1), $M_I(\ddot{q}) \in \mathbb{R}$ denotes the inertial effects of the shank-foot complex about the
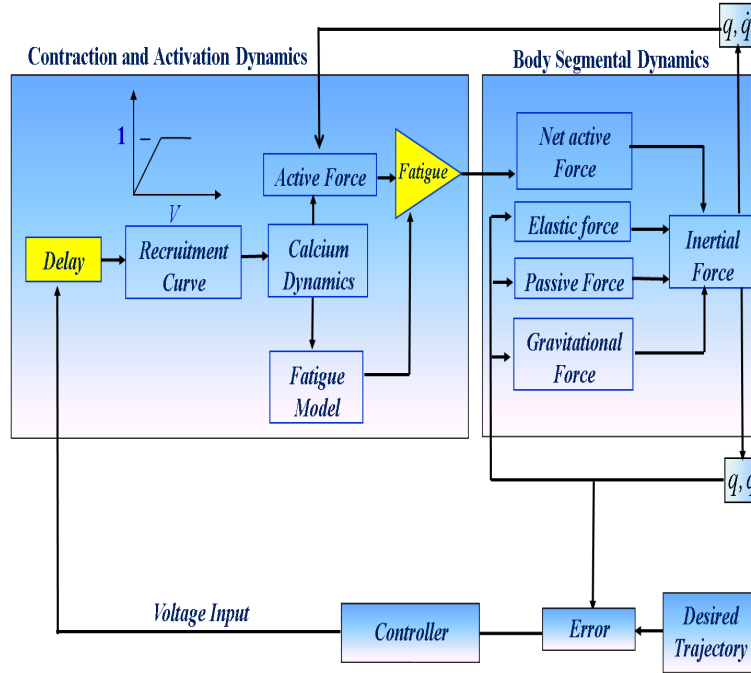
Figure 2-1. Muscle activation and limb model. The force generating contraction and activation dynamics in the muscle is denoted by an unknown nonlinear function $\eta(q, \dot{q}) \in \mathbb{R}$ in the dynamics. The detailed contraction and activation dynamics including fatigue and calcium dynamics are introduced in Chapter 4.

knee-joint, $M_e(q) \in \mathbb{R}$ denotes the elastic effects due to joint stiffness, $M_g(q) \in \mathbb{R}$ denotes the gravitational component, $M_v(\dot{q}) \in \mathbb{R}$ denotes the viscous effects due to damping in the musculotendon complex [97], $\tau_d(t) \in \mathbb{R}$ is considered as an unknown bounded disturbance which represents an unmodeled reflex activation of the muscle (e.g., muscle spasticity) and other unknown unmodeled phenomena (e.g., dynamic fatigue, electromechanical delays), and $\tau(t) \in \mathbb{R}$ denotes the torque produced at the knee joint. In the subsequent development, the unknown disturbance $\tau_d(t)$ is assumed to be bounded and its first and second time derivatives are assumed to exist and be bounded. These are reasonable assumptions for typical disturbances such as muscle spasticity, fatigue, and load changes during functional tasks. For simplicity, the passive damping and elastic force of muscle and joints are considered together. The inertial and gravitational effects in (2–1) can be modeled as

$$M_I(\ddot{q}(t)) = J\ddot{q}(t), \qquad M_g(q(t)) = -mgl\sin(q(t)), \qquad (2\text{–}2)$$

where $q(t)$, $\dot{q}(t)$, $\ddot{q}(t) \in \mathbb{R}$ denote the angular position, velocity, and acceleration of the lower shank about the knee-joint, respectively (see Fig. 2-2), $J \in \mathbb{R}$ denotes the unknown inertia of the combined shank and foot, $m \in \mathbb{R}$ denotes the unknown combined mass of the shank and foot, $l \in \mathbb{R}$ is the unknown distance between the knee-joint and the lumped center of mass of the shank and foot, and $g \in \mathbb{R}$ denotes the gravitational acceleration. The elastic effects are modeled on the empirical findings by Ferrarin and Pedotti in [97] as

$$M_e(q) = -k_1(\exp(-k_2 q(t)))(q(t) - k_3), \qquad (2\text{–}3)$$

where k_1, k_2, $k_3 \in \mathbb{R}$ are unknown positive coefficients. As shown in [6], the viscous moment $M_v(\dot{q})$ can be modelled as

$$M_v(\dot{q}(t)) = B_1 \tanh(-B_2\dot{q}(t)) - B_3\dot{q}(t), \qquad (2\text{–}4)$$

where B_1, B_2, and $B_3 \in \mathbb{R}$ are unknown positive constants.

Figure 2-2. The left image illustrates a person's left leg in a relaxed state. The right image shows the left leg during stimulation. The angle q(t) is measured with respect to the vertical line as shown.

The torque produced about the knee is controlled through muscle forces that are elicited by NMES. For simplicity (and without loss of generality), the development in this chapter focuses on producing knee torque through muscle tendon forces, denoted by $F_T(t) \in \mathbb{R}$, generated by electrical stimulation of the quadriceps (i.e., antagonistic muscle forces are not considered). The knee torque is related to the muscle tendon force as

$$\tau(t) = \zeta(q(t))F_T(t), \tag{2–5}$$

where $\zeta(q(t)) \in \mathbb{R}$ denotes a positive moment arm that changes with the extension and flexion of the leg as shown in studies by [98] and [99]. The tendon force $F_T(t)$ in (2–5) is defined as

$$F_T = F \cos a(q) \tag{2–6}$$

where $a(q(t))$ is defined as the pennation angle between the tendon and the muscle. The pennation angle of human quadriceps muscle changes monotonically during quadriceps contraction and is a continuously differentiable, positive, monotonic, and bounded function with a bounded first time derivative [100]. The relationship between muscle force and applied voltage is denoted by the unknown function $\eta(q, \dot{q}) \in \mathbb{R}$ as

$$F(t) = \eta(q, \dot{q})V(t), \tag{2–7}$$

where $V(t) \in \mathbb{R}$ is the voltage applied to the quadriceps muscle by electrical stimulation. While exact force versus voltage models are debatable and contain parametric uncertainty, the generally accepted empirical relationship between the applied voltage (or similarly, current, frequency [101, 102], or pulse width) is well established. The empirical data in [101] and [102] indicates the function $\eta(q, \dot{q})$ is a continuously differentiable, non-zero, positive, monotonic, and bounded function, and its first time derivative is bounded.

The total force generated at the tendon could be considered as the sum of forces generated by an active element (often denoted by F_{CE}), the tension generated by a passive elastic element (often denoted by F_{PE}), and forces generated by viscous fluids (often denoted by F_{VE}). These forces have dynamic characteristics. For example, the passive element increases with increasing muscle length, and the muscle stiffness has been reported to change by greater than two orders of magnitude [34] under dynamic contractions. The muscle model in the chapter considers the total muscle force composed of the sum of these elements as the function of an unknown nonlinear function $\eta(q, \dot{q})$ and an applied voltage $V(t)$. The introduction of the unknown nonlinear function $\eta(q, \dot{q})$ enables the muscle contraction to be considered under general dynamic conditions in the subsequent control development. Expressing the muscle contraction forces in this manner enables the development of a control method that is robust to changes in the forces, because these effects are included in the uncertain nonlinear muscle model that is incorporated in the stability analysis. The model developed in (2–1)-(2–7) is used to examine the stability of the subsequently developed controller, but the controller does not explicitly depend on these models. The following assumptions are used to facilitate the subsequent control development and stability analysis.

Assumption 1: The moment arm $\zeta(q)$ is assumed to be a non-zero, positive, bounded function [98, 99] whose first two time derivatives exist, and based on the empirical data [101, 102], the function $\eta(q, \dot{q})$ is assumed to be a non-zero, positive, and bounded function with a bounded first and second time derivatives.

Assumption 2: The auxiliary non-zero unknown scalar function $\Omega(q, \dot{q}) \in \mathbb{R}$ is defined as

$$\Omega = \zeta \eta \cos a, \qquad\qquad (2\text{–}8)$$

where the first and second time derivatives of $\Omega(q, \dot{q})$ are assumed to exist and be bounded (see Assumption 1).

Assumption 3: The unknown disturbance $\tau_d(t)$ is bounded and its first and second derivatives with respect to time exist and are bounded. Based on Assumptions 1 and 2, the ratio $\tau_d(t)/\Omega(q, \dot{q})$ is also assumed to be bounded and its first and second derivatives with respect to time exist and are bounded.

CHAPTER 3
NONLINEAR NEUROMUSCULAR ELECTRICAL STIMULATION (NMES) TRACKING CONTROL OF A HUMAN LIMB

3.1 Introduction

An open-loop error system for a general uncertain nonlinear muscle model is developed in the chapter by grouping terms in a manner that facilitates the development of a new continuous feedback method (coined RISE for Robust Integral of the Sign of the Error in [11, 12])and its extension through combining NN-based feedforward method. Through this error-system development, the continuous RISE controller and its modification is proven (through a Lyapunov-based stability analysis) to yield an asymptotic stability result despite the uncertain nonlinear muscle model and the presence of additive bounded disturbances (e.g., muscle spasticity, fatigue, changing loads in functional tasks). The performance of the two nonlinear controllers is experimentally verified for human leg tracking by applying the controller as a voltage potential across external electrodes attached to the distal-medial and proximal-lateral portion of the quadriceps femoris muscle group. The RISE and NN + RISE controllers are implemented by a voltage modulation scheme with a fixed frequency and a fixed pulse width. Other modulation strategies (e.g., frequency or pulse-width modulation) could have also been implemented (and applied to other skeletal muscle groups) without loss of generality.

Third section of the chapter discusses the development of RISE controller for uncertain nonlinear muscle model. The experiments illustrate the ability of the controller to enable the leg shank to track single and multiple period trajectories with different periods and ranges of motion, and also track desired step changes with changing loads. In fourth section the RISE-based method is modified with a NN to develop a new NMES controller for the uncertain muscle model. The experimental results indicate that the addition of the NN reduces the root mean squared (RMS) tracking error for similar stimulation effort when compared to the first result (RISE method without the NN

feedforward component). A preliminary test was also conducted on a healthy volunteer to test the capability of the controller to enable the person to perform a sit-to-stand task.

3.2 Control Development

A high-level objective of NMES is to enable a person to achieve some functional task (i.e., functional electrical stimulation (FES)). Towards this goal, the objective of the current effort is to develop a NMES controller to produce a knee position trajectory that will enable a human shank to track a desired trajectory, denoted by $q_d(t) \in \mathbb{R}$. The desired trajectory can be any continuous signal (or a simple constant setpoint). In the subsequent experimental results, the desired trajectories were selected as periodic signals (for simplicity and without loss of generality) of different frequencies and step functions with changes in the dynamic load. Although such trajectories may not be truly functional, trajectory-based movements are necessary for the performance of many FES augmented tasks (e.g., repetitive stepping during walking). Whether the desired trajectories are based on limb position, as in the current result, or other information (e.g., desired joint kinetics or kinematics), the ability to precisely track a desired pattern is fundamental to eliciting reproducible movement patterns during functional tasks.

To quantify the objective, a position tracking error, denoted by $e_1(t) \in \mathbb{R}$, is defined as

$$e_1(t) = q_d(t) - q(t), \tag{3--1}$$

where $q_d(t)$ is an a priori trajectory which is designed such that $q_d(t), q_d^i(t) \in \mathcal{L}_\infty$, where $q_d^i(t)$ denotes the ith derivative for $i = 1, 2, 3, 4$. To facilitate the subsequent analysis, filtered tracking errors, denoted by $e_2(t)$ and $r(t) \in \mathbb{R}$, are defined as

$$e_2(t) = \dot{e}_1(t) + \alpha_1 e_1(t), \tag{3--2}$$

$$r(t) = \dot{e}_2(t) + \alpha_2 e_2(t), \tag{3--3}$$

where α_1, $\alpha_2 \in \mathbb{R}$ denote positive constants. The filtered tracking error $r(t)$ is introduced to facilitate the closed-loop error system development and stability analysis but is not used in the controller because of a dependence on acceleration measurements.

3.3 Nonlinear NMES Control of a Human Limb via Robust Integral of Signum of Error (RISE) method

After multiplying (3–3) by J and utilizing the expressions in (2–1) and (2–5)-(3–2), the following expression can be obtained:

$$Jr = W - \Omega V + \tau_d, \tag{3–4}$$

where $W(\dot{e}_1, e_2, t) \in \mathbb{R}$ is an auxiliary signal defined as

$$W = J(\ddot{q}_d + \alpha_1 \dot{e}_1 + \alpha_2 e_2) + M_e + M_g + M_v, \tag{3–5}$$

and the continuous, positive, monotonic, and bounded auxiliary function $\Omega(q, t) \in \mathbb{R}$ is defined in (2–8). After multiplying (3–4) by $\Omega^{-1}(q, t) \in \mathbb{R}$, the following expression is obtained:

$$J_\Omega r = W_\Omega - V + \tau_{d\Omega}, \tag{3–6}$$

where $J_\Omega(q, t) \in \mathbb{R}$, $\tau_{d\Omega}(q, t) \in \mathbb{R}$, and $W_\Omega(\dot{e}_1, e_2, t) \in \mathbb{R}$ are defined as

$$J_\Omega = \frac{J}{\Omega}, \qquad \tau_{d\Omega} = \frac{\tau_d}{\Omega} \tag{3–7}$$

$$W_\Omega = \frac{W}{\Omega} = J_\Omega(\ddot{q}_d + \alpha_1 \dot{e}_1 + \alpha_2 e_2) + M_{e\Omega} + M_{g\Omega} + M_{v\Omega}. \tag{3–8}$$

To facilitate the subsequent stability analysis, the open-loop error system for (3–6) can be determined as

$$J_\Omega \dot{r} = -\frac{1}{2} \dot{J}_\Omega r + N - \dot{V} - e_2, \tag{3–9}$$

where $N(e_1, e_2, r, t) \in \mathbb{R}$ denotes the unmeasurable auxiliary term

$$N = \dot{W}_\Omega + e_2 - \frac{1}{2} \dot{J}_\Omega r + \dot{\tau}_{d\Omega}(q, t). \tag{3–10}$$

32

To further facilitate the analysis, another unmeasurable auxiliary term, $N_d(q_d, \dot{q}_d, \ddot{q}_d, \dddot{q}_d, t) \in \mathbb{R}$, is defined as

$$N_d = \dot{J}_\Omega(q_d)\ddot{q}_d + J_\Omega(q_d)\dddot{q}_d + \dot{M}_{e_\Omega}(q_d) + \dot{M}_{g_\Omega}(q_d) + \dot{M}_{v_\Omega}(q_d) + \dot{\tau}_{d_\Omega}(q_d, t). \qquad (3\text{--}11)$$

After adding and subtracting (3–11) to (3–9), the open-loop error system can be expressed as

$$J_\Omega \dot{r} = -\dot{V} - e_2 + \tilde{N} + N_d - \frac{1}{2}\dot{J}_\Omega r, \qquad (3\text{--}12)$$

where the unmeasurable auxiliary term $\tilde{N}(e_1, e_2, r, t) \in \mathbb{R}$ is defined as

$$\tilde{N}(t) = N - N_d. \qquad (3\text{--}13)$$

Motivation for expressing the open-loop error system as in (3–12) is given by the desire to segregate the uncertain nonlinearities and disturbances from the model into terms that are bounded by state-dependent bounds and terms that are upper bounded by constants. Specifically, the Mean Value Theorem can be applied to upper bound $\tilde{N}(e_1, e_2, r, t)$ by state-dependent terms as

$$\left\| \tilde{N} \right\| \leq \rho\left(\|z\|\right)\|z\|, \qquad (3\text{--}14)$$

where $z(t) \in \mathbb{R}^3$ is defined as

$$z(t) \triangleq [e_1^T \ e_2^T \ r^T]^T, \qquad (3\text{--}15)$$

and the bounding function $\rho\left(\|z\|\right)$ is a positive, globally invertible, nondecreasing function. The fact that $q_d(t)$, $q_d^i(t) \in \mathcal{L}_\infty \ \forall \ i = 1, 2, 3, 4$ can be used to upper bound $N_d(q_d, \dot{q}_d, \ddot{q}_d, \dddot{q}_d, t)$ as

$$\|N_d\| \leq \zeta_{N_d} \qquad \left\| \dot{N}_d \right\| \leq \zeta_{\dot{N}_d}, \qquad (3\text{--}16)$$

where ζ_{N_d} and $\zeta_{\dot{N}_d} \in \mathbb{R}$ are known positive constants.

Based on the dynamics given in (2–1)-(2–7), the RISE-based voltage control input $V(t)$ is designed as

$$V(t) \triangleq (k_s + 1)e_2(t) - (k_s + 1)e_2(0) + \nu(t), \tag{3–17}$$

where $k_s \in \mathbb{R}$ denotes positive constant adjustable control gain, and $\nu(t) \in \mathbb{R}$ is the generalized solution to

$$\dot{\nu}(t) = (k_s + 1)\alpha_2 e_2(t) + \beta sgn(e_2(t)), \quad \nu(0) = 0, \tag{3–18}$$

where $\beta \in \mathbb{R}$ denotes positive constant adjustable control gain, and $sgn(\cdot)$ denotes the signum function. Although the control input is present in the open-loop error system in (3–4), an extra derivative is used to develop the open-loop error system in (3–12) to facilitate the design of the RISE-based controller. Specifically, the time-derivative of the RISE input in (3–17) looks like a discontinuous sliding mode controller. Sliding mode control is desirable because it is a method that can be used to reject the additive bounded disturbances present in the muscle dynamics (e.g., muscle spasticity, load changes, electromechanical delays) while still obtaining an asymptotic stability result. The disadvantage of a sliding mode controller is that it is discontinuous. By structuring the open-loop error system as in (3–12), the RISE controller in (3–17) can be implemented as a continuous controller (i.e., the unique integral of the sign of the error) and still yield an asymptotic stability result. Without loss of generality, the developed voltage control input can be implemented through various modulation methods (i.e., voltage, frequency, or pulse width modulation).

3.3.1   Stability Analysis

Theorem 1. *The controller given in (3–17) ensures that all system signals are bounded under closed-loop operation. The position tracking error is regulated in the sense that*

$$\|e_1(t)\| \to 0 \qquad as \ \ t \to \infty, \tag{3–19}$$

and the controller yields semi-global asymptotic tracking provided the control gain k_s, introduced in (3–17) is selected sufficiently large, and β is selected according to the following sufficient condition:

$$\beta > \left(\zeta_{N_d} + \frac{1}{\alpha_2} \zeta_{\dot{N}_d} \right), \tag{3–20}$$

where ζ_{N_d} and $\zeta_{\dot{N}_d}$ are introduced in (3–16).

Proof for Theorem 1: Let $\mathcal{D} \subset \mathbb{R}^4$ be a domain containing $y(t) = 0$, where $y(t) \in \mathbb{R}^{3+1}$ is defined as

$$y(t) \triangleq \left[\begin{array}{cc} z^T & \sqrt{P(t)} \end{array} \right]^T, \tag{3–21}$$

and the auxiliary function $P(t) \in \mathbb{R}$ is the generalized solution to the differential equation

$$\dot{P}(t) = -L(t), \quad P(0) = \beta |e_2(0)| - e_2(0) N_d(0). \tag{3–22}$$

The auxiliary function $L(t) \in \mathbb{R}$ in (3–22) is defined as

$$L(t) \triangleq r(N_d(t) - \beta sgn(e_2)). \tag{3–23}$$

Provided the sufficient conditions stated in Theorem 1 are satisfied, then $P(t) \geq 0$.

Let $V_L(y,t) : \mathcal{D} \times [0,\infty) \to \mathbb{R}$ denote a Lipschitz continuous regular positive definite functional defined as

$$V_L(y,t) \triangleq e_1^T e_1 + \frac{1}{2} e_2^T e_2 + \frac{1}{2} r^T J_\Omega r + P, \tag{3–24}$$

which satisfy the inequalities

$$U_1(y) \leq V_L(y,t) \leq U_2(y), \tag{3–25}$$

provided the sufficient condition introduced Theorem 1 is satisfied, where $U_1(y), U_2(y) \in \mathbb{R}$ are continuous, positive definite functions. After taking the time derivative of (3–24), $\dot{V}_L(y,t)$ can be expressed as

$$\dot{V}_L(y,t) \triangleq 2e_1\dot{e}_1 + \frac{1}{2} e_2\dot{e}_2 + J_\Omega r\dot{r} + \frac{1}{2}\dot{J}_\Omega r^2 + \dot{P}. \tag{3–26}$$

From (3–2), (3–3), (3–12), (3–22), and (3–23), some of the differential equations describing the closed-loop system for which the stability analysis is being performed have discontinuous right-hand sides as

$$\dot{e}_1 = e_2 - \alpha_1 e_1, \tag{3–27a}$$

$$\dot{e}_2 = r - \alpha_2 e_2, \tag{3–27b}$$

$$J_\Omega \dot{r} = -\frac{1}{2} \dot{J}_\Omega r + \tilde{N} + N_d - e_2 - (k_s + 1) r - \beta sgn(e_2), \tag{3–27c}$$

$$\dot{P}(t) = -r (N_d(t) - \beta sgn(e_2)). \tag{3–27d}$$

Let $f(y,t) \in \mathbb{R}^4$ denote the right hand side of (3–27). Since the subsequent analysis requires that a solution exists for $\dot{y} = f(y,t)$, it is important to show the existence of the solution to (3–27). As described in [103–106], the existence of Filippov's generalized solution can be established for (3–27). First, note that $f(y,t)$ is continuous except in the set $\{(y,t)|e_2 = 0\}$. From [103–106], an absolute continuous Filippov solution $y(t)$ exists almost everywhere (a.e.) so that

$$\dot{y} \in K[f](y,t) \quad a.e. \tag{3–28}$$

Except the points on the discontinuous surface $\{(y,t)|e_2 = 0\}$, the Filippov set-valued map includes unique solution. Under Filippov's framework, a generalized Lyapunov stability theory can be used (see [106–109] for further details) to establish strong stability of the closed-loop system. The generalized time derivative of (3–24) exists a.e., and $\dot{V}_L(y,t) \in^{a.e.} \dot{\tilde{V}}_L(y,t)$ where

$$
\begin{aligned}
\dot{\tilde{V}}_L &= \bigcap_{\xi \in \partial V_L(y,t)} \xi^T K \begin{bmatrix} \dot{e}_1 & \dot{e}_2 & \dot{r} & \frac{1}{2}P^{-\frac{1}{2}}\dot{P} & 1 \end{bmatrix}^T. \\
&= \nabla V_L^T K \begin{bmatrix} \dot{e}_1 & \dot{e}_2 & \dot{r} & \frac{1}{2}P^{-\frac{1}{2}}\dot{P} & 1 \end{bmatrix}^T \\
&\subset \begin{bmatrix} 2e_1 & e_2 & rJ_\Omega & 2P^{\frac{1}{2}} & \frac{1}{2}\dot{J}_\Omega r^2 \end{bmatrix} K \begin{bmatrix} \dot{e}_1 & \dot{e}_2 & \dot{r} & \frac{1}{2}P^{-\frac{1}{2}}\dot{P} & 1 \end{bmatrix}^T,
\end{aligned}
$$

where ∂V is the generalized gradient of V [107], and $K[\cdot]$ is defined as [108, 109]

$$K[f](y) \triangleq \bigcap_{\delta > 0} \bigcap_{\mu N = 0} \overline{co} f(B(x, \delta) - N),$$

where $\bigcap_{\mu N = 0}$ denotes the intersection of all sets N of Lebesgue measure zero, $\overline{co}$ denotes convex closure, and $B(x, \delta)$ represents a ball of radius δ around x. After utilizing (3–2), (3–3), (3–12), (3–17), (3–18), (3–22), and (3–23)

$$
\begin{aligned}
\dot{\tilde{V}}_L(y, t) \quad \subset \quad & 2e_1 e_2 - 2\alpha_1 e_1^2 + e_2 r - \alpha_2 e_2^2 + \frac{1}{2}\dot{J}_\Omega r^2 + r\tilde{N} + r N_d - r e_2 - (k_s + 1)\,r^2 \\
& -\beta r K[sgn(e_2)] - \frac{1}{2}\dot{J}_\Omega r^2 - r N_d(t) + \beta r K[sgn(e_2)],
\end{aligned}
\tag{3–29}
$$

where [108]

$$K[sgn(e_2)] = SGN(e_2),\tag{3–30}$$

such that

$$
SGN(e_2) =
\begin{cases}
1 & e_2 > 0 \\
[-1, 1] & e_2 = 0 \\
-1 & e_2 < 0
\end{cases}.
\tag{3–31}
$$

Cancelling common terms and based on the fact that

$$2e_1 e_2 \leq \|e_2\|^2 + \|e_1\|^2,\tag{3–32}$$

(3–29) can be written as

$$\dot{\tilde{V}}_L(y, t) \subset -(2\alpha_1 - 1)e_1^2 - (\alpha_2 - 1)e_2^2 - r^2 + r\tilde{N} - k_s r^2.\tag{3–33}$$

As shown in (3–29)-(3–33), the unique integral signum term in the RISE controller is used to compensate for the disturbance terms included in $N_d(q_d, \dot{q}_d, \ddot{q}_d, \dddot{q}_d, t)$, provided the control gain β is selected according to (3–20). Using (3–14), the term $r(t)\tilde{N}(e_1, e_2, r, t)$, can be upper bounded by following inequality:

$$\left\|r\tilde{N}\right\| \leq \rho\left(\|z\|\right)\|z\|\|r\|,\tag{3–34}$$

to obtain

$$\dot{\tilde{V}}_L(y,t) \subset -\min\{2\alpha_1 - 1, \alpha_2 - 1, 1\} \|z\|^2 + [\rho(\|z\|)\|z\|\|r\| - k_s\|r\|^2]. \qquad (3\text{--}35)$$

Completing the squares for the bracketed terms in (3–35) yields

$$\dot{\tilde{V}}_L(y,t) \subset -\min\{2\alpha_1 - 1, \alpha_2 - 1, 1\} \|z\|^2 + \frac{\rho^2(\|z\|)\|z\|^2}{4k_s}. \qquad (3\text{--}36)$$

The following expression can be obtained from (3–36):

$$\dot{\tilde{V}}_L(y,t) \subset -U(y), \qquad (3\text{--}37)$$

where $U(y)$ is a continuous positive definite function, provided k_s is selected sufficiently large based on the initial conditions of the system. That is, the region of attraction can be made arbitrarily large to include any initial conditions by increasing the control gain k_s (i.e., a semi-global type of stability result), and hence

$$c\|z(t)\|^2 \to 0 \qquad \text{as } t \to \infty \qquad \forall y(0) \in \mathcal{S}. \qquad (3\text{--}38)$$

Based on the definition of $z(t)$ in (3–15), (3–38) can be used to show that

$$\|e_1(t)\| \to 0 \qquad \text{as } t \to \infty \qquad \forall y(0) \in \mathcal{S}. \qquad (3\text{--}39)$$

3.3.2 Experimental Results

Experiments were performed using the RISE controller given in (3–17). The voltage controller was implemented through an amplitude modulation scheme composed of a variable amplitude positive square wave with a fixed pulse width of 100 μ sec and fixed frequency of 30 Hz. The 100 μsec pulse width and the 30 Hz stimulation frequency were chosen a-priori and represent parametric settings that are within the ranges typically reported during NMES studies. During stimulation at 100 μsec pulse widths, human skeletal muscle response to changes in stimulation amplitude (force-amplitude relationship) and frequency (force-frequency relationship) are highly predictable and thus deemed

appropriate for use in the present study. The 30 Hz stimulation was selected based on force-frequency curves [110] which show that as stimulation frequency is increased muscle force increases to a saturation limit. Higher frequencies can be chosen to generate more force up to a saturation limit, but muscles tend to fatigue faster at higher frequencies. The 30 Hz pulse wave yields reduced fatigue in comparison to higher frequencies but lower frequencies tend to produce rippled knee motion [35, 110]. Therefore stimulation frequencies in the range of 30-40 Hz is an optimal choice for conducting external electrical stimulation. The following results indicate that the RISE algorithm was able to minimize the knee angle error while dynamically tracking a desired trajectory.

3.3.2.1 Testbed and protocol

The testbed consists of a custom computer controlled stimulation circuit and a modified leg extension machine (LEM). The LEM was modified to include optical encoders. The LEM allows seating adjustments to ensure the rotation of the knee is about the encoder axis. A 4.5 kg (10 lb.) load was attached to the weight bar of the LEM, and a mechanical stop was used to prevent hyperextension.

In the experiment, bipolar self-adhesive neuromuscular stimulation electrodes were placed over the distal-medial and proximal-lateral portion of the quadriceps femoris muscle group and connected to the custom stimulation circuitry. Prior to participating in the study, written informed consent was obtained from all the subjects, as approved by the Institutional Review Board at the University of Florida. Tracking experiments for a two period desired trajectory were conducted on both legs of five subjects. The subjects included two healthy females and three healthy males in the age group of 22 to 26 years. The electrical stimulation responses of healthy subjects have been reported as similar to paraplegic subjects' responses [16, 22, 39, 111]. Therefore healthy subjects were used in NMES experiments as substitute for paraplegic patients which were not available. As described in Section 3.3.2.2, the results were approximately equal across the subjects (i.e., a standard deviation of 0.53 degrees of Root Mean Squared (RMS) tracking error).

Therefore, additional experiments were conducted on a single subject's leg to illustrate the applicability of the controller for different conditions.

During the experiments each subject was instructed to relax and to allow the stimulation to control the limb motion (i.e., the subjects were not supposed to influence the leg motion voluntarily and were not allowed to observe the desired trajectory). Varying the time period and range of motion may also help to reduce any possible trajectory learning and anticipation by a healthy subject. To experimentally examine if any trajectory learning occurred, four successive tests were conducted on a healthy subject with a two minute interval between trials. The experiments were conducted for 15 seconds on a dual period trajectory of 4 and 6 seconds. The resulting RMS errors are given in Table 3-1. The results in Table 3-1 illustrate that trajectory learning by the subject is not apparent since the standard deviation between the successive trials is 0.039 degrees.

Trial	RMS error (in deg.)
1	4.35
2	4.28
3	4.26
4	4.29

Table 3-1. Tabulated results indicate that the test subject was not learning the desired trajectory since the RMS errors are relatively equal for each trial.

3.3.2.2   Results and discussion

The experimental results of five subjects tested for the two period desired trajectory depicted in Fig. 3-1, are summarized in Table 3-2. In Table 3-2, the maximum steady-state error is defined as the maximum absolute value of error that occurs after 4 seconds of the trial. The maximum steady-state errors range from 4.25 to 7.55 degrees with a mean of 6.32 degrees and a standard deviation of 1.18 degrees. The RMS tracking errors range from $2°$ to $3.47°$ with a mean RMS error of 2.75 degrees and a standard deviation of 0.53 degrees. The tracking error results for Subject B and the corresponding output voltages computed by the RISE method (prior to voltage modulation) are shown in Fig. 3-1. The

results successfully illustrate the ability of the RISE controller to track the desired two period trajectory.

Subject	Leg	RMS Error	Max. Steady State Error
A	Left	2.89°	7.55°
A	Right	2.36°	7.14°
B	Left	2.00°	5.40°
B	Right	2.35°	6.99°
C	Left	2.07°	4.25°
C	Right	2.94°	4.51°
D	Left	3.47°	7.30°
D	Right	2.89°	6.94°
E	Left	3.11°	6.80°
E	Right	3.45°	6.30°
Mean		**2.75°**	**6.32°**
Std. Dev.		**0.53°**	**1.18°**

Table 3-2. Experimental results for two period desired trajectory

To further illustrate the performance of the controller, experiments were also conducted for trajectories with faster and slower periods and larger ranges of motion. Specifically, the controller's performance was tested for a desired trajectory with a constant 2 second period, a constant 6 second period, a triple periodic trajectory with cycles of 2, 4, and 6 seconds and for a higher range of motion of 65 degrees. As indicated in Table 3-1, the results for the two period trajectory yielded similar results for all the subjects. Hence, these additional tests were performed on a single individual simply to illustrate the capabilities of the controller, with the understanding that some variations would be apparent when implemented on different individuals. The RMS tracking errors and maximum steady-state errors are provided in Table 3-3. The RMS error and the maximum steady state errors are lowest for a constant 6 second period desired trajectory and higher for faster trajectories and higher range of motion. These results are an expected outcome since tracking more aggressive trajectories generally yields more error. The triple periodic trajectory consists of a mix of slower and faster period
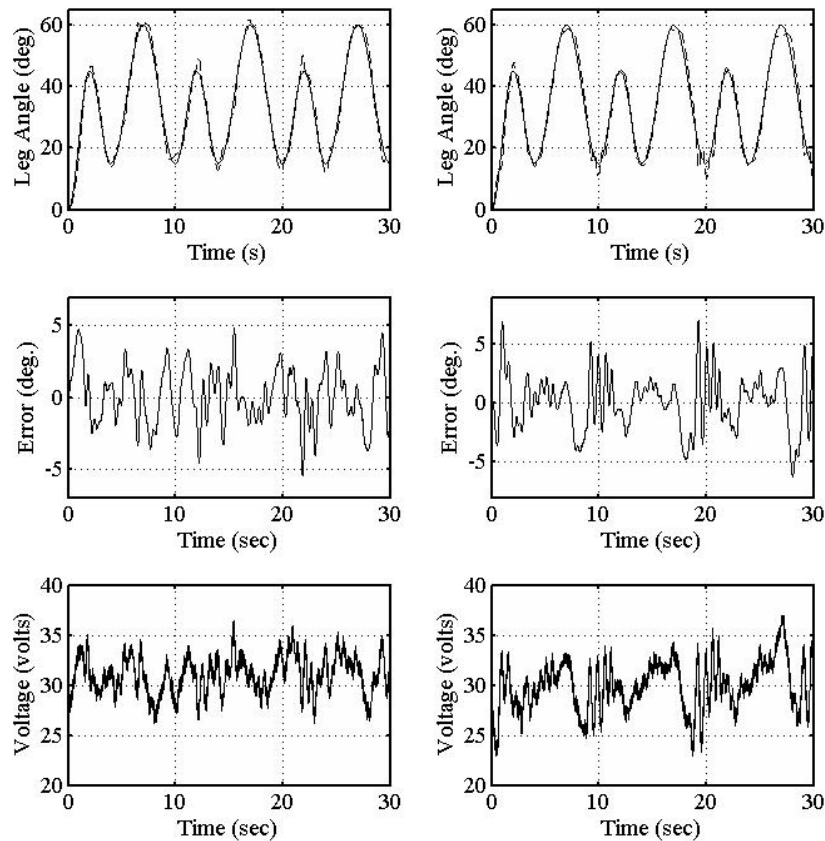
Figure 3-1. Top plots: Actual left limb trajectory of a subject (solid line) versus the desired two periodic trajectory (dashed line) input. (left leg - top left plot and right leg - top right plot). Middle plots: The tracking error (desired angle minus actual angle) of a subject's leg tracking a two periodic desired trajectory. (left leg - middle left plot and right leg - middle right plot). Bottom plots: The computed RISE voltage during knee joint tracking for the case of two period trajectory (left leg - bottom left plot and right leg - bottom right plot).

trajectories, therefore the RMS and the maximum steady state errors are in between the respective errors obtained for more aggressive 2 second period and higher range of motion desired trajectories. Figs. 3-2 - 3-5 depict the errors for the experiments summarized in Table 3-3.

Additional experiments were also conducted to examine the performance of the controller in response to step changes and changing loads. Specifically, a desired trajectory of a step input was commanded with a 10 pound load attached to the LEM. An additional

Trajectory	A	B
Constant 6 sec.	2.88	6.13
Constant 2 sec.	4.11	10.67
Triple periodic $(6, 4, 2)$ sec.	3.27	7.82
Triple periodic $(6, 4, 2)$ sec with higher range of motion	5.46	12.48

Table 3-3. Summarized experimental results for multiple, higher frequencies and higher range of motion. Column (A) indicates RMS error in degrees, and column (B) indicates maximum steady state error in degrees.
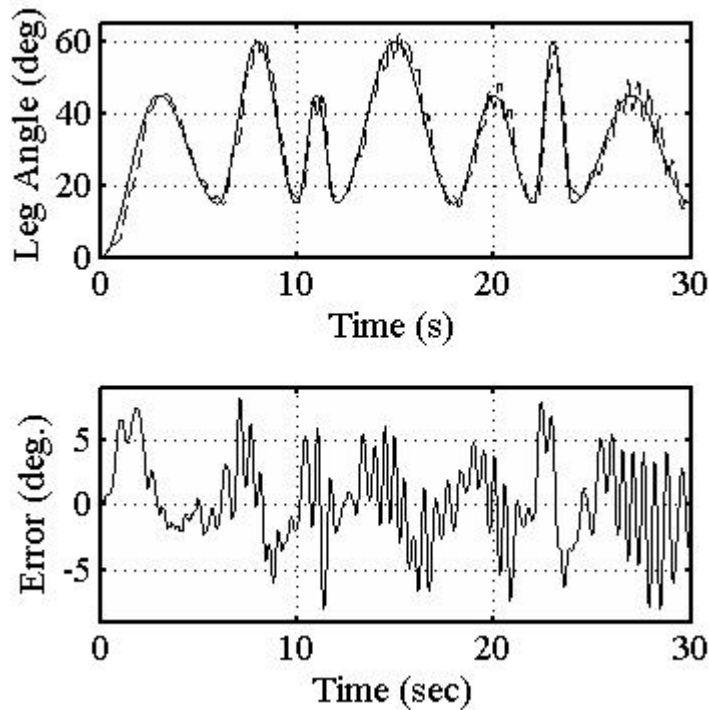
Figure 3-2. Top plot: Actual limb trajectory (solid line) versus the desired triple periodic trajectory (dashed line). Bottom plot: The limb tracking error (desired angle minus actual angle) of a subject tracking a triple periodic desired trajectory.

10 pound load was added once the limb stabilized after a step down of 15 degrees. The limb was again commanded to perform a step response to raise the limb back up an additional 15 degrees with the total load of 20 pounds. The results are shown in Fig. 3-6. The steady state error was within ±1 degree. A maximum error of 3 degrees was observed when the external load was added. The results give some indication of the controller's
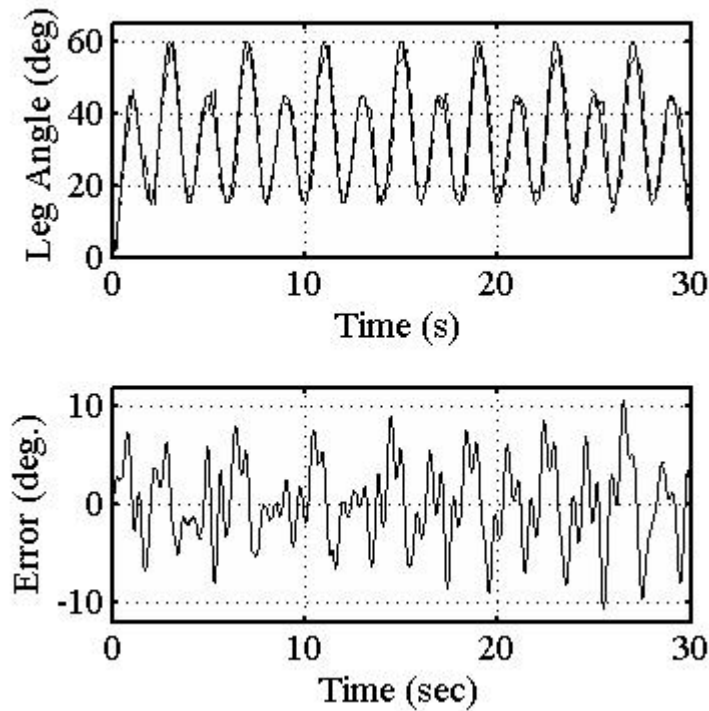
Figure 3-3. Top plot: Actual limb trajectory (solid line) versus the desired constant period (2 sec) trajectory (dashed line). Bottom plot: The limb tracking error (desired angle minus actual angle) of a subject tracking a constant period (2 sec) desired trajectory.

ability to adapt to changes in load and step inputs and motivate possible future case studies with neurologically impaired individuals that express muscle spasticity.

For each experiment, the computed voltage input was modulated by a fixed pulse width of 100 μ sec and fixed frequency of 30 Hz. The stimulation frequency was selected based on subject comfort and to minimize fatigue. During preliminary experiments with stimulation frequencies of 100 Hz, the subjects fatigued approximately two times faster than in the current results. The results also indicate that a 100 μ sec pulse width was acceptable, though future studies will investigate higher pulse widths in the range of $300 - 350\mu$ sec which recruit more slow fatiguing motor units [110]. Our previous preliminary experiments indicated that longer pulse widths (e.g., 1 msec) produced similar effects as a direct current voltage.
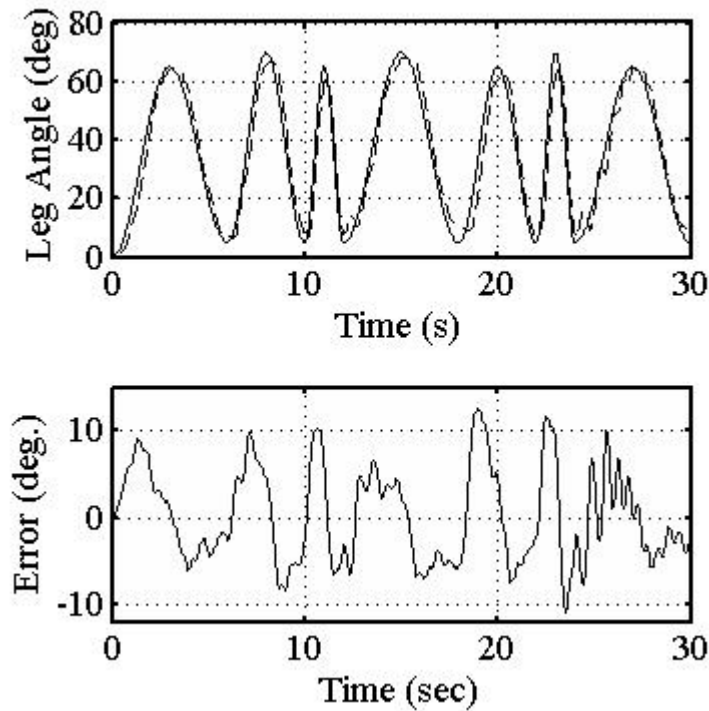
Figure 3-4. Top plot: Actual limb trajectory (solid line) versus the triple periodic desired trajectory with higher range of motion (dashed line). Bottom plot: The limb tracking error (desired angle minus actual angle) of a subject tracking a triple periodic desired trajectory with higher range of motion

The use of the RISE control structure is motivated by its implicit learning characteristics [96] and its ability to compensate for additive system disturbances and parametric uncertainties in the system. The advantage of the RISE controller is that it does not require muscle model knowledge and guarantees asymptotic stability of the nonlinear system. The experimental results indicate that this feedback method may have promise in some clinical applications.

Although the RISE controller was successfully implemented, the performance of the controller may be improved by including a feedforward control structure such as neural networks (a black box function approximation technique) or physiological/phenomenological muscle models. Since the RISE controller is a high gain feedback controller that yields asymptotic performance, adding a feedforward control element may improve transient and
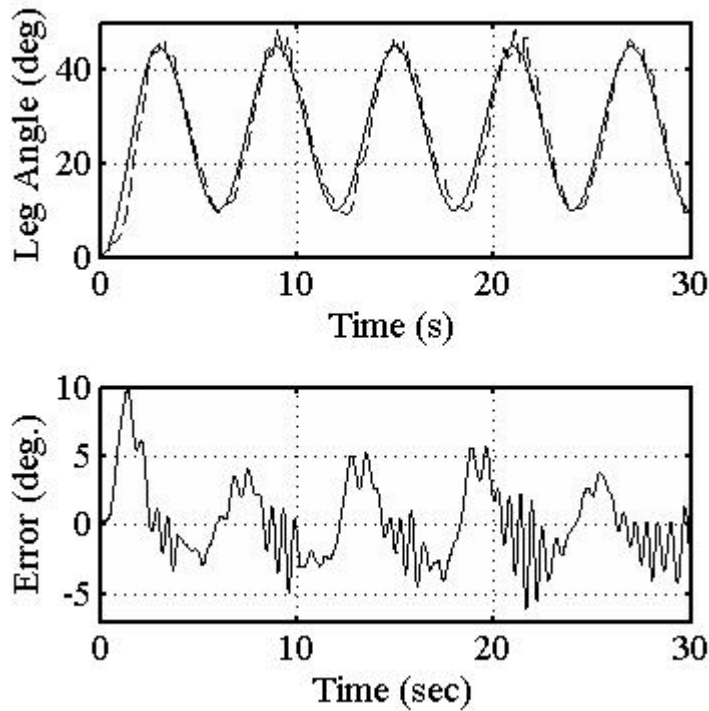
Figure 3-5. Top plot: Actual limb trajectory (solid line) versus the desired constant period (6 sec) trajectory (dashed line). Bottom plot: The limb tracking error (desired angle minus actual angle) of a subject tracking a constant period (6 sec) desired trajectory.

steady state performance and reduce the overall control effort, thereby reducing muscle fatigue. Another possible improvement to the controller is to account for fatigue. Fatigue can be reduced for short durations by selecting optimal stimulation parameters, but functional electrical stimulation (FES) may require a controller that adapts with fatigue to yield performance gains for longer time durations. Therefore our future goal will be to include a fatigue model in the system to enhance the controller performance.

3.3.3 Conclusion

A Lyapunov-based stability analysis indicates that the closed-loop nonlinear control method yields asymptotic tracking for a nonlinear muscle activation and limb dynamics, even in the presence of additive disturbances. Experiments using external electrodes on human subjects demonstrated the ability of the RISE controller to enable a limb to track a desired trajectory composed of varying amplitude and frequency sinusoids, step
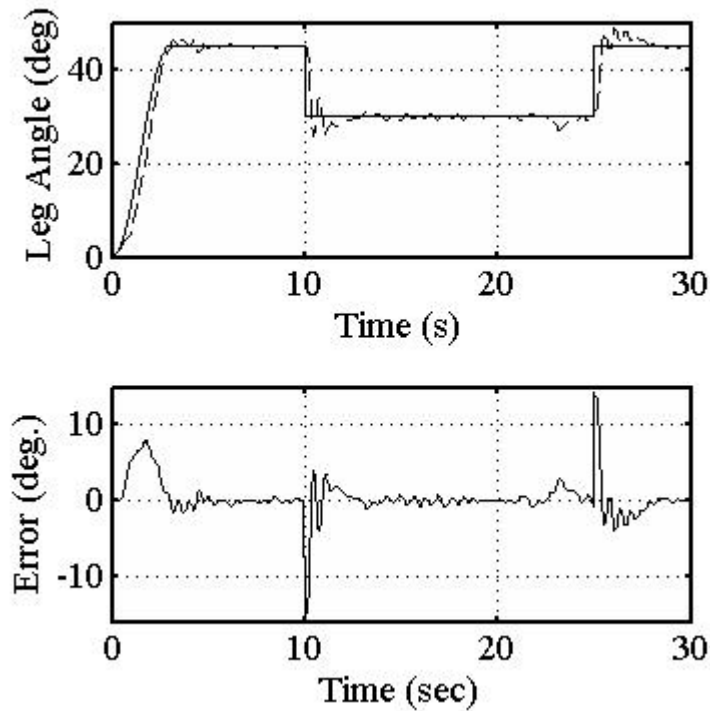
Figure 3-6. Top plot : Actual limb trajectory (solid line) versus desired step trajectory (dashed line). The limb is tested for two step inputs. The load is added once the limb stabilizes (between 23 and 24 second interval). Bottom plot: The limb tracking error for step inputs.

changes, and changes in the load. Specifically, the experimental results indicated that with no muscle model (and only voltage amplitude modulation), the RISE algorithm could determine the appropriate stimulation voltage for the tracking objective. For the fastest tested trajectory the maximum steady-state tracking errors were approximately 10 degrees, whereas the maximum steady-state error in slower trajectories were as little as approximately 4 degrees. An advantage of this controller is that it can be applied without knowledge of patient specific parameters like limb mass or inertia, limb center of gravity location, parameters that model passive and elastic force elements. Thus, its application would not require specific expertise or extensive testing prior to use. The control development also accounts for unmodeled disturbance (e.g. muscle spasticity) that are commonly observed in clinical populations. The proposed strategy holds promise for

47

clinical implementation of the controller as a therapeutic tool to enhance muscle function during isolated joint movements. However, results have yet to demonstrate functional movements (e.g. walking) in populations without the ability to voluntarily activate their muscles. As such, future directions will focus on studies to demonstrate the effectiveness of the controller under such conditions. Although the trajectories used in the experiments may not be truly functional, the controller can be applied to any continuous trajectory. This is clinically relevant because trajectory-based movements are necessary for the performance of many FES augmented tasks (e.g., repetitive stepping during walking). Whether the desired trajectories are based on limb position, as in the current result, or other information (e.g., desired joint kinetics or kinematics), the ability to precisely track a desired pattern is fundamental to eliciting reproducible movement patterns during functional tasks. An advantage of the control development is that it allows for inter- as well as intra-individual variations in trajectory tracking (i.e. task performance) to be accounted for both within and between sessions (e.g. during rehabilitation training), thus potentially providing a tool to aid in the future advancement of rehabilitation. A possible disadvantage of the controller is that high gains are used to achieve the robustness to disturbances and unmodeled effects. The next section will investigate augmenting the RISE structure with feedforward control architectures that can accommodate for disturbances without requiring high gain feedback.

3.4 Modified Neural Network-based Electrical Stimulation for Human Limb Tracking

NN-based estimation methods are well suited for NMES because the muscle model contains unstructured nonlinear disturbances as given in (2–1). Due to the universal approximation property, NN-based estimation methods can be used to represent the unknown nonlinear muscle model by a three-layer NN as [112]

$$f(x) = W^T \sigma(U^T x) + \epsilon(x), \tag{3–40}$$

for some input $x(t) \in \mathbb{R}^{N_1+1}$. In (3–40), $U \in \mathbb{R}^{(N_1+1) \times N_2}$ and $W \in \mathbb{R}^{(N_2+1) \times n}$ are bounded constant ideal weight matrices for the first-to-second and second-to-third layers respectively, where N_1 is the number of neurons in the input layer, N_2 is the number of neurons in the hidden layer, and n is the number of neurons in the output layer. The sigmoid activation function in (3–40) is denoted by $\sigma(\cdot) : \mathbb{R}^{N_1+1} \rightarrow \mathbb{R}^{N_2+1}$, and $\epsilon(x) : \mathbb{R}^{N_1+1} \rightarrow \mathbb{R}^n$ is the functional reconstruction error. The additional term "1" in the input vector $x(t)$ and activation term $\sigma(\cdot)$ allows for thresholds to be included as the first columns of the weight matrices [112]. Thus, any tuning of W and U then includes tuning of thresholds. Based on (3–40), the typical three layer NN approximation for $f(x)$ is given as [112]

$$\hat{f}(x) = \hat{W}^T \sigma(\hat{U}^T x), \tag{3–41}$$

where $\hat{U} \in \mathbb{R}^{(N_1+1) \times N_2}$ and $\hat{W} \in \mathbb{R}^{(N_2+1) \times n}$ are subsequently designed estimates of the ideal weight matrices. The estimate mismatch for the ideal weight matrices, denoted by $\tilde{U}(t) \in R^{(N_1+1) \times N_2}$ and $\tilde{W}(t) \in R^{(N_2+1) \times n}$, are defined as

$$\tilde{U} = U - \hat{U}, \qquad \tilde{W} = W - \hat{W}, \tag{3–42}$$

and the mismatch for the hidden-layer output error for a given $x(t)$, denoted by $\tilde{\sigma}(x) \in R^{N_2+1}$, is defined as

$$\tilde{\sigma} = \sigma - \hat{\sigma} = \sigma(U^T x) - \sigma(\hat{U}^T x). \tag{3–43}$$

The NN estimate has ceratin properties and assumptions that facilitate the subsequent development.

Property 1: (Taylor Series Approximation) The Taylor series expansion for $\sigma(U^T y)$ for a given $y(t)$ may be written as [112]

$$\sigma(U^T y) = \sigma(\hat{U}^T y) + \sigma'(\hat{U}^T y)\tilde{U}^T y + O(\tilde{U}^T y)^2, \tag{3–44}$$

where $\sigma'(\hat{U}^T y) = d\sigma(U^T y)/d(U^T y)_{|U^T y = \hat{U}^T y}$, and $O(\tilde{U}^T y)^2$ denotes the higher order terms. After substituting (3–44) into (3–43) the following expression can be obtained:

$$\tilde{\sigma} = \hat{\sigma}' \tilde{U}^T y + O(\tilde{U}^T y)^2, \tag{3–45}$$

where $\hat{\sigma}' = \sigma'(\hat{U}^T y)$.

Assumption 1: (Boundedness of the Ideal Weights) The ideal weights are assumed to exist and are bounded by known positive values so that

$$\|U\|_F^2 = tr(U^T U) = vec(U)^T vec(U) \leq \bar{U}_B, \tag{3–46}$$

$$\|W\|_F^2 = tr(W^T W) = vec(W)^T vec(W) \leq \bar{W}_B, \tag{3–47}$$

where $\|\cdot\|_F$ is the Frobenius norm of a matrix, $tr(\cdot)$ is the trace of a matrix. The ideal weights in a NN are bounded, but knowledge of this bound is a non-standard assumption in typical NN literature (although this assumption is also used in textbooks such as [112, 113]). If the ideal weights are constrained to stay within some predefined threshold, then the function reconstruction error will be larger. Typically, this would yield a larger ultimate steady-state bound. Yet, in the current result, the mismatch resulting from limiting the magnitude of the weights is compensated through the RISE feedback structure (i.e., the RISE structure eliminates the disturbance due to the function reconstruction error).

3.4.1 Open-Loop Error System

The open-loop tracking error system can be developed by multiplying (3–3) by J and by utilizing the expressions in (2–1) and (2–5)–(3–2) as

$$Jr = J(\alpha_2 e_2 + \alpha_1 \dot{e}_1 + \ddot{q}_d) + M_e + M_g + M_v - \Omega V + \tau_d, \tag{3–48}$$

50

where $\Omega(q, \dot{q})$ is defined in (2–8). The dynamics in (3–48) can be rewritten as

$$J_\Omega r = f_d + S - V + \tau_{d\Omega}, \tag{3–49}$$

where the auxiliary functions $f_d(q_d, \dot{q}_d, \ddot{q}_d) \in \mathbb{R}$ and $S(q, q_d, \dot{q}, \dot{q}_d, \ddot{q}_d) \in \mathbb{R}$ are defined as

$$f_d = L_\Omega(q_d, \dot{q}_d) + J_\Omega(q_d)\ddot{q}_d, \tag{3–50}$$

$$S = J_\Omega(q)(\alpha_2 e_2 + \alpha_1 \dot{e}_1) + J_\Omega(q)\ddot{q}_d - J_\Omega(q_d)\ddot{q}_d + L_\Omega(q, \dot{q}) - L_\Omega(q_d, \dot{q}_d)$$

and $J_\Omega(q, \dot{q}) \in \mathbb{R}$, $L_\Omega(q, \dot{q}) \in \mathbb{R}$, and $\tau_{d\Omega}(q, t) \in \mathbb{R}$ are defined as

$$J_\Omega = \frac{J}{\Omega}, \qquad \tau_{d\Omega} = \frac{\tau_d}{\Omega}, \qquad L_\Omega = \frac{M_e + M_g + M_v}{\Omega}. \tag{3–51}$$

The expression in (3–50) can be represented by a three-layer NN as

$$f_d = W^T \sigma(U^T x_d) + \epsilon(x_d), \tag{3–52}$$

where $x_d(t) \in \mathbb{R}^4$ is defined as $x_d(t) = [1 \; q_d(t) \; \dot{q}_d(t) \; \ddot{q}_d(t)]$. Based on the assumption that the desired trajectory is bounded, the following inequalities hold

$$\|\epsilon(x_d)\| \le \epsilon_{b_1} \qquad \|\dot{\epsilon}(x_d)\| \le \epsilon_{b_2} \qquad \|\ddot{\epsilon}(x_d)\| \le \epsilon_{b_3}, \tag{3–53}$$

where ϵ_{b_1}, ϵ_{b_2} and $\epsilon_{b_3} \in \mathbb{R}$ are known positive constants.

3.4.2 Closed-Loop Error System

The control development in this section is motivated by several technical challenges related to blend the NN feedforward term with the RISE feedback method. One of the challenges is that the NN structure must be developed in terms if the desired trajectories to avoid the use of acceleration measurements. Also, while the NN estimates are upper bounded by constants, the time derivatives of these terms are state dependent, and hence violate the traditional RISE assumptions. To address this issue, the closed-loop error system development requires a strategic separation and regrouping of terms. In this section, the control is designed and the closed-loop error system is presented. Based on the

open-loop error system in (3–49) and the subsequent stability analysis, the control torque input is designed as [27]

$$V = \hat{f}_d + \mu \tag{3–54}$$

where $\hat{f}_d(t) \in R$ is the three-layer NN feedforward estimate designed as

$$\hat{f}_d = \hat{W}^T \sigma(\hat{U}^T x_d) \tag{3–55}$$

and $\mu(t) \in \mathbb{R}$ is the RISE feedback term designed as [11, 96, 114, 115]

$$\mu(t) \triangleq (k_s + 1)e_2(t) - (k_s + 1)e_2(0) + \nu(t). \tag{3–56}$$

The estimates for the NN weights in (3–55) are generated on-line using a projection algorithm as

$$\dot{\hat{W}} = proj\left(\Gamma_1 \hat{\sigma}' \hat{U}^T \dot{x}_d e_2^T\right) \qquad \dot{\hat{U}} = proj\left(\Gamma_2 \dot{x}_d \left(\hat{\sigma}'^T \hat{W} e_2\right)^T\right), \tag{3–57}$$

where $\Gamma_1 \in \mathbb{R}^{(N_2+1)\times(N_2+1)}$ and $\Gamma_2 \in \mathbb{R}^{4\times4}$ are constant, positive definite, symmetric gain matrices. In (3–56), $k_s \in \mathbb{R}$ denotes positive constant adjustable control gain, and $\nu(t) \in \mathbb{R}$ is the generalized solution to

$$\dot{\nu}(t) = (k_s + 1)\alpha_2 e_2(t) + \beta_1 sgn(e_2(t)), \quad \nu(0) = 0, \tag{3–58}$$

where $\beta_1 \in \mathbb{R}$ denotes positive constant adjustable control gain, and $sgn(\cdot)$ denotes the signum function. The closed-loop tracking error system can be developed by substituting (3–54) into (3–49) as

$$J_\Omega r = \tilde{f}_d + S - \mu + \tau_{d\Omega}, \tag{3–59}$$

where

$$\tilde{f}_d(x_d) = f_d - \hat{f}_d. \tag{3–60}$$

To facilitate subsequent closed loop stability analysis, the time derivative of (3–59) can be determined as

$$J_\Omega \dot{r} = -\dot{J}_\Omega r + \dot{\tilde{f}}_d + \dot{S} - \dot{\mu} + \dot{\tau}_{d\Omega}. \tag{3–61}$$

Although the voltage control input $V(t)$ is present in the open loop error system in (3–49), an additional derivative is taken to facilitate the design of the RISE-based feedback controller. After substituting the time derivative of (3–60) into (3–61) by using (3–52) and (3–55), the closed loop system can be expressed as

$$J_\Omega \dot{r} = -\dot{J}_\Omega r + W^T \sigma'(U^T x_d) U^T \dot{x}_d - \dot{\hat{W}}^T \sigma(\hat{U}^T x_d) - \hat{W}^T \sigma'(\hat{U}^T x_d)\hat{U}^T \dot{x}_d - \hat{W}^T \sigma'(\hat{U}^T x_d)\dot{\hat{U}}^T x_d$$
$$+ \dot{\epsilon}(x_d) + \dot{S} - \dot{\mu} + \dot{\tau}_{d\Omega}, \tag{3–62}$$

where $\sigma'(\hat{U}^T x) = d\sigma(U^T x)/d(U^T x) \mid_{U^T x = \hat{U}^T x}$. After adding and subtracting the terms $W^T \hat{\sigma}' \hat{V}^T \dot{x}_d + \hat{W}^T \hat{\sigma}' \tilde{V}^T \dot{x}_d$ to (3–62), the following expression can be obtained:

$$J_\Omega \dot{r} = -\dot{J}_\Omega r + \hat{W}^T \hat{\sigma}' \tilde{V}^T \dot{x}_d + \tilde{W}^T \hat{\sigma}' \hat{V}^T \dot{x}_d - \hat{W}^T \hat{\sigma}' \tilde{V}^T \dot{x}_d - W^T \hat{\sigma}' \hat{V}^T \dot{x}_d \tag{3–63}$$
$$+ W^T \sigma' U^T \dot{x}_d + \dot{\epsilon}(x_d) - \hat{W}^T \hat{\sigma}' \dot{\hat{U}}^T x_d - \dot{\hat{W}}^T \hat{\sigma} + \dot{S} - \dot{\mu} + \dot{\tau}_{d\Omega},$$

where the notation $\hat{\sigma}(\cdot)$ is introduced in (3–43). Using the NN weight tuning laws described in (3–57), the expression in (3–63) can be rewritten as

$$J_\Omega \dot{r} = -\frac{1}{2}\dot{J}_\Omega r + \tilde{N} + N - e_2 - (k_s + 1)r - \beta sgn(e_2), \tag{3–64}$$

where the unmeasurable auxiliary terms $\tilde{N}(e_1, e_2, r, t)$ and $N(\hat{W}, \hat{U}, x_d, t) \in \mathbb{R}$ given in (3–64) are defined as

$$\tilde{N}(t) = -\frac{1}{2}\dot{J}_\Omega r + \dot{S} + e_2 - proj\left(\Gamma_1 \hat{\sigma}' \hat{U}^T \dot{x}_d e_2^T\right)^T \hat{\sigma} - \hat{W}^T \hat{\sigma}' proj\left(\Gamma_2 \dot{x}_d \left(\hat{\sigma}'^T \hat{W} e_2\right)^T\right)^T x_d \tag{3–65}$$

$$N = N_B + N_d. \tag{3–66}$$

In (3–66), $N_d(q, \dot{q}, x_d, \dot{x}_d, t) \in \mathbb{R}$ is defined as

$$N_d = W^T \sigma' U^T \dot{x}_d + \dot{\epsilon}(x_d) + \dot{\tau}_{d\Omega}, \tag{3–67}$$

while $N_B(\hat{W}, \hat{U}, x_d, \dot{x}_d, t) \in \mathbb{R}$ is defined as

$$N_B = N_{B_1} + N_{B_2}, \tag{3–68}$$

where $N_{B_1}(\hat{W}, \hat{U}, x_d, \dot{x}_d, t)$ and $N_{B_2}(\hat{W}, \hat{U}, x_d, \dot{x}_d, t) \in \mathbb{R}$ are defined as

$$N_{B_1} = -\hat{W}^T \hat{\sigma}' \tilde{U}^T \dot{x}_d - W^T \hat{\sigma}' \hat{U}^T \dot{x}_d, \tag{3–69}$$

and

$$N_{B_2} = \hat{W}^T \hat{\sigma}' \tilde{U}^T \dot{x}_d + \tilde{W}^T \hat{\sigma}' \hat{U}^T \dot{x}_d. \tag{3–70}$$

Motivation for the definitions in (3–65)-(3–67) are based on the need to segregate terms that are bounded by state-dependent bounds and terms that are upper bounded by constants for the development of the NN weight update laws and the subsequent stability analysis. The auxiliary term in (3–68) is further segregated to develop gain conditions in the stability analysis. Based on the segregation of terms in (3–65), the Mean Value Theorem can be applied to upper bound $\tilde{N}(e_1, e_2, r, t)$ as

$$\left\| \tilde{N} \right\| \leq \rho \left(\|z\| \right) \|z\|, \tag{3–71}$$

where $z(t) \in \mathbb{R}^3$ is defined as

$$z(t) \triangleq [e_1^T \ e_2^T \ r^T]^T, \tag{3–72}$$

and the bounding function $\rho \left(\|z\| \right) \in \mathbb{R}$ is a positive globally invertible nondecreasing function. Based on Assumption 3 in Chapter 2, (3–46), (3–47), (3–53), and (3–68)-(3–70), the following inequalities can be developed [27]:

$$\|N_d\| \leq \zeta_1 \qquad \|N_B\| \leq \zeta_2 \qquad \left\| \dot{N}_d \right\| \leq \zeta_3 \tag{3–73}$$

$$\left\| \dot{N}_B \right\| \leq \zeta_4 + \zeta_5 \|e_2\|$$

where $\zeta_i \in \mathbb{R}$,$(i = 1, 2, ...5)$ are known positive constants.

3.4.3 Stability Analysis

Theorem 2. *The composite NN and RISE controller given in (3–54)-(3–58) ensures that all system signals are bounded under closed-loop operation and that the position tracking error is regulated in the sense that*

$$\|e_1(t)\| \to 0 \qquad as \ \ t \to \infty, \tag{3–74}$$

within some set $\mathcal{S}$ containing the initial conditions of the system, provided the control gains in (3–56) and (3–58) are selected sufficiently large.

Proof for Theorem 2: Let $\mathcal{D} \subset \mathbb{R}^5$ be a domain containing $y(t) = 0$, where $y(t) \in \mathbb{R}^5$ is defined as

$$y(t) \triangleq \begin{bmatrix} z^T & \sqrt{P(t)} & \sqrt{Q(t)} \end{bmatrix}^T, \tag{3–75}$$

where the auxiliary function $Q(t) \in \mathbb{R}$ is defined as

$$Q(t) \triangleq \frac{\alpha_2}{2} tr\left(\tilde{W}^T \Gamma_1^{-1} \tilde{W}\right) + \frac{\alpha_2}{2} tr\left(\tilde{U}^T \Gamma_2^{-1} \tilde{U}\right). \tag{3–76}$$

and $P(t) \in \mathbb{R}$ is the generalized solution to the differential equation

$$\dot{P}(t) = -L(t), \quad P(0) = \beta_1 |e_2(0)| - e_2(0) N(0). \tag{3–77}$$

Since Γ_1 and Γ_2 in (3–76) are constant, symmetric, and positive definite matrices, and $\alpha_2 > 0$, it is straightforward that $Q(t) \geq 0$. The auxiliary function $L(t) \in \mathbb{R}$ in (3–77) is defined as

$$L(t) \triangleq r\left(N_{B_1}(t) + N_d(t) - \beta_1 sgn(e_2)\right) + \dot{e}_2 N_{B_2}(t) - \beta_2 e_2(t)^2, \tag{3–78}$$

where β_1, $\beta_2 \in \mathbb{R}$ introduced in (3–58) and (3–78) respectively, are positive constants chosen according to the following sufficient conditions

$$\beta_1 > \zeta_1 + \zeta_2 + \frac{1}{\alpha_2}\zeta_3 + \frac{1}{\alpha_2}\zeta_4, \quad \beta_2 > \zeta_5, \tag{3–79}$$

where $\zeta_i \in R$, $(i = 1, 2, ..., 5)$ are known positive constants introduced in (3–73). Provided the sufficient conditions in (3–79) are satisfied, then $P(t) \geq 0$.

Let $V_L(y, t) : \mathcal{D} \times [0, \infty) \to \mathbb{R}$ denote a Lipschitz continuous regular positive definite functional defined as

$$V_L(y, t) \triangleq e_1^2 + \frac{1}{2}e_2^2 + \frac{1}{2}J_\Omega r^2 + P + Q, \tag{3–80}$$

which satisfies the inequalities

$$U_1(y) \leq V_L(y, t) \leq U_2(y), \tag{3–81}$$

provided the sufficient conditions in (3–79) are satisfied, where $U_1(y), U_2(y) \in \mathbb{R}$ are continuous, positive definite functions defined as

$$U_1(y) = \lambda_1 \|y\|^2, \qquad U_2(y) = \lambda_2 \|y\|^2, \tag{3–82}$$

where λ_1, $\lambda_2 \in \mathbb{R}$ are known positive functions or constants. From (3–2), (3–3), (3–64), (3–77), (3–78), and after taking the time derivative of (3–76), some of the differential equations describing the closed-loop system for which the stability analysis is being performed have discontinuous right-hand sides as

$$\dot{e}_1 = e_2 - \alpha_1 e_1, \tag{3–83a}$$

$$\dot{e}_2 = r - \alpha_2 e_2, \tag{3–83b}$$

$$J_\Omega \dot{r} = -\frac{1}{2}\dot{J}_\Omega r + \tilde{N} + N - e_2 - (k_s + 1)r - \beta sgn(e_2), \tag{3–83c}$$

$$\dot{P}(t) = -r(N_{B_1}(t) + N_d(t) - \beta_1 sgn(e_2)) - \dot{e}_2 N_{B_2}(t) + \beta_2 e_2(t)^2, \tag{3–83d}$$

$$\dot{Q}(t) = tr\left(\alpha_2 \tilde{W}^T \Gamma_1^{-1} \dot{\tilde{W}}\right) + tr\left(\alpha_2 \tilde{U}^T \Gamma_2^{-1} \dot{\tilde{U}}\right). \tag{3–83e}$$

Let $f(y, t) \in \mathbb{R}^5$ denote the right hand side of (3–83). $f(y, t)$ is continuous except in the set $\{(y, t)|e_2 = 0\}$. From [103–106], an absolute continuous Filippov solution $y(t)$ exists almost everywhere (a.e.) so that

$$\dot{y} \in K[f](y, t) \quad a.e.$$

The generalized time derivative of (3–80) exists a.e., and $\dot{V}_L(y,t) \in^{a.e.} \dot{\tilde{V}}_L(y,t)$ where

$$\dot{\tilde{V}}_L(y,t) = \bigcap_{\xi \in \partial V_L(y,t)} \xi^T K \begin{bmatrix} \dot{e}_1 & \dot{e}_2 & \dot{r} & \frac{1}{2}P^{-\frac{1}{2}}\dot{P} & \frac{1}{2}Q^{-\frac{1}{2}}\dot{Q} & 1 \end{bmatrix}^T \tag{3–84}$$

$$= \nabla V_L^T K \begin{bmatrix} \dot{e}_1 & \dot{e}_2 & \dot{r} & \frac{1}{2}P^{-\frac{1}{2}}\dot{P} & \frac{1}{2}Q^{-\frac{1}{2}}\dot{Q} & 1 \end{bmatrix}^T,$$

$$\subset \begin{bmatrix} 2e_1 & e_2 & rJ_\Omega & 2P^{\frac{1}{2}} & 2Q^{\frac{1}{2}} & \frac{1}{2}\dot{J}_\Omega r^2 \end{bmatrix} K \begin{bmatrix} \dot{e}_1 & \dot{e}_2 & \dot{r} & \frac{1}{2}P^{-\frac{1}{2}}\dot{P} & \frac{1}{2}Q^{-\frac{1}{2}}\dot{Q} & 1 \end{bmatrix}^T.$$

For more details of the notations used in 3–83 to 3–84 and discussion, see Section 3.3.1.

After utilizing (3–2), (3–3), (3–64), (3–77), (3–78), the expression in 3–84 can be rewritten as

$$\dot{\tilde{V}}_L(y,t) \subset 2e_1e_2 - 2\alpha_1 e_1^2 + e_2 r - \alpha_2 e_2^2 + \frac{1}{2}\dot{J}_\Omega r^2 + r\tilde{N} + rN - re_2 - (k_s+1)r^2 - \beta r K[sgn(e_2)]$$

$$- \frac{1}{2}\dot{J}_\Omega r^2 - rN_{B_1} - rN_d(t) + \beta r K[sgn(e_2)] - \dot{e}_2 N_{B_2}(t) + \beta_2 e_2^2 + tr\left(\alpha_2 \tilde{W}^T \Gamma_1^{-1} \dot{\tilde{W}}\right)$$

$$+ tr\left(\alpha_2 \tilde{U}^T \Gamma_2^{-1} \dot{\tilde{U}}\right). \tag{3–85}$$

Using (3–57), (3–66), (3–68), (3–70), cancelling common terms, and based on the fact that

$$2e_1e_2 \leq \|e_2\|^2 + \|e_1\|^2,$$

(3–85) can be written as

$$\dot{\tilde{V}}_L(y,t) \subset -(2\alpha_1 - 1)e_1^2 - (\alpha_2 - \beta_2 - 1)e_2^2 - r^2 + r\tilde{N} - k_s r^2. \tag{3–86}$$

As shown in (3–85)-(3–86), the unique integral signum term in the RISE controller is used to compensate for the disturbance terms included in $N_d(q_d, \dot{q}_d, \ddot{q}_d, \dddot{q}_d, t)$ and $N_{B_1}(\hat{W}, \hat{U}, x_d, \dot{x}_d, t)$, provided the control gain β_1 and β_2 are selected according to (3–79). Further the term $N_{B_2}(\hat{W}, \hat{U}, x_d, \dot{x}_d, t)$ is partially rejected by the unique integral signum term and partially cancelled by adaptive update law. Using (3–71), the term

$r^T(t)\tilde{N}(e_1, e_2, r, t)$, can be upper bounded by following inequality:

$$\left| r\tilde{N} \right| \leq \rho\left(\|z\|\right) \|z\| \, |r| \, ,$$

to obtain

$$\dot{\tilde{V}}_L(y, t) \subset -\min\left\{2\alpha_1 - 1, \alpha_2 - \beta_2 - 1, 1\right\} \|z\|^2 + \left[\rho\left(\|z\|\right) \|z\| \, |r| - k_s r^2\right]. \qquad (3\text{--}87)$$

Completing the squares for the bracketed terms in (3–87) yields

$$\dot{\tilde{V}}_L(y, t) \subset -\min\left\{2\alpha_1 - 1, \alpha_2 - \beta_2 - 1, 1\right\} \|z\|^2 + \frac{\rho^2\left(\|z\|\right) \|z\|^2}{4k_s}. \qquad (3\text{--}88)$$

The following expression can be obtained from (3–88):

$$\dot{\tilde{V}}_L(y, t) \subset -U(y), \qquad (3\text{--}89)$$

where $U(y) = c\|z\|^2$, for some positive constant $c \in \mathbb{R}$, is a continuous positive semi-definite function that is defined on the following domain:

$$\mathcal{D} \triangleq \left\{ y \in \mathbb{R}^5 \mid \|y\| \leq \rho^{-1}\left(2\sqrt{\lambda_3 k_s}\right) \right\}$$

where $\lambda_3 \triangleq \min\left\{2\alpha_1 - 1, \alpha_2 - \beta_2 - 1, 1\right\}$. Let $\mathcal{S} \subset \mathcal{D}$ denote a set defined as follows:

$$\mathcal{S} \triangleq \left\{ y(t) \subset \mathcal{D} \mid U_2\left(y(t)\right) \leq \lambda_1 \left(\rho^{-1}\left(2\sqrt{\lambda_3 k_s}\right)\right)^2 \right\}, \qquad (3\text{--}90)$$

where $\mathcal{S} \subset \mathcal{D}$ is introduced in Theorem 2. The region of attraction in (3–90) can be made arbitrarily large to include any initial conditions by increasing the control gain k_s (i.e., a semi-global type of stability result), and hence

$$c\|z(t)\|^2 \to 0 \qquad \text{as } t \to \infty \qquad \forall y(0) \in \mathcal{S}. \qquad (3\text{--}91)$$

Based on the definition of $z(t)$ in (3–72), (3–91) can be used to show that

$$\|e_1(t)\| \to 0 \qquad \text{as } t \to \infty \qquad \forall y(0) \in \mathcal{S}. \qquad (3\text{--}92)$$

3.4.4 Experimental Results

Results are provided in this section that examine the performance of the controller given in (3–54)-(3–58) in experiments with volunteer subjects. These results were compared with the previous results in [116] that used the RISE feedback structure without the NN feedforward term. The NMES controller was implemented as an amplitude modulated voltage composed of a positive rectangular pulse with a fixed width of 400 μ sec and fixed frequency of 30 Hz. The a priori chosen stimulation parameters are within the ranges typically reported during NMES studies [110, 116]. Without loss of generality, the controller is applicable to different stimulation protocols (i.e., voltage, frequency, or pulse width modulation). The following results indicate that the developed controller (henceforth denoted as NN+RISE) was able to minimize the knee angle error while dynamically tracking a desired trajectory.

3.4.4.1 Testbed and protocol

The testbed consists of a custom computer controlled stimulation circuit and a modified leg extension machine (LEM). The LEM was modified to include optical encoders. The LEM allows seating adjustments to ensure the rotation of the knee is about the encoder axis. A 4.5 kg (10 lb.) load was attached to the weight bar of the LEM and a mechanical stop was used to prevent hyperextension.

The objective in one set of experiments was to enable the knee and lower leg to follow an angular trajectory, whereas, the objective of a second set of experiments was to regulate the knee and lower leg to a constant desired setpoint. An additional preliminary test was also performed to test the capability of the controller for a sit-to-stand task. For each set of experiments, bipolar self-adhesive neuromuscular stimulation electrodes were placed over the distal-medial and proximal-lateral portion of the quadriceps femoris muscle group of volunteers and connected to custom stimulation circuitry. The experiments were conducted on non-impaired male and female subjects (as in our previous study in [116]) with age ranges of 20 to 35 years, with written informed consent as approved by

the Institutional Review Board at the University of Florida. The electrical stimulation responses of non-impaired subjects have been reported as similar to paraplegic subjects' responses [16, 22, 39, 111]. The volunteers were instructed to relax as much as possible and to allow the stimulation to control the limb motion (i.e., the subject was not supposed to influence the leg motion voluntarily and was not allowed to see the desired trajectory).

The NN+RISE controller was implemented with a three input layer neurons, twenty-five hidden layer neurons, and one output layer neuron. The neural network weights were estimated on-line according to the adaptive algorithm in (3–57). For each experiment, the computed voltage input was modulated by a fixed pulse width of 400 μ sec and fixed frequency of 30 Hz. The stimulation frequency was selected based on subject comfort and to minimize fatigue. Nine subjects (8 males, 1 female) were included in the study. The study was conducted for different types of desired trajectories including: a 1.5 second periodic trajectory, a dual periodic trajectory (4-6 second), and a step trajectory. For the 1.5 second periodic trajectory, controllers were implemented on both legs of four subjects, while the rest of the tests were performed on only one leg of the other three subjects since they were not available for further testing. Three subjects (1 male, 1 female (both legs); 1 male (one leg)) were asked to volunteer for the dual periodic desired trajectory tests while regulation tests were performed on one of the legs of two subjects. Each subject participated in one trial per criteria (e.g., one result was obtained in a session for a given desired trajectory). For each session, a pre-trial test was performed on each volunteer to find the appropriate initial voltage for the controller to reduce the initial transient error. After the pre-trial test, the RISE controller was implemented on each subject for a thirty second duration and its performance was recorded. A rest period of five minutes was provided before the NN+RISE controller was implemented for an additional thirty second duration.

Figure 3-7. The top plot shows the actual limb trajectory (solid line) obtained from the RISE controller versus the desired 1.5 second period desired trajectory (dashed line). The middle plot shows the tracking error (desired angle minus actual angle). The maximum steady state error obtained is 5.95° (at 20.7 sec.). The bottom plot shows the computed RISE voltage. The maximum steady state voltage obtained is 28.1 V (at 21.47 sec.).

3.4.4.2 Results and discussion

The knee/lower limb tracking results for a representative subject with stimulation from the RISE and the NN+RISE controllers are shown in Figs. 3-7-3-8 and are summarized in Table 3-4. In Table 3-4, the maximum steady state voltage (SSV) and maximum steady state error (SSE) are defined as the computed voltage and absolute value of error respectively, that occur after 1.5 seconds of the trial. Paired one tailed t-tests (across the subject group) were performed with a level of significance set at $\alpha = 0.05$. The results indicate that the developed controller demonstrates the ability of the knee angle to track a desired trajectory with a mean (for eleven tests) RMS error of 2.92 degrees with a mean maximum steady state error of 7.01 degrees. Combining the NN with the RISE feedback structure in [116] yields (statistically significant) reduced mean RMS error

Figure 3-8. The top plot shows the actual limb trajectory (solid line) obtained from the NN+RISE controller versus the desired 1.5 second period desired trajectory (dashed line). The middle plot shows the tracking error (desired angle minus actual angle). The maximum steady state error obtained is 4.24° (at 28.6 sec.). The bottom plot shows the computed NN+RISE voltage. The maximum steady state voltage obtained is 26.95 V (at 29.1 sec.).

for approximately the same input stimulus. The maximum steady state voltages for the RISE and NN+RISE controllers revealed no statistical differences. To illustrate that the performance of NN+RISE controller (in comparison to the RISE controller alone) can be more significant for different desired trajectories, both controllers were implemented on three subjects (2 male, 1 female) with the control objective to track a dual periodic $(4 - 6$ second) desired trajectory with a higher range of motion. The stimulation results from the RISE and the NN+RISE controllers are shown in Figs. 3-9 and 3-10 and are summarized in Table 3-5. In Table 3-5, the maximum SSV and SSE were observed after 4 seconds of the trial. The results illustrate NN+RISE controller yields reduced mean RMS error (across the group) and reduced mean maximum SSE (across the group) for

Subject	Leg	RMS Error		Max SSE		RMS Voltage [V]		Max SSV [V]	
		RISE	**NNR**	**RISE**	**NNR**	**RISE**	**NNR**	**RISE**	**NNR**
A	Left	3.59°	2.92°	12.42°	7.59°	22.91	23.98	29.5	31
A	Right	2.60°	2.63°	5.74°	6.51°	27.70	25.40	32.95	31.5
B	Left	2.47°	2.23°	5.95°	4.24°	22.41	22.81	28.1	26.95
B	Right	2.83°	2.74°	6.28°	6.76°	25.10	23.03	29.8	30.5
C	Left	3.18°	2.46°	8.1	6.17°	41.35	40.14	48.9	44.8
C	Right	2.97°	3.01°	6.9°	9.63°	36.32	35.15	46.4	42.3
D	Left	3.23°	3.71°	6.04°	5.86°	25.25	28.24	30	34.1
D	Right	3.53°	2.96°	8.8°	7.58°	13.62	14.95	24.2	23.4
E	Left	3.92°	3.26°	11.15°	7.92°	30.89	31.46	45	40.5
F	Left	3.38°	2.83°	7.99°	6.41°	26.15	28.13	31.8	34.1
G	Left	3.52°	3.32°	8.2°	8.45°	41.59	43.44	49.8	50
Mean		**3.20°**	***2.92°**	**7.96°**	**7.01°**	**28.48**	**28.79**	**36.04**	**35.38**
Std. Dev.		**0.45°**	**0.41°**	**2.18°**	**1.44°**	**8.49**	**8.29**	**9.44**	**8.08**
p-value		**0.02**		**0.08**		**0.28**		**0.22**	

Table 3-4. Summarized experimental results and P values of one tailed paired T-test for a 1.5 second period desired trajectory. * indicates statistical difference. NNR stands for NN+RISE controller.

approximately the same input stimulus. Paired one tailed t-tests (across the subject group) were performed with a level of significance set at $\alpha = 0.05$. The results show that the difference in mean RMS error and mean maximum SSE were statistically significant. The P value for the mean RMS error (0.00043) and mean maximum SSE (0.0033) t-test obtained in the case of dual periodic trajectory is smaller when compared to the P values (0.02 and 0.08, respectively) obtained for the 1.5 second trajectory. This difference indicates the increased role of the NN for slower trajectories (where the adaptation gains can be increased).

As in [117], additional experiments were also conducted to examine the performance of the NN+RISE controller in response to step changes and changing loads. Specifically, a desired trajectory of a step input was commanded with a 10 pound load attached to the LEM. An additional 10 pound load was added once the limb stabilized at 15 degrees. The limb was again commanded to perform a step response to raise the limb back up an
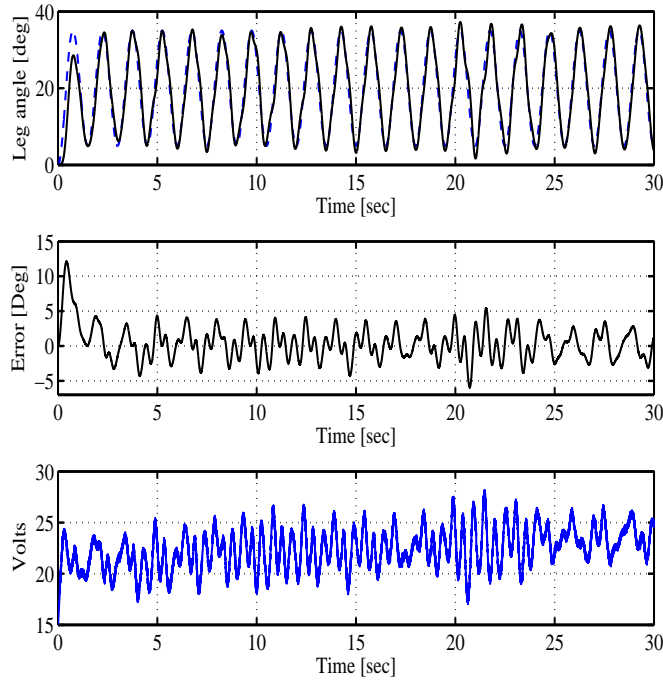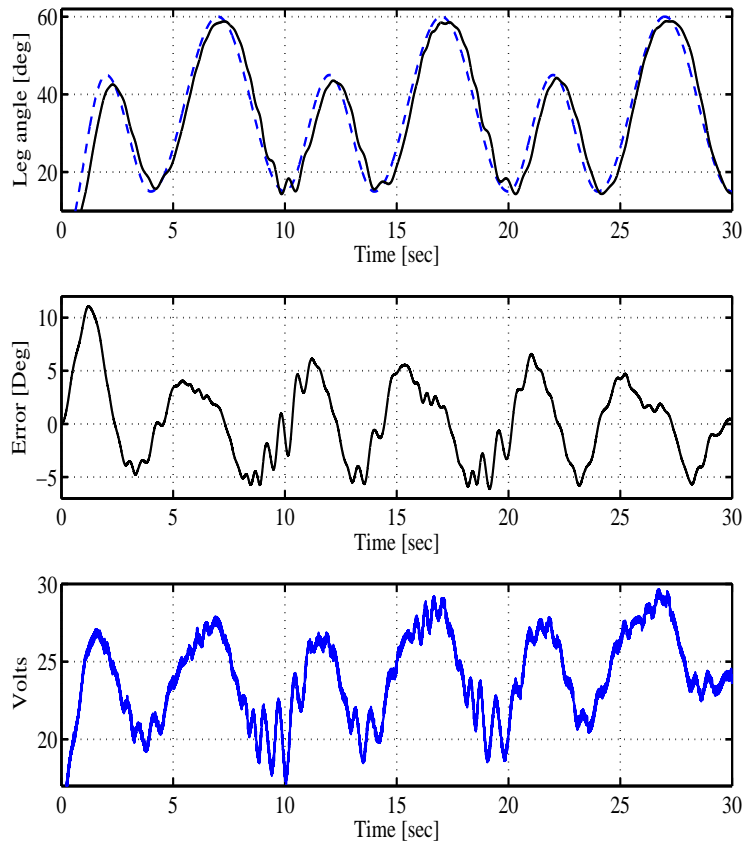
Figure 3-9. The top plot shows the actual limb trajectory (solid line) obtained from the RISE controller versus the dual periodic desired trajectory (dashed line). The middle plot shows the tracking error (desired angle minus actual angle). The maximum steady state error obtained is 6.56° (at 21 sec). The bottom plot shows the computed RISE volatge. The maximum steady state voltage obtained is 29.67 V (at 26.7 sec.).

additional 15 degrees with the total load of 20 pounds. The results from a representative subject using NN+RISE controller are shown in Fig. 3-11. The experimental results for the step response and load addition are given in Table 3-6. The results give some indication of the controller's ability to adapt to changes in load and step inputs and motivate possible future case studies.

Experiments were also performed to test the NN+RISE controller for a sit-to-stand task. These tests were conducted on a healthy individual initially seated on a chair (see Fig. 3-12). The knee angle was measured using a goniometer (manufactured by Biometrics
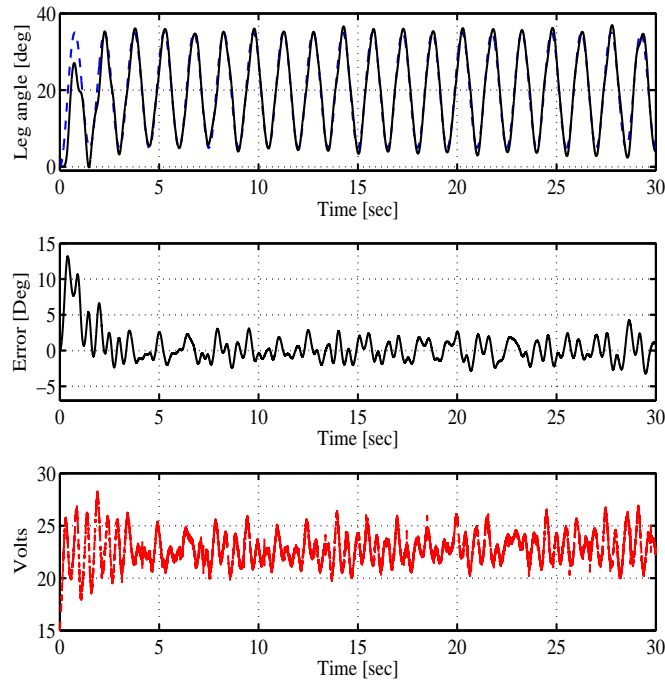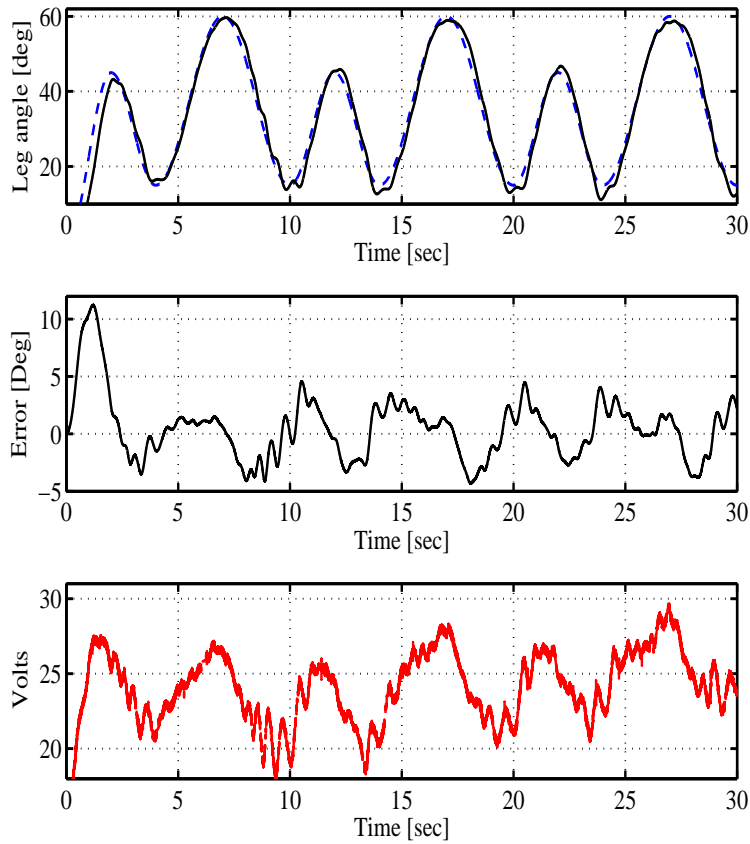
Figure 3-10. The top plot shows the actual limb trajectory (solid line) obtained from the NN+RISE controller versus the dual periodic desired trajectory (dashed line). The middle plot shows the tracking error (desired angle minus actual angle). The maximum steady state error obtained is 4.57° (at 10.5 sec.). The bottom plot shows the computed NN+RISE volatge. The maximum steady state voltage obtained is 29.68 V (at 26.9 sec.

Ltd.) attached to both sides of the subject's knee, where the initial knee angle is set to zero (sitting position). The goniometer was interfaced with the custom computer controlled stimulation circuit via an angle display unit (ADU301). The objective was to control the angular knee trajectory that resulted in the volunteer rising from a seated position, with a final desired angle of 90° (standing position). The error, voltage, and desired versus actual knee angle plots are shown in Fig. 3-13. The RMS error and voltage during this experiment were obtained as 2.92° and 26.88 *V*, respectively. The final steady state error reached within −0.5°, the maximum transient error was observed as 8.23°,

Subject	Leg	RMS Error		Max SSE		RMS Voltage [V]		Max SSV [V]	
		RISE	NNR	RISE	NNR	RISE	NNR	RISE	NNR
A	Left	2.35°	1.85°	6.12°	4.30°	29.08	29.19	34.10	34.09
A	Right	1.73°	1.26°	4.49°	3.9°	30.00	29.67	35.75	34.62
B	Left	3.52°	2.62°	6.45°	5.64°	37.09	36.34	44.04	43.47
B	Right	3.39°	2.89°	6.53°	6.00°	37.88	38.57	45.30	46.19
C	Right	3.84°	2.82°	6.56°	4.57°	23.99	24.09	29.67	29.68
Mean		2.97°	*2.29°	6.03°	*4.88°	31.61	31.57	37.77	37.61
Std. Dev.		0.89°	0.71°	0.88°	0.90°	5.84	5.85	6.69	6.93
p-value		0.00043		0.0033		0.43		0.29	

Table 3-5. Summarized experimental results and P values of one tailed paired T-test for dual periodic (4-6 second) desired trajectory. * indicates statistical difference. NNR stands for NN+RISE controller.

Subject	Leg	Max. SSE (after step input)	Max. Transient Error	Max. Error (during disturbance)	Max. SSV (after step input) [Volts]
A	Left	0.7°	9.5°	2.8°	42.2
B	Right	0.6°	9.52°	2.0°	19.2

Table 3-6. Experimental results for step response and changing loads

and the maximum voltage was obtained as 35.1 V. The significance of these tests is to depict the applicability of the controller on clinical tasks such as sit to stand maneuvers. Although the experiments were conducted on a healthy individual, these preliminary results show that the controller holds promise to provide satisfactory performance on patients in a clinical-type scenario.

The NN+RISE structure is motivated by the desire to blend a NN-based feedforward method with a continuous feedback RISE structure to obtain asymptotic limb tracking despite an uncertain nonlinear muscle response. The ability of the neural networks to learn uncertain and unknown muscle dynamics is complemented by the ability of RISE to compensate for additive system disturbances (hyperactive somatosensory reflexes that may be present in impaired individuals) and NN approximation error. Although the NN+RISE controller was successfully implemented and compared to RISE controller in the present work, the performance of the controller may be further improved in efforts to reduce the
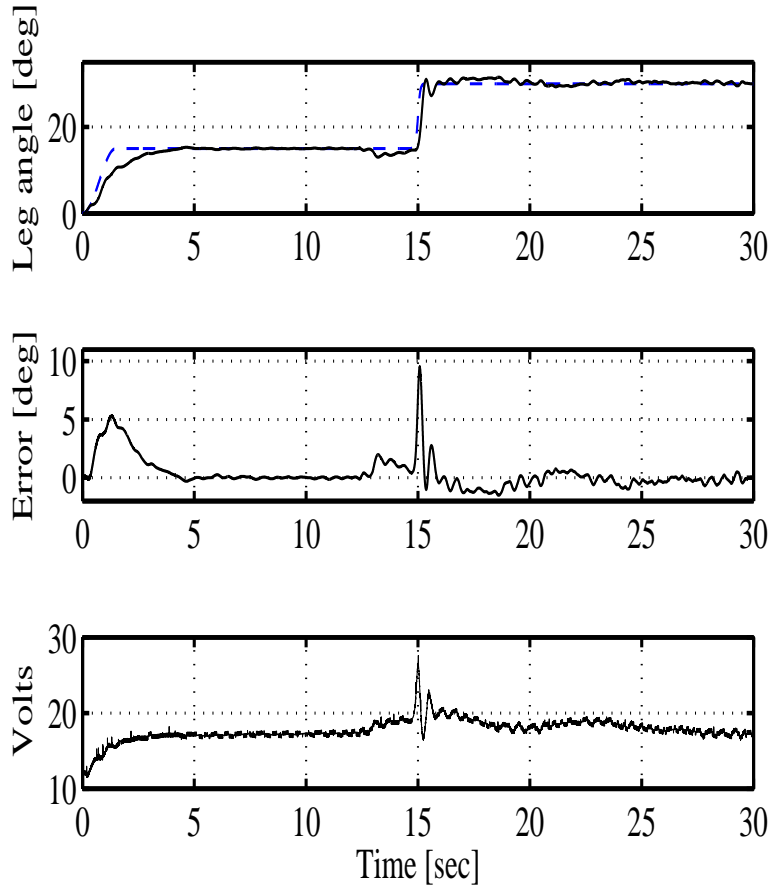
Figure 3-11. Experimental plots for step change and load addition obtained from NN+RISE controller. Top plot shows actual limb trajectory (solid line) versus desired step trajectory (dashed line). The load is added once the limb stabilizes (between 13-15 second interval). After load addition the limb is tested for the step input. Middle plot shows the limb tracking error obtained during the experiment. Bottom plot shows computed voltage for the experiment.

effects of muscle fatigue in future studies. Fatigue can be reduced for short durations by selecting optimal stimulation parameters, but functional electrical stimulation (FES) may require a controller that adapts with fatigue to yield performance gains for longer time durations. Therefore our future goal will be to include a fatigue model and incorporating calcium dynamics in the muscle dynamics to enhance the controller performance.

67
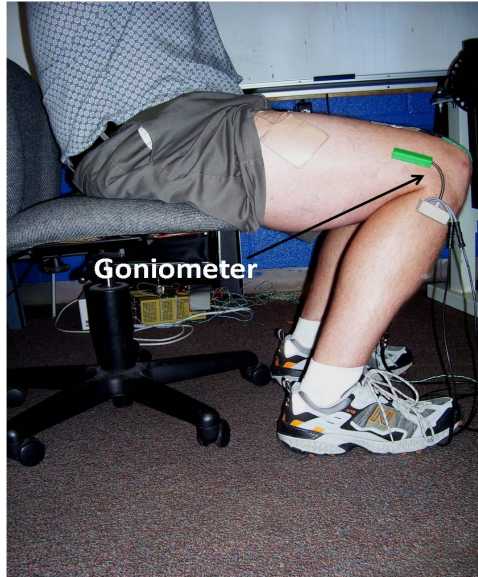
Figure 3-12. Initial sitting position during sit-to-stand experiments. The knee-angle was measured using a goniometer attached around the knee-axis of the subject's leg.

3.4.5 Limitations

The results illustrate the added value of including a NN feedforward component in comparison to only using the RISE feedback structure in [116]. However, several limitations exist in the experimental study. The contribution from the NN component was observed to increase but the RISE contribution did not decline proportionally. A possible reason for this observation is that the 1.5 second period desired trajectory has a large desired acceleration $\ddot{q}_d(t)$, which is an input to the NN that can lead to large voltage swings during the transient stage. To reduce large voltage variants during the transient due to $\ddot{q}_d(t)$, the update law gains are reduced in comparison to gains that could be employed during less aggressive trajectories. The experimental results with slower trajectories (dual periodic - 4-6 second period) illustrate that the NN component can play a larger role depending on the trajectory. Specifically, the dual periodic trajectory results indicate that the RMS error obtained with the NN+RISE controller is lower than the RMS error obtained with the RISE controller with a lower P value (0.00043) compared to the P value (0.02) obtained with the 1.5 second period trajectory.
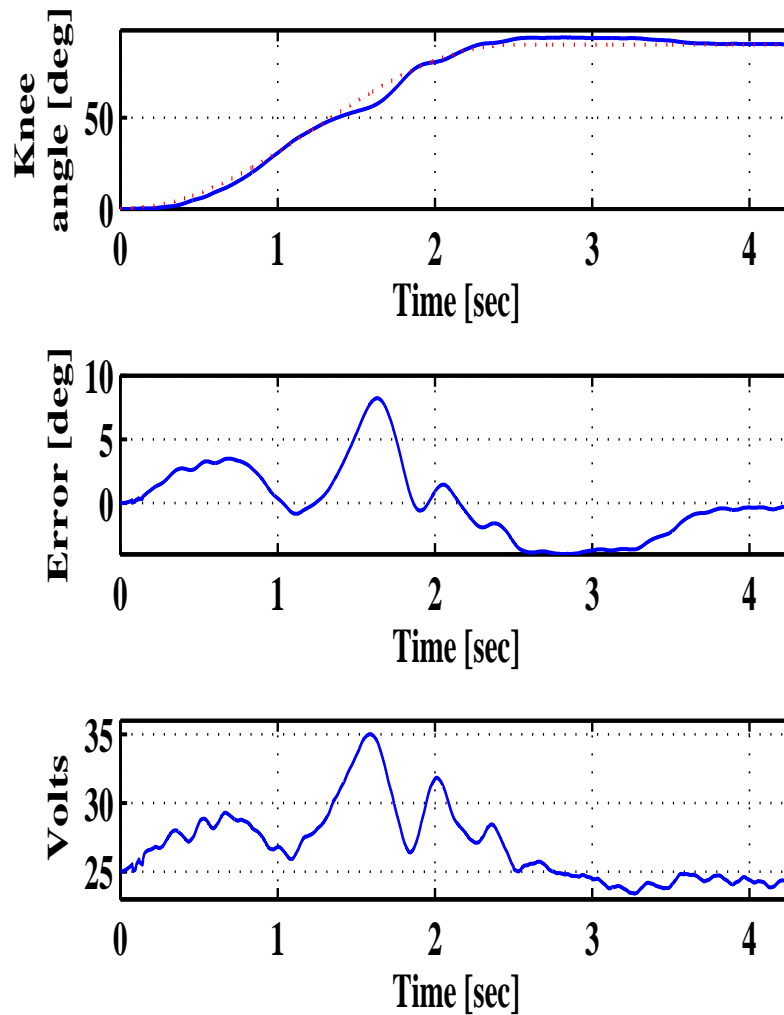
Figure 3-13. The top plot shows the actual leg angle trajectory (solid line) versus desired trajectory (dotted line) obtained during the standing experiment. The middle plot shows the error obtained during the experiment. The bottom plot shows the voltage produced during the experiment.

Since a trajectory for a specific functional task was not provided, the desired trajectory used in the first set of experiments was simply selected as a continuous sinusoid with a constant 1.5 second period. The desired trajectory was arbitrarily selected, but the period of the sinusoid is inspired by a typical walking gait trajectory. As the work transitions to applications where a specific functional trajectory is generated, the control

results should directly translate. Furthermore, some clinical goals may be better expressed as a desired force profile rather than a desired limb trajectory. The results from this work could be directly applied to these cases by altering the control objective and open-loop error system, but the form of the control method (i.e., NN+RISE) would remain intact.

An analysis of RMS errors during extension and flexion phase of the leg movements across different subjects, trajectories (1.5 second and dual periodic), and both controllers showed that the mean RMS error is more when leg is moving upwards (extension phase) compared to periods when leg is moving downwards (flexion phase). A t-test analysis showed that the results are statistically significant with p values of 0.00013 and 0.0014 obtained from RISE and NN+RISE controllers, respectively. The mean RMS errors during extension phase for RISE and NN+RISE controllers were 3.49° and 2.68°, respectively while mean RMS errors during flexion phase for RISE and NN+RISE controllers were 2.96° and 2.42°, respectively. Summarized RMS errors for both phases are shown in Table 3-7. An increased error during extension phase can be attributed to higher control effort required during extension. The performance during the extension phase can also be aggravated by increased time delay and muscle fatigue due to the requirement for higher muscle force compared to the flexion phase. This analysis indicates a possible need for separate control strategies during extension and flexion phase of the leg movement. Particularly, future efforts will investigate a hybrid control approach for each phase of motion.

Currently the experiments were performed on non-impaired persons. In future studies with impaired individuals, our untested hypothesis is that the added value of the NN feedforward component will be even more pronounced (and that the controller will remain stable) as disturbances due to more rapid fatigue and more sensitive somatosensory reflexes may be present in impaired individuals. To delay the onset of fatigue, different researchers have proposed different stimulation strategies [32, 33, 118] such as choosing different stimulation patterns and parameters. The NMES controller in this study was

Subject	Leg	Trajectory	RMS Error (RISE)		RMS Error (NN+RISE)	
			Extension	Flexion	Extension	Flexion
A	Left	Dual period	4.35°	2.41°	3.30°	1.68°
A	Right	Dual period	3.98°	2.68°	3.39°	2.28°
B	Left	Dual period	2.74°	1.86°	1.77°	1.92°
B	Right	Dual period	1.78°	1.69°	1.35°	1.17°
C	Right	Dual period	4.22°	3.43°	3.27°	2.28°
D	Left	1.5 second	2.87°	2.00°	2.54°	1.88°
D	Right	1.5 second	3.21°	2.38°	3.07°	2.38°
E	Left	1.5 second	3.87°	3.30°	3.30°	2.49°
E	Right	1.5 second	2.56°	2.65°	2.34°	2.88°
F	Left	1.5 second	3.81°	2.51°	4.00°	3.40°
F	Right	1.5 second	3.59°	3.47	2.96°	2.96°
G	Left	1.5 second	3.93°	2.18°	2.86°	1.97°
G	Right	1.5 second	2.98°	2.95°	2.82°	3.19°
H	Left	1.5 second	4.18°	2.70°	3.92°	2.58°
I	Left	1.5 second	3.97°	2.66°	3.11°	2.51°
J	Right	1.5 second	3.79°	4.05°	3.38°	3.13°
Mean			**3.49°**	**2.68°**	**2.96°**	**2.42°**
p-value			0.00013		0.0014	

Table 3-7. The table shows the RMS errors during extension and flexion phase of the leg movement across different subjects, trajectories (1.5 second and dual periodic), and controllers (RISE/NN+RISE). The results show that the mean RMS error is more during the extension phase than during the flexion phase.

implemented using constant pulse width amplitude modulation of the voltage. However, the controller can be implemented using other modulation schemes such as pulse width and frequency modulation without any implications on the stability analysis, but the effects of using frequency modulation or varying pulse trains (e.g. a pulse train containing doublets) remain to be investigated clinically.

3.4.6 Conclusion

A Lyapunov-based stability analysis indicates that the developed closed-loop nonlinear NMES control method yields asymptotic tracking for a unknown nonlinear muscle activation and limb dynamics, even in the presence of uncertain additive disturbances. Experiments using external electrodes on non-impaired volunteers

demonstrated the ability of the NN+RISE controller to enable the knee and lower leg to track a desired trajectory composed of sinusoids, step changes, and changes in the load. Statistical analysis of the experimental results indicates that the NN+RISE algorithm yields reduced RMS tracking error when compared to the RISE controller for statistically insignificant differences in voltage input. A preliminary experiment (a sit-to-stand task) to test the controller for a clinical-type functional task showed a promising control performance. These experiments suggest that future efforts can be made to test the performance on patients with movement disorders. Specifically, experiments should be conducted for functional tasks such as walking and sit-to-stand maneuvers.

CHAPTER 4
NONLINEAR CONTROL OF NMES: INCORPORATING FATIGUE AND CALCIUM DYNAMICS

4.1   Introduction

The focus of this chapter is to address muscle fatigue by incorporating an uncertain fatigue model (i.e., the model developed in [35]) in the NMES controller. The contribution of the method is that only best guess estimates of patient specific fatigue time constants and natural frequency of calcium dynamics are required and the mismatch between the estimated parameters and actual parameters is included in a stability analysis. The fatigue model is defined as a function of a normalized muscle activation variable. The normalized muscle activation variable denotes the calcium (Ca^{2+} ion) dynamics which act as an intermediate variable between contractile machinery and external stimulus. The calcium dynamics are modeled as a first order differential equation based on [6] and [39]. An open-loop error system for an uncertain nonlinear muscle model is developed that includes the fatigue and calcium dynamics. A virtual control input is designed using nonlinear backstepping technique which is composed of a NN based feedforward signal and an error based feedback signal. The NN based control structure is exploited not only to feedforward muscle dynamics but also to approximate the error generated due to parametric uncertainties in the assumed fatigue model. The actual external control input (applied voltage) is designed based on the backstepping error. Through this error-system development, the continuous NN based controller is proven (through a Lyapunov-based stability analysis) to yield an uniformly ultimately bounded stability result despite the uncertain nonlinear muscle model and the presence of additive bounded disturbances (e.g., muscle spasticity, changing loads in functional tasks, and delays).

4.2   Muscle Activation and Limb Model

The musculoskeletal model given in Chapter 2 is modified to consider calcium and fatigue dynamics during neuromuscular electrical stimulation. The additional dynamics

of calcium ions and muscle fatigue are incorporated in the contraction and activation dynamics while the body segmental dynamics remains the same as provided in Chapter 2.

The torque produced about the knee is generated through muscle forces that are elicited by NMES. The active moment generating force at the knee joint is the tendon force $F_T(t) \in \mathbb{R}$ defined as [119]

$$F_T = F \cos a, \tag{4–1}$$

where $a(q(t)) \in \mathbb{R}$ is defined as the pennation angle between the tendon and the muscle, where $q(t)$, $\dot{q}(t) \in \mathbb{R}$ denote the angular position and velocity of the lower shank about the knee-joint, respectively (see Fig. 2-2). The pennation angle of the human quadriceps muscle changes monotonically during quadriceps contraction and is a continuously differentiable, positive, monotonic, and bounded function with a bounded first time derivative [100]. The muscle force $F(t) \in \mathbb{R}$ in (4–1) is defined as [36]

$$F = F_m \eta_1 \eta_2 \varphi(x) x, \tag{4–2}$$

where $F_m \in \mathbb{R}$ is the maximum isometric force generated by the muscle. The uncertain nonlinear functions $\eta_1(q)$, $\eta_2(q, \dot{q}) \in \mathbb{R}$ in (4–2) are force-length and force-velocity relationships, respectively, defined as [36, 120, 121]

$$\eta_1(q) = \exp\left(-\left(\frac{\bar{l}(q) - 1}{b}\right)^2\right), \tag{4–3}$$

$$\eta_2(q, \dot{q}) = c_1 \arctan(c_2 \bar{v}(q, \dot{q}) + c_3) + c_4, \tag{4–4}$$

where $b, \bar{l}(q) \in \mathbb{R}$ in (4–3) denote the unknown shape factor and the normalized length with respect to the optimal muscle length, respectively, and $\bar{v}(q, \dot{q}) \in \mathbb{R}$ is an unknown non-negative normalized velocity with respect to the maximal contraction velocity of the muscle, and c_1, c_2, c_3, c_4 are unknown, bounded, positive constants.

Assumption: The force-velocity relationship η_2 is lower bounded by a known constant ε_η. The lower bound on the force-velocity relationship is practical in the sense

that $\eta_2(q, \dot{q}) = 0$ (i.e., no force output) only occurs when the muscle shortening velocity (a concentric contraction) is at the maximum rate.

The definitions in (4–3) and (4–4) are not directly used in the control development. Instead, the structure of the relationships in (4–3) and (4–4) is used to conclude that $\eta_1(q)$ and $\eta_2(q, \dot{q})$ are continuously differentiable, non-zero, positive, monotonic, and bounded functions, with bounded first time derivatives. The muscle force in (4–2) is coupled to the actual external voltage control input $V(t) \in \mathbb{R}$ through an intermediate normalized muscle activation variable $x(t) \in \mathbb{R}$. The muscle activation variable is governed by following differential equation [34, 119]

$$2\dot{x} = -wx + wsat[V(t)], \tag{4–5}$$

where $w \in \mathbb{R}$ is the constant natural frequency of the calcium dynamics. The function $sat[V(t)] \in \mathbb{R}$ (i.e., recruitment curve) is denoted by a piecewise linear function as

$$sat[V(t)] = \begin{cases} 0 & V < V_{\min} \\ \frac{V - V_{\min}}{V_{\max} - V_{\min}} & V_{\min} \leq V \leq V_{\max} \\ 1 & V > V_{\max}, \end{cases} \tag{4–6}$$

where $V_{\min} \in \mathbb{R}$ is the minimum voltage required to generate noticeable movement or force production in a muscle, and $V_{\max} \in \mathbb{R}$ is the voltage of the muscle at which no considerable increase in force or movement is observed. Based on (4–5) and (4–6), a linear differential inequality can be developed to show that $x(t) \in [0, 1]$. Muscle fatigue is included in (4–2) through the invertible, positive, bounded fatigue function $\varphi(x) \in \mathbb{R}$ that is generated from the first order differential equation [35, 36]

$$\dot{\varphi} = \frac{1}{T_f}(\varphi_{\min} - \varphi)x + \frac{1}{T_r}(1 - \varphi)(1 - x), \tag{4–7}$$

where $\varphi_{\min}$ is the unknown minimum fatigue constant of the muscle, and T_f, T_r are unknown time constants for fatigue and recovery in the muscle, respectively.
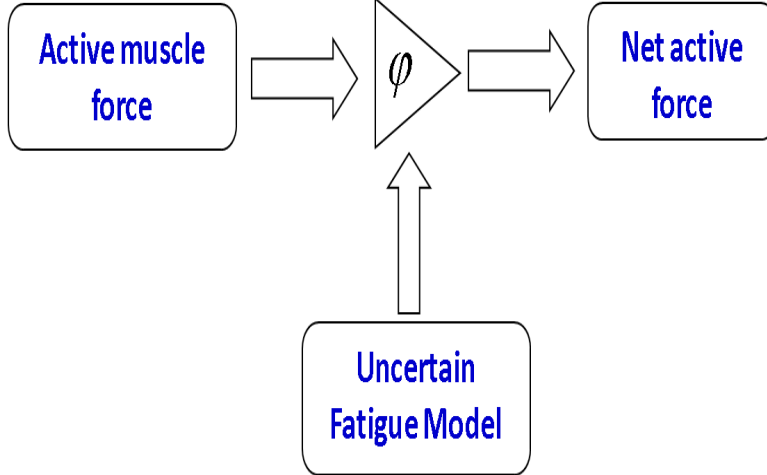
Figure 4-1. An uncertain fatigue model is incorporated in the control design to address muscle fatigue. Best guess estimates are used for unknown model parameters.

4.3 Control Development

The objective is to develop a NMES controller to produce a knee torque trajectory that will enable a human shank to track a desired trajectory, denoted by $q_d(t) \in \mathbb{R}$, despite the uncertain fatigue effects and coupled muscle force and calcium dynamics. Without loss of generality, the developed controller is applicable to different stimulation protocols (i.e., voltage, frequency, or pulse width modulation). To quantify the objective, a position tracking error, denoted by $e(t) \in \mathbb{R}$, is defined as

$$e(t) = q_d(t) - q(t), \tag{4--8}$$

where $q_d(t)$ is an a priori trajectory which is designed such that $q_d(t), q_d^i(t) \in \mathcal{L}_\infty$, where $q_d^{(i)}(t)$ denotes the ith derivative for $i = 1, 2, 3, 4$. To facilitate the subsequent analysis, a filtered tracking error, denoted by $r(t)$, is defined as

$$r(t) = \dot{e}(t) + \alpha e(t), \tag{4--9}$$

where $\alpha \in \mathbb{R}$ denotes a positive constant.

4.3.1   Open-Loop Error System

The open-loop tracking error system can be developed by taking the time derivative of (4–9), multiplying the resulting expression by J, and then utilizing the expressions in (4–1), (4–2), (2–1), (2–5) and (4–8) as

$$J\dot{r} = J(\alpha\dot{e} + \ddot{q}_d) + M_e + M_g + M_v + \tau_d - \rho\varphi x, \qquad (4\text{–}10)$$

where the auxiliary function $\rho(q, \dot{q}) \in \mathbb{R}$ is defined as

$$\rho = \varsigma \cos(a) F_m \eta_1 \eta_2. \qquad (4\text{–}11)$$

After multiplying (4–10) by $\rho^{-1}(q, \dot{q}) \in \mathbb{R}$, the following expression is obtained:

$$J_\rho \dot{r} = J_\rho(\alpha\dot{e} + \ddot{q}_d) + L_\rho + \tau_{d\rho} - \varphi x, \qquad (4\text{–}12)$$

where $J_\rho(q, t)$, $\tau_{d\rho}(q, t)$, $L_\rho(q, \dot{q}) \in \mathbb{R}$ are defined as

$$J_\rho = \rho^{-1} J, \qquad \tau_{d\rho} = \rho^{-1} \tau_d,$$
$$L_\rho = \rho^{-1}(M_e + M_g + M_v).$$

Property 3: Based on the assumptions and properties (in Section 4.2), $\rho(q, \dot{q})$ is continuously differentiable, positive, monotonic, and bounded. Also the function $\rho^{-1}(q, \dot{q})$ is bounded. The first time derivatives of $\rho(q, \dot{q})$ and $\rho^{-1}(q, \dot{q})$ exist and are bounded. The inertia function J_ρ is positive definite and can be upper and lower bounded as

$$a_1 \|\gamma\|^2 \leq \gamma^T J_\rho \gamma \leq a_2 \|\gamma\|^2 \quad \forall \gamma \in \mathbb{R}^n, \qquad (4\text{–}13)$$

where $a_1, a_2 \in \mathbb{R}$ are some known positive constants. Also using the boundedness of $\rho(q, \dot{q})$, $\dot{\rho}(q, \dot{q})$, $\rho^{-1}(q, \dot{q})$

$$\left|\dot{J}_\rho\right| \leq \xi_j, \quad |\tau_{d\rho}| \leq \xi_\tau, \qquad (4\text{–}14)$$

where ξ_j, $\xi_\tau \in \mathbb{R}$ are some known positive constants.

77

Based on (4–7) a positive estimate $\hat{\varphi}(\hat{x})$ is generated as

$$\dot{\hat{\varphi}} = \frac{1}{\hat{T}_f}(\varphi_{\min} - \hat{\varphi})\hat{x} + \frac{1}{\hat{T}_r}(1 - \hat{\varphi})(1 - \hat{x}),$$

(4–15)

$$1 \geq \hat{\varphi}(0) > 0,$$

where $\hat{T}_f$, $\hat{T}_r \in \mathbb{R}$ denote constant best guess estimates of the time constants T_f and T_r, respectively, $\varphi_{\min} \in \mathbb{R}$ is a non zero positive constant, and $\hat{x}(t) \in \mathbb{R}$ is the estimated normalized muscle activation variable which is generated based on (4–5) as

$$2\dot{\hat{x}} = -\hat{w}\hat{x} + \hat{w}sat[V(t)],$$

(4–16)

where $\hat{w} \in \mathbb{R}$ denotes the constant best guess estimate of natural frequency of calcium dynamics w. The estimated function $\hat{\varphi}(\hat{x})$ is upper bounded by a positive constant $\bar{\varphi} \in \mathbb{R}$. Specifically, $\bar{\varphi}$ can be determined as

$$\bar{\varphi} = \hat{\varphi}(0) + 1 + \frac{\hat{T}_r}{\hat{T}_f}\hat{\varphi}_{\min}.$$

(4–17)

The algorithm used in (4–15) ensures that $\hat{\varphi}(\hat{x})$ remains strictly positive. Based on (4–6) and (4–16), a linear differential inequality can be developed to show that $\hat{x}(t) \in [0, 1]$.

To facilitate the control development, the terms $\varphi(x)\hat{x} + \varphi(\hat{x})\hat{x} + \hat{\varphi}(\hat{x})\hat{x}$ are added and subtracted to (4–12) to yield

$$J_\rho \dot{r} = S + \tau_{d\rho} - \frac{1}{2}\xi_j r - e - \varphi\tilde{x} - \varphi_e\hat{x} - \hat{\varphi}\hat{x},$$

(4–18)

where the auxiliary function $S(q, \dot{q}, \ddot{q}_d, e, r, \hat{x}) \in \mathbb{R}$ is defined as

$$S = J_\rho(\ddot{q}_d + \alpha\dot{e}) + L_\rho(q, \dot{q}) + \frac{1}{2}\xi_j r + e - \tilde{\varphi}\hat{x}$$

(4–19)

and the error functions $\varphi_e(x, \hat{x})$, $\tilde{\varphi}(\hat{x})$, $\tilde{x}(t) \in \mathbb{R}$ are denoted as

$$\tilde{\varphi}(\hat{x}) = \varphi(\hat{x}) - \hat{\varphi}(\hat{x}),$$

(4–20)

$$\varphi_e(x, \hat{x}) = \varphi(x) - \varphi(\hat{x}),$$

(4–21)

$$\tilde{x} = x - \hat{x}. \tag{4-22}$$

Since $\varphi(\hat{x})$ and $\varphi(x)$ are bounded functions, the error function $\varphi_e(t)$ can be upper bounded as

$$|\varphi_e| \leq \xi_\varphi, \tag{4-23}$$

where $\xi_\varphi \in \mathbb{R}$ is some known positive constant. The auxiliary function $S(q, \dot{q}, \ddot{q}_d, e, r, \hat{x})$ can be represented by a three-layer NN as

$$S = W^T \sigma(U^T y) + \epsilon(y), \tag{4-24}$$

where $y(t) \in \mathbb{R}^7$ is defined as

$$y(t) = \begin{bmatrix} 1 & q(t) & \dot{q}(t) & \ddot{q}_d(t) & e(t) & r(t) & \hat{x}(t) \end{bmatrix}, \tag{4-25}$$

and $\epsilon(y)$ is a functional reconstruction error that is bounded by a constant as

$$|\epsilon(y)| \leq \delta. \tag{4-26}$$

4.3.2 Closed-Loop Error System

Since a direct control input does not appear in the open-loop system in (4–18), a backstepping-based approach is used to inject a virtual control input $x_d(t) \in \mathbb{R}$ (i.e., desired calcium dynamics) as

$$J_\rho \dot{r} = S + \tau_{d\rho} - \varphi\tilde{x} - \varphi_e\hat{x} - \frac{1}{2}\xi_j r - e - \hat{\varphi}\hat{x} + \hat{\varphi}x_d - \hat{\varphi}x_d. \tag{4-27}$$

Based on (4–27), the virtual control input is designed as a three layer NN feedforward term plus a feedback term as

$$x_d = \hat{\varphi}^{-1}(\hat{S} + k_s r), \tag{4-28}$$

where $k_s \in \mathbb{R}$ denotes a positive constant adjustable control gain. The feedforward NN component in (4–28), denoted by $\hat{S}(t) \in \mathbb{R}$ is generated as

$$\hat{S} = \hat{W}^T \sigma(\hat{U}^T y). \tag{4-29}$$

The estimates for the NN weights in (4–29) are generated on-line using projection algorithm as [27]

$$\dot{\hat{W}} = proj(\Gamma_1 \hat{\sigma} r^T), \qquad \dot{\hat{U}} = proj(\Gamma_2 y(\hat{\sigma}'^T \hat{W} r)^T), \tag{4–30}$$

where $\Gamma_1 \in \mathbb{R}^{(N_2+1)\times(N_2+1)}$ and $\Gamma_2 \in \mathbb{R}^{(N_1+1)\times(N_1+1)}$ are constant, positive definite, symmetric gain matrices. The closed-loop tracking error system can be developed by substituting (4–28) into (4–27) as

$$J_\rho \dot{r} = -\frac{1}{2}\xi_j r - e + \tilde{S} + \tau_{d\rho} - \varphi\tilde{x} - \varphi_e\hat{x} - k_s r - \hat{\varphi}e_x, \tag{4–31}$$

where $\tilde{S}(y) \in \mathbb{R}$ is defined as

$$\tilde{S}(y) = S - \hat{S}, \tag{4–32}$$

and $e_x(t) \in \mathbb{R}$ is the backstepping error defined as

$$e_x = \hat{x} - x_d. \tag{4–33}$$

The closed loop system can be expressed as

$$J_\rho \dot{r} = -\frac{1}{2}\xi_j r - e + W^T\sigma(U^T y) - \hat{W}^T\sigma(\hat{U}^T y) + \epsilon(y) + \tau_{d\rho} - \varphi\tilde{x} - \varphi_e\hat{x} - k_s r - \hat{\varphi}e_x. \tag{4–34}$$

After adding and subtracting the terms $W^T\hat{\sigma} + \hat{W}^T\tilde{\sigma}$ to (4–34), the following expression can be obtained:

$$J_\rho \dot{r} = -\frac{1}{2}\xi_j r - e + \tilde{W}^T\hat{\sigma} + \hat{W}^T\tilde{\sigma} + \tilde{W}^T\tilde{\sigma} + \epsilon(y) + \tau_{d\rho} - \varphi\tilde{x} - \varphi_e\hat{x} - k_s r - \hat{\varphi}e_x, \tag{4–35}$$

where the notations $\hat{\sigma}\,(\cdot)$ and $\tilde{\sigma}\,(\cdot)$ are introduced in (3–43). The Taylor series approximation described in (3–44) and (3–45) can now be used to rewrite (4–35) as

$$J_\rho \dot{r} = -\frac{1}{2}\xi_j r - e + N + \tilde{W}^T\hat{\sigma} + \hat{W}^T\hat{\sigma}'\tilde{U}^T y - k_s r - \hat{\varphi}e_x, \tag{4–36}$$

where $\sigma'(\hat{U}^T y) = d\sigma(U^T y)/d(U^T y)_{|U^T y = \hat{U}^T y}$. The unmeasurable auxiliary term $N(\tilde{W}, \tilde{U}, y, \rho^{-1}, t)$ $\in \mathbb{R}$ is defined as

$$N = \tilde{W}^T \hat{\sigma}' \tilde{U}^T y + W^T O(\tilde{U}^T y)^2 + \epsilon(y) + \tau_{d\rho} - \varphi\tilde{x} - \varphi_e \hat{x}. \qquad (4\text{--}37)$$

Based on (4–14), (4–23), (4–26), (4–30), the fact that $x(t)$, $\hat{x}(t) \in [0, 1]$, and the assumption that desired trajectories are bounded, the following inequality can be developed [122]:

$$|N| \leq \zeta_1 + \zeta_2 \|z\|, \qquad (4\text{--}38)$$

where $\zeta_i \in \mathbb{R}$, $(i = 1, 2)$ are known positive constants and $z \in \mathbb{R}^2$ is defined as

$$z \triangleq \begin{bmatrix} e^T & r^T \end{bmatrix}^T. \qquad (4\text{--}39)$$

4.3.3 Backstepping Error System

To facilitate the subsequent stability analysis, the time derivative of the backstepping error (4–33) can be determined by using (4–16) as

$$\dot{e}_x = -\frac{\hat{w}}{2}\hat{x} + \frac{\hat{w}}{2}sat[V(t)] - \dot{x}_d. \qquad (4\text{--}40)$$

Based on (4–6) and (4–40), and assumption that control input remains below the saturation voltage $V_{\max}$, the control input (Voltage input) $V(t) \in \mathbb{R}$ is designed as

$$V(t) = (V_{\max} - V_{\min}) \left\{ \left(\frac{\hat{w}}{2}\right)^{-1} (\dot{x}_d + \frac{\hat{w}}{2}\hat{x} + \hat{\varphi}r - ke_x) \right\} + V_{\min}, \qquad (4\text{--}41)$$

where $k \in \mathbb{R}$ denotes a positive constant adjustable control gain. Substituting (4–41) into (4–40), yields

$$\dot{e}_x = \hat{\varphi}r - ke_x. \qquad (4\text{--}42)$$

4.4 Stability Analysis

Theorem 3. *The controller given in (4–28) and (4–41) ensures that all system signals are bounded under closed-loop operation and that the position tracking error is regulated in the*

sense that

$$|e(t)| \leq \epsilon_0 \exp(-\epsilon_1 t) + \epsilon_2, \tag{4–43}$$

provided the control gains α, k_{s_1} introduced in (4–9), (4–49), (4–50) are selected according to the following sufficient condition:

$$\min(\alpha_1, k_{s_1}) > \zeta_2, \tag{4–44}$$

where ϵ_0, ϵ_1, $\epsilon_2 \in \mathbb{R}$ denote positive constants, and ζ_2 is a known positive constant introduced in (4–38).

Proof: Let $V_L(t) \in \mathbb{R}$ denote a continuously differentiable, non negative, radially unbounded function defined as

$$V_L(t) \triangleq \frac{1}{2}e^T e + \frac{1}{2}r^T J_\rho r + \frac{1}{2}e_x^T e_x + \frac{1}{2}tr(\tilde{W}^T \Gamma_1^{-1} \tilde{W}) + \frac{1}{2}tr(\tilde{U}^T \Gamma_2^{-1} \tilde{U}). \tag{4–45}$$

By using (4–13) and typical NN properties [112], $V_L(t)$ can be upper and lower bounded as

$$\lambda_1 \|X\|^2 \leq V_L(t) \leq \lambda_2 \|X\|^2 + \theta, \tag{4–46}$$

where $\lambda_1, \lambda_2, \theta \in \mathbb{R}$ are known positive constants, and $X(t) \in \mathbb{R}^3$ is defined as

$$X(t) \triangleq \begin{bmatrix} z(t) & e_x(t) \end{bmatrix}^T. \tag{4–47}$$

Taking the time derivative of (4–45), utilizing (4–9), (4–36), (4–42), and canceling similar terms yields

$$\dot{V}_L = -e^T \alpha e + r^T N - r^T k_s r + r^T \tilde{W}^T \hat{\sigma} + r^T \hat{W}^T \hat{\sigma}' \tilde{U}^T y - e_x^T k e_x - r^T (\xi_j - \dot{J}_\rho) r$$
$$- tr(\tilde{W}^T \Gamma_1^{-1} \dot{\tilde{W}}) - tr(\tilde{U}^T \Gamma_2^{-1} \dot{\tilde{U}}). \tag{4–48}$$

Using (4–14) and (4–38), the expression in (4–48) can be upper bounded as

$$\dot{V}_L \leq -\alpha e^2 - k_{s_1} r^2 + \zeta_2 \|z\| |r| + [|r| \zeta_1 - k_{s_2} r^2] - k e_x^2 + r^T \tilde{W}^T \hat{\sigma} + r^T \hat{W}^T \hat{\sigma}' \tilde{U}^T y - tr(\tilde{W}^T \Gamma_1^{-1} \dot{\hat{W}})$$
$$- tr(\tilde{U}^T \Gamma_2^{-1} \dot{\hat{U}}), \tag{4–49}$$

82

where $k_{s_1}, k_{s_2} \in \mathbb{R}$ are positive constant gains that satisfy

$$k_s = k_{s_1} + k_{s_2}. \tag{4–50}$$

Completing the squares for the bracketed term in (4–49) and using the update laws in (4–30) yields

$$\dot{V}_L \leq -[\min(\alpha_1, k_{s_1}) - \zeta_2] \|z\|^2 - k e_x^2 + \frac{\zeta_1^2}{4k_{s_2}}. \tag{4–51}$$

The inequality in (4–46) can be used to rewrite (4–51) as

$$\dot{V}_L \leq -\frac{\beta}{\lambda_2} V_L + \varepsilon, \tag{4–52}$$

where $\varepsilon \in \mathbb{R}$ is a positive constant defined as

$$\varepsilon = \frac{\zeta_1^2}{4k_{s_2}} + \frac{\beta}{\lambda_2}\theta, \tag{4–53}$$

and $\beta \in \mathbb{R}$ is defined as

$$\beta = \min[(\min(\alpha_1, k_{s_1}) - \zeta_2), k]. \tag{4–54}$$

The linear differential inequality in (4–52) can be solved as

$$V_L(t) \leq V_L(0)e^{-\frac{\beta}{\lambda_2}t} + \varepsilon\frac{\lambda_2}{\beta}\left[1 - e^{-\frac{\beta}{\lambda_2}t}\right]. \tag{4–55}$$

Provided the sufficient condition in (4–44) is satisfied, the expressions in (4–45) and (4–55) indicate that $e(t)$, $r(t)$, $e_x(t)$, $\tilde{W}(t)$, $\tilde{U}(t) \in \mathcal{L}_\infty$. Given that $e(t)$, $r(t)$, $q_d(t)$, $\dot{q}_d(t) \in \mathcal{L}_\infty$, (4–8) and (4–9) indicate that $q(t)$, $\dot{q}(t) \in \mathcal{L}_\infty$. Since $\tilde{W}(t)$, $\tilde{U}(t) \in \mathcal{L}_\infty$, (3–42) and Assumption 1 (3.4) can be used to conclude that $\hat{W}(t)$, $\hat{U}(t) \in \mathcal{L}_\infty$. Based on (4–5), it can be shown that $\hat{x}(t) \in [0, 1]$. Given that $\ddot{q}_d(t)$, $e(t)$, $r(t)$, $q(t)$, $\dot{q}(t)$, $\hat{x}(t) \in \mathcal{L}_\infty$, the NN input vector $y(t) \in \mathcal{L}_\infty$ from (4–25). Since $e_x(t)$, $\hat{x}(t) \in \mathcal{L}_\infty$, (4–33) can be used to show that $x_d(t) \in \mathcal{L}_\infty$. Given that $r(t)$, $\hat{W}(t)$, $\hat{U}(t)$, $x_d(t) \in \mathcal{L}_\infty$, (4–28) and (4–29) indicate that $\hat{S}(t)$, $\hat{\varphi}^{-1}(t) \in \mathcal{L}_\infty$. Since $e(t)$, $r(t)$, $\hat{W}(t)$, $\tilde{W}(t)$, $\tilde{U}(t)$, $e_x(t)$ $\hat{\varphi}(t) \in \mathcal{L}_\infty$, (4–36) and (4–38) indicate that $\dot{r}(t) \in \mathcal{L}_\infty$. As $r(t)$, $y(t)$, $\hat{W}(t) \in \mathcal{L}_\infty$, the update laws $\dot{\hat{W}}(t)$, $\dot{\hat{U}}(t) \in \mathcal{L}_\infty$. Since $\hat{\varphi}(t)$, $\hat{x}(t) \in \mathcal{L}_\infty$, it can be shown that $\dot{\hat{\varphi}}(t) \in \mathcal{L}_\infty$. Given that the $\dot{\hat{\varphi}}(t)$, $\hat{\varphi}^{-1}(t)$, $\dot{r}(t)$,

$r(t)$, $\hat{W}(t)$, $\hat{U}(t)$, $\dot{\hat{W}}(t)$, $\dot{\hat{U}}(t) \in \mathcal{L}_\infty$, it can be shown that $\dot{x}_d(t) \in \mathcal{L}_\infty$. Because $\hat{\varphi}(t)$, $\dot{x}_d(t)$, $r(t)$, $\hat{x}(t)$, $e_x(t) \in \mathcal{L}_\infty$, it can be concluded that the voltage control input $V(t)$ is bounded.

4.5   Simulations

Simulations are performed to illustrate the performance of the controller. The model parameters were chosen from [6, 36, 123]. The RISE and the proposed controller are tested for two different desired trajectories: 1) slow trajectory with 6 second period, 2) fast trajectory with 2 second period.

Figure 4-2. Top plot shows the knee angle error for a 6 second period trajectory using the proposed controller. Middle plot shows the pulsewidth computed by the proposed controller. Bottom plot shows the actual leg angle (dashed line) vs desired trajectory (solid line).

From the results shown in Figs. 4-2-4-8, it is clear that the proposed controller tracks both time varying desired trajectories better than the RISE controller. Figs. 4-4 and 4-5 illustrate the performance of the RISE controller when implemented on muscle dynamics without including the fatigue dynamics. The steady state error from the RISE controller is between $\pm 8°$ for desired trajectory with period 6 seconds. The steady state error in the case of RISE controller increases to $\pm 14°$ when faster trajectory with period 2 seconds is used. Fig. 4-6 depicts that the control performance degrades later in time when RISE

Figure 4-3. Top plot shows the knee angle error for a 2 second period trajectory using the proposed controller. Middle plot shows the pulsewidth computed by the proposed controller. Bottom plot shows the actual leg angle (dashed line) vs desired trajectory (solid line).

controller is implemented on muscle dynamics with fatigue model included. The proposed controller was implemented on the complete muscle dynamics that included the fatigue dynamics. Figs. 4-2, 4-3 and 4-7 show that the steady state error in the case of proposed controller remains within $\pm 0.5°$ for both slow and fast trajectories. Fig. 4-8 shows how the fatigue variable evolves with time as a deceasing input gain. The proposed controller is able to compensate for the decreasing control gain, and the performance does not degrade over time as shown in Fig. 4-7.

4.6   Conclusion

A NN based nonlinear control algorithm is developed to elicit non-isometric contractions of the human quadriceps muscle via NMES. The primary objective of the developed method is to incorporate an uncertain muscle fatigue model and unknown calcium dynamics in the nonlinear muscle dynamics. The unknown muscle model and the parametric uncertainties in the fatigue model are approximated by the NN structure through an estimate of the calcium dynamics. A Lyapunov based stability analysis is

85

Figure 4-4. Top plot shows the knee angle error for a 6 second period trajectory using the RISE controller. Middle plot shows the pulsewidth computed by the RISE controller. Bottom plot shows the actual leg angle (dashed line) vs desired trajectory (solid line).

performed to prove uniformly ultimately bounded result in the presence of bounded disturbances (e.g muscle spasticity), parametric uncertainties. Simulation results clearly illustrate that the proposed controller performs better in terms of reduced error in comparison to the RISE controller. However, the performance of the controller on volunteers or patients remains to be seen. The controller's dependence on acceleration and mathematical fatigue and calcium models hinder its implementation on volunteers. The mathematical calcium and fatigue models were incorporated due to the fact that the measurement of actual fatigue state and calcium variable is difficult. Future efforts can be made to incorporate an observer-based design in the controller in order to estimate the fatigue and calcium states.
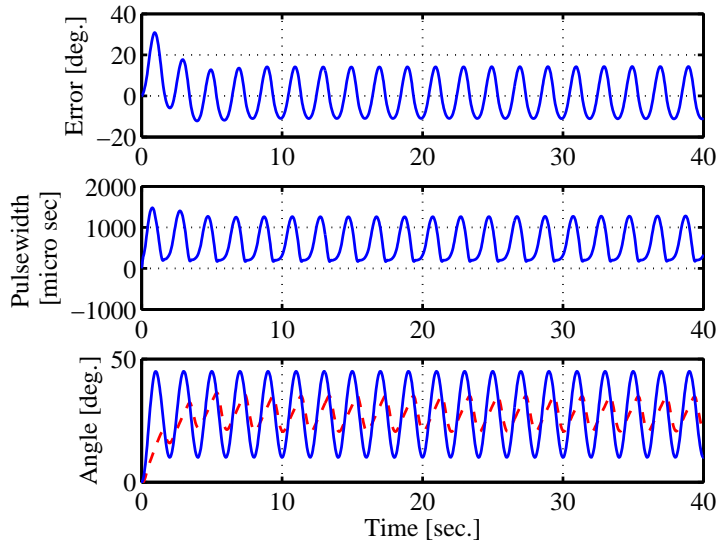
Figure 4-5. Top plot shows the knee angle error for a 2 second period trajectory using the RISE controller. Middle plot shows the pulsewidth computed by the RISE controller. Bottom plot shows the actual leg angle (dashed line) vs desired trajectory (solid line).
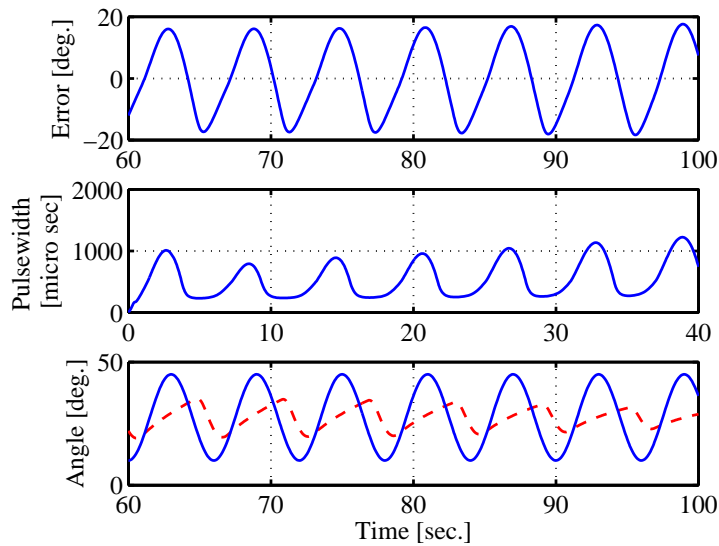
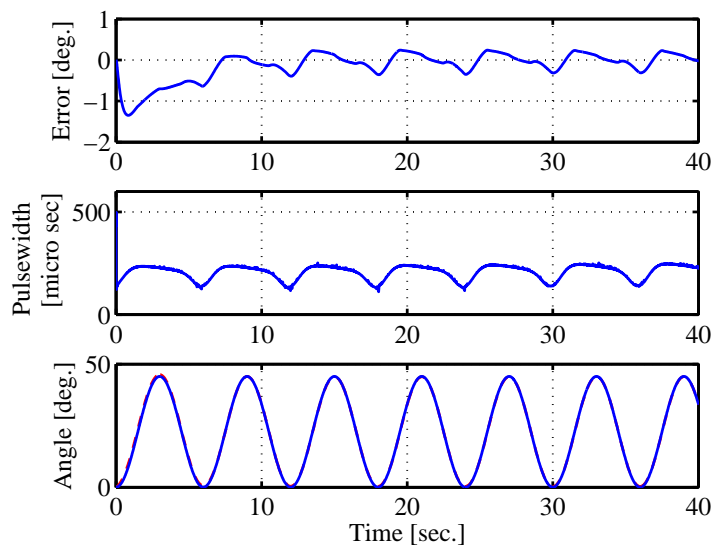Figure 4-6. RISE controller with fatigue in the dynamics: Top plot shows the knee angle error for a 6 second period trajectory using the RISE controller. Middle plot shows the pulsewidth computed by the RISE controller. Bottom plot shows the actual leg angle (dashed line) vs desired trajectory (solid line).
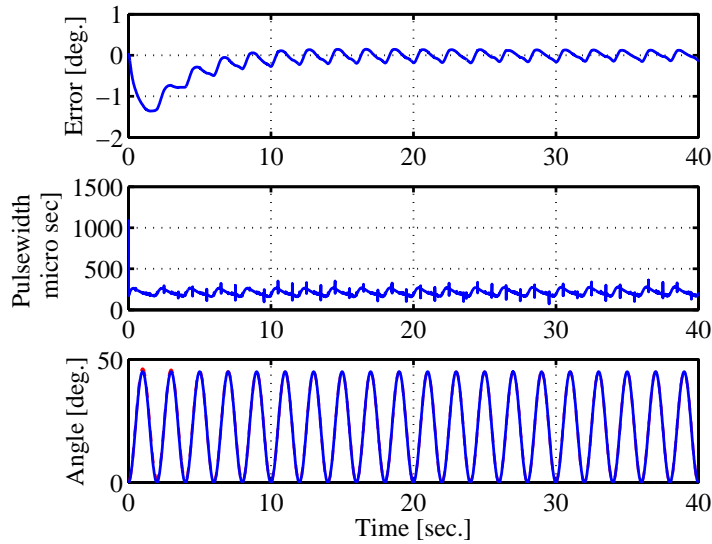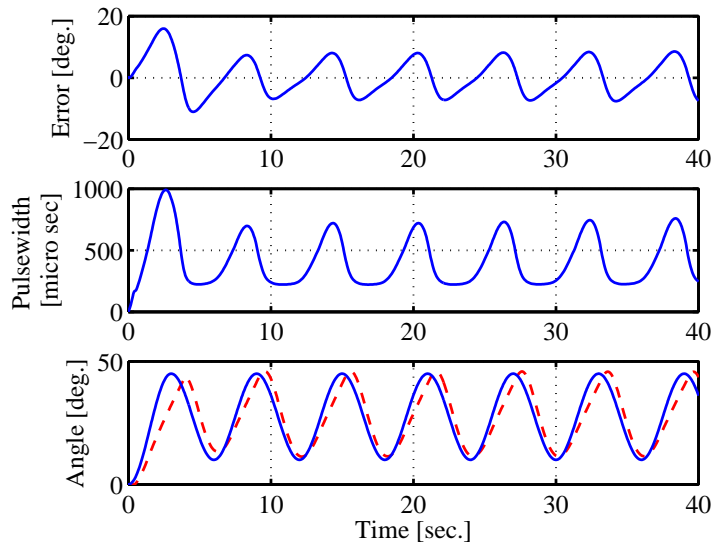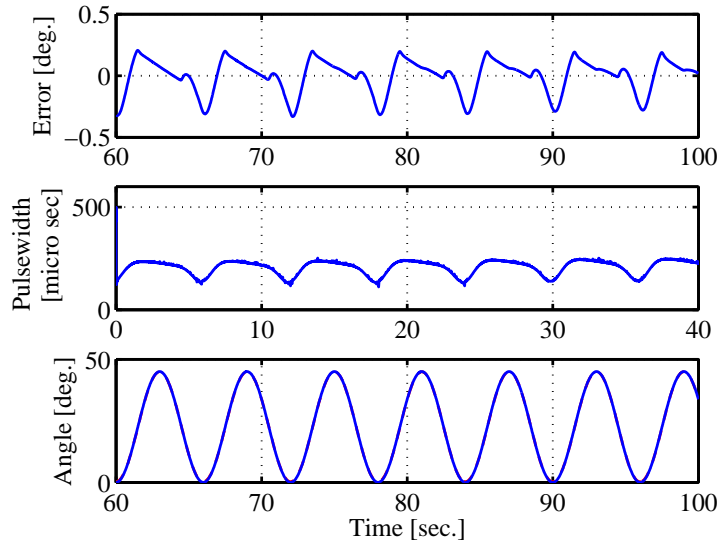
Figure 4-7. Performance of the proposed controller: Top plot shows the knee angle error for a 6 second period trajectory using the proposed controller. Middle plot shows the pulsewidth computed by the proposed controller. Bottom plot shows the actual leg angle (dashed line) vs desired trajectory (solid line).
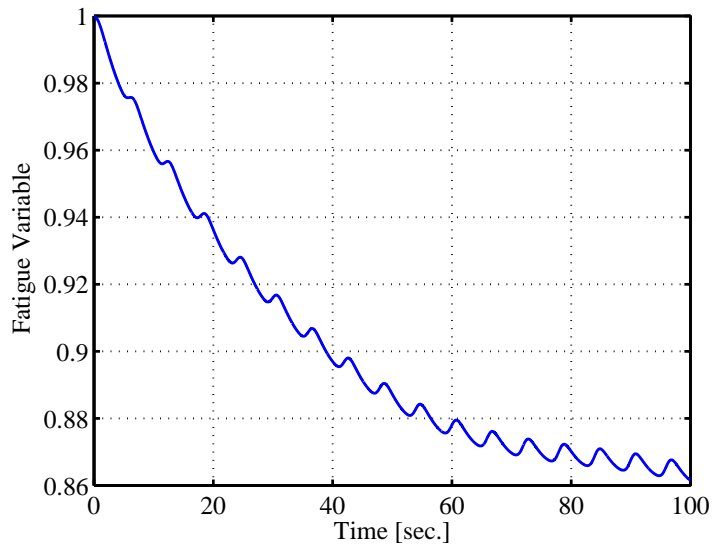
Figure 4-8. Fatigue variable

CHAPTER 5
PREDICTOR-BASED CONTROL FOR AN UNCERTAIN EULER-LAGRANGE SYSTEM WITH INPUT DELAY

5.1   Introduction

This chapter focuses on the development of tracking controllers for an uncertain nonlinear Euler-Lagrange system with input delay. The input time delay is assumed to be a known constant and can be arbitrarily large. The dynamics are assumed to contain parametric uncertainty and additive bounded disturbances. The first developed controller is based on the assumption that the inertia matrix is known. The known inertia case is provided to illustrate how a proportional integral (PID) controller can be augmented to compensate for input delay. The second controller removes the assumption that inertia matrix is known, and different design/analysis efforts are used to yield a PD controller with an augmented predictor component. The key contributions of this effort is the design of a delay compensating auxiliary signal to obtain a time delay free open-loop error system and the construction of LK functionals to cancel the time delayed terms. The auxiliary signal leads to the development of a predictor-based controller that contains a finite integral of past control values. This delayed state to delay free transformation is analogous to the Artstein model reduction approach, where a similar predictor-based control is obtained. LK functionals containing finite integrals of control input values are used in a Lyapunov-based analysis that proves the tracking errors are semi-global uniformly ultimately bounded. Experimental results are obtained for a two-link direct drive robot. The results illustrate the robustness and added value of the developed predictor-based controllers.

The primary motive of this research is to develop and implement a controller that compensates for electromechanical delay (EMD) in NMES. The last section of the chapter focusses on characterizing EMD during NMES. Experiments results obtained from healthy volunteers are provided which describe the effect of stimulation parameters on the EMD during NMES. Finally, a PD controller with an augmented predictor component

is implemented on the healthy volunteers. Experiments show that the controller can be applied to compensate EMD in NMES. A comparison with the traditional PD controller shows that the PD controller with delay compensation provides a better performance.

5.2 Dynamic Model and Properties

Consider the following input delayed Euler-Lagrange dynamics

$$M(q)\ddot{q} + V_m(q, \dot{q})\dot{q} + G(q) + F(\dot{q}) + d(t) = u(t - \tau). \qquad (5\text{–}1)$$

In (5–1), $M(q) \in \mathbb{R}^{n \times n}$ denotes a generalized inertia matrix, $V_m(q, \dot{q}) \in \mathbb{R}^{n \times n}$ denotes a generalized centripetal-Coriolis matrix, $G(q) \in \mathbb{R}^n$ denotes a generalized gravity vector, $F(\dot{q}) \in \mathbb{R}^n$ denotes generalized friction, $d(t) \in \mathbb{R}^n$ denotes an exogenous disturbance (e.g., unmodeled effects), $u(t - \tau) \in \mathbb{R}^n$ represents the generalized delayed input control vector, where $\tau \in \mathbb{R}$ is a constant time delay, and $q(t)$, $\dot{q}(t)$, $\ddot{q}(t) \in \mathbb{R}^n$ denote the generalized states. The subsequent development is based on the assumptions that $q(t)$ and $\dot{q}(t)$ are measurable, $V_m(q, \dot{q})$, $G(q)$, $F(\dot{q})$, $d(t)$ are unknown, the time delay constant $\tau \in \mathbb{R}$ is known[1] , and the control input vector $u(t)$ and its past values (i.e., $u(t - \theta) \ \forall \ \theta \in [0 \quad \tau]$) are measurable. For the controller developed in Section 5.3.2, $M(q)$ is assumed to be known to illustrate the development of a PID-like controller. In Section 5.3.3, this assumption is removed and a PD-like controller is developed. Throughout the paper, a time dependent delayed function is denoted as $x(t - \tau)$ (or as x_τ) and a time dependent function (without time delay) is denoted as $x(t)$ (or as x). The following assumptions are used in the subsequent development.

---

[1] Experimental results (where the time delay is artificially injected in a desired manner) illustrate the performance of the developed controllers when the time delay has as much as 100% error between the assumed and actual delay.

Assumption 1: The inertia matrix $M(q)$ is symmetric, positive definite, and satisfies the following inequality $\forall \; \xi(t) \in \mathbb{R}^n$:

$$m_1 \left\| \xi \right\|^2 \leq \xi^T M \xi \leq m_2 \left\| \xi \right\|^2 , \tag{5--2}$$

where m_1, $m_2 \in \mathbb{R}^+$ are known constants and $\left\| \cdot \right\|$ denotes the standard Euclidean norm.

Assumption 2: The desired trajectory $q_d(t)$ is designed such that $q_d(t)$, $q_d^{(i)}(t) \in \mathcal{L}_\infty$, where $q_d^{(i)}(t)$ denotes the ith time derivative for $i = 1, 2, 3$.

Assumption 3: If $q(t)$, $\dot{q}(t) \in \mathcal{L}_\infty$, then $M(q)$, $V_m(q, \dot{q})$, $G(q)$, and $F(\dot{q})$ are bounded. Moreover, if $q(t)$, $\dot{q}(t)$, $\ddot{q}(t) \in \mathcal{L}_\infty$, then the first time derivatives of $M(q)$, $V_m(q, \dot{q})$, $G(q)$, $F(\dot{q})$ exist and are bounded. The infinity norm of $M(q)$ and its inverse can be upper bounded as

$$\left\| M(q) \right\|_\infty \leq \zeta_1 \quad \left\| M^{-1}(q) \right\|_\infty \leq \zeta_2, \tag{5--3}$$

where ζ_1, $\zeta_2 \in \mathbb{R}^+$ are known constants.

Assumption 4: The nonlinear disturbance term and its first time derivative are bounded, i.e., $d(t)$, $\dot{d}(t) \in \mathcal{L}_\infty$.

5.3   Control Development

5.3.1   Objective

The objective is to develop a controller that will enable the input delayed system in (5–1) to track a desired trajectory, denoted by $q_d(t) \in \mathbb{R}^n$. To quantify the objective, a position tracking error, denoted by $e_1(t) \in \mathbb{R}^n$, is defined as

$$e_1 = q_d(t) - q(t). \tag{5--4}$$

5.3.2   Control development given a Known Inertia Matrix

To facilitate the subsequent analysis, a filtered tracking error, denoted by $e_2(t) \in \mathbb{R}^n$, is defined as

$$e_2 = \dot{e}_1 + \alpha_1 e_1, \tag{5--5}$$

where $\alpha_1 \in \mathbb{R}^+$ denotes a constant. To reduce the input delayed system in (5–1) to an input delay free system, an auxiliary signal denoted by $r(t) \in \mathbb{R}^n$, is also defined as

$$r = \dot{e}_2 + \alpha_2 e_2 + M^{-1}(q)(u(t-\tau) - u(t)), \tag{5–6}$$

where $\alpha_2 \in \mathbb{R}^+$ denotes a constant. The auxiliary signal $r(t)$ is only introduced to facilitate the subsequent analysis, and is not used in the control design since the expression in (5–6) depends on the unmeasurable generalized state $\ddot{q}(t)$.

After multiplying (5–6) by $M(q)$ and utilizing the expressions in (5–1), (5–4), and (5–5), the transformed open-loop tracking error system can be expressed in an input delay free form as

$$M(q)r = M(q)\ddot{q}_d + V_m(q,\dot{q})\dot{q} + G(q) + F(\dot{q}) + \alpha_1 M(q)\dot{e}_1 + \alpha_2 M(q)e_2 + d - u(t). \tag{5–7}$$

Based on (5–7) and the subsequent stability analysis, the control input $u(t) \in \mathbb{R}^n$ is designed as

$$u = k_a \left(e_2 + \int_0^t \alpha_2 e_2(\theta) + M^{-1}(\theta)(u(\theta - \tau) - u(\theta))d\theta \right) - k_a e_2(0), \tag{5–8}$$

where $k_a \in \mathbb{R}^+$ is a known constant that can be expanded as

$$k_a = k_{a_1} + k_{a_2} + 1, \tag{5–9}$$

to facilitate the subsequent stability analysis, where k_{a_1}, $k_{a_2} \in \mathbb{R}^+$ are known constants. The controller $u(t)$ in (5–8) is a proportional integral derivative (PID) controller modified by a predictor like feedback term for time delay compensation. Although the control input $u(t)$ is present in the open loop error system in (5–7), an additional derivative is taken to facilitate the subsequent stability analysis. The time derivative of (5–7) can be expressed as

$$M(q)\dot{r} = -\frac{1}{2}\dot{M}(q)r + N + \dot{d} - k_a r, \tag{5–10}$$

where $N(e_1, e_2, r, t) \in \mathbb{R}^n$ is an auxiliary term defined as

$$
\begin{aligned}
N = {}& -\frac{1}{2}\dot{M}(q)r + M(q)\dddot{q}_d + \dot{M}(q)\ddot{q}_d + \dot{V}_m(q,\dot{q})\dot{q} + V_m(q,\dot{q})\ddot{q} + \dot{G}(q) + \dot{F}(\dot{q}) \quad (5\text{--}11)\\
& + (\alpha_1 + \alpha_2)\, M(q)r - \alpha_1\alpha_2 M(q)e_2 - \alpha_1^2 M(q)e_1 - \alpha_2^2 M(q)e_2 + \alpha_1 \dot{M}(q)\dot{e}_1\\
& + \alpha_2 \dot{M}(q)e_2 - (\alpha_1 + \alpha_2)\,(u_\tau - u) - \alpha_1^2 M(q)\dot{e}_1,
\end{aligned}
$$

and (5–6) is used to write the time derivative of (5–8) as

$$
\dot{u} = k_a r.
$$

After adding and subtracting the auxiliary function $N_d(q_d, \dot{q}_d, \ddot{q}_d, \dddot{q}_d, t) \in \mathbb{R}^n$ defined as

$$
N_d = M(q_d)\dddot{q}_d + \dot{M}(q_d)\ddot{q}_d + \dot{V}_m(q_d,\dot{q}_d)\dot{q}_d + V_m(q_d,\dot{q}_d)\ddot{q}_d + \dot{G}(q_d) + \dot{F}(\dot{q}_d),
$$

to (5–10), the following expression is obtained:

$$
M(q)\dot{r} = -\frac{1}{2}\dot{M}(q)r + \tilde{N} + S - e_2 - k_a r, \qquad (5\text{--}12)
$$

where the auxiliary functions $\tilde{N}(e_1, e_2, r, t) \in \mathbb{R}^n$ and $S(q_d, \dot{q}_d, \ddot{q}_d, \dddot{q}_d, t) \in \mathbb{R}^n$ are defined as

$$
\tilde{N} = N - N_d + e_2, \qquad S = N_d + \dot{d}. \qquad (5\text{--}13)
$$

Some terms in the closed-loop dynamics in (5–12) are segregated into auxiliary terms in (5–13) because of differences in how the terms can be upper bounded. For example, Assumptions 2, 3 and 4, can be used to upper bound $S(q_d, \dot{q}_d, \ddot{q}_d, \dddot{q}_d, t)$ as

$$
\|S\| \le \varepsilon_1, \qquad (5\text{--}14)
$$

where $\varepsilon_1 \in \mathbb{R}^+$ is a known constant and the Mean Value Theorem can be used to upper bound $\tilde{N}(e_1, e_2, r, t)$ as

$$
\tilde{N} \le \rho_1(\|z\|)\,\|z\|, \qquad (5\text{--}15)
$$

where $z \in \mathbb{R}^{4n}$ is defined as

$$z = \begin{bmatrix} e_1^T & e_2^T & r^T & e_z^T \end{bmatrix}^T, \tag{5-16}$$

and the bounding function $\rho_1 \left(\|z\| \right) \in \mathbb{R}$ is a known positive globally invertible nondecreasing function. In (5–16), $e_z \in \mathbb{R}^n$ is defined as

$$e_z \triangleq u - u_\tau = \int_{t-\tau}^{t} \dot{u}(\theta) d\theta,$$

based on the Leibnitz-Newton formula.

Theorem 4. *The controller given in (5–8) ensures semi-globally uniformly ultimately bounded (SUUB) tracking in the sense that*

$$\|e_1(t)\| \leq \epsilon_0 \exp(-\epsilon_1 t) + \epsilon_2, \tag{5-17}$$

where ϵ_0, ϵ_1, $\epsilon_2 \in \mathbb{R}^+$ denote constants, provided the control gains α_1, α_2, and k_a introduced in (5–5), (5–6), and (5–8), respectively are selected according to the following sufficient conditions:

$$\alpha_1 > \frac{1}{2}, \quad \alpha_2 > 1 + \frac{\zeta_2^2 \gamma^2}{4}, \quad k_a^2 < \frac{1}{\omega \tau}, \quad \omega \gamma^2 > 2\tau, \tag{5-18}$$

where ω, $\gamma \in \mathbb{R}^+$ are subsequently defined control gains.

Proof: Let $y(t) \in \mathcal{D} \subset \mathbb{R}^{3n+1}$ be defined as

$$y(t) \triangleq \begin{bmatrix} e_1^T & e_2^T & r^T & \sqrt{Q} \end{bmatrix}^T, \tag{5-19}$$

where $Q(t) \in \mathbb{R}$ is defined as [45, 76]

$$Q = \omega \int_{t-\tau}^{t} \left(\int_{s}^{t} \|\dot{u}(\theta)\|^2 d\theta \right) ds, \tag{5-20}$$

where $\omega \in \mathbb{R}^+$ is a known constant. A positive definite Lyapunov functional candidate $V(y,t) : \mathcal{D} \times [0 \quad \infty) \rightarrow \mathbb{R}$ is defined as

$$V(y,t) \triangleq e_1^T e_1 + \frac{1}{2} e_2^T e_2 + \frac{1}{2} r^T M(q) r + Q, \tag{5-21}$$

and satisfies the following inequalities

$$\lambda_1 \|y\|^2 \leq V \leq \lambda_2 \|y\|^2, \tag{5-22}$$

where $\lambda_1, \lambda_2 \in \mathbb{R}^+$ are known constants defined as

$$\lambda_1 = \frac{1}{2} \min[m_1, 1], \qquad \lambda_2 = \max[\frac{1}{2} m_2, 1], \tag{5-23}$$

where m_1 and m_2 are defined in (5–2).

After utilizing (5–5), (5–6), and (5–12) and cancelling the similar terms, the time derivative of (5–21) is

$$\dot{V} = 2e_1^T e_2 - 2\alpha_1 e_1^T e_1 - \alpha_2 e_2^T e_2 - k_a r^T r + e_2^T M^{-1}(q) e_z + r^T S + r^T \tilde{N} + \omega \tau \|\dot{u}\|^2 - \omega \int_{t-\tau}^t \|\dot{u}(\theta)\|^2 \, d\theta, \tag{5-24}$$

where the Leibniz integral rule was applied to determine the time derivative of $Q(t)$ in (5–20) (see the Appendix 7.2). The expression in (5–24) can be upper bounded by using (5–3), (5–14) and (5–15) as

$$
\begin{aligned}
\dot{V} \leq \ & -(2\alpha_1 - 1) \|e_1\|^2 - (\alpha_2 - 1) \|e_2\|^2 - k_a \|r\|^2 + \zeta_2 \|e_2\| \|e_z\| \\
& + \omega \tau \|\dot{u}\|^2 + \varepsilon_1 \|r\| + \rho_1(\|z\|) \|z\| \|r\| - \omega \int_{t-\tau}^t \|\dot{u}(\theta)\|^2 \, d\theta.
\end{aligned}
\tag{5-25}
$$

The following term in (5–25) can be upper bounded by using Young's inequality:

$$\zeta_2 \|e_2\| \|e_z\| \leq \frac{\zeta_2^2 \gamma^2}{4} \|e_2\|^2 + \frac{1}{\gamma^2} \|e_z\|^2, \tag{5-26}$$

where $\gamma \in \mathbb{R}^+$ is a known constant. Further, by using the Cauchy Schwarz inequality, the following term in (5–26) can be upper bounded as

$$\|e_z\|^2 \leq \tau \int_{t-\tau}^t \|\dot{u}(\theta)\|^2 \, d\theta. \tag{5-27}$$

Adding and subtracting $\frac{\tau}{\gamma^2} \int_{t-\tau}^{t} \|\dot{u}(\theta)\|^2 \, d\theta$ in (5–25) yields

$$
\begin{aligned}
\dot{V} \leq\ & -(2\alpha_1 - 1) \|e_1\|^2 - (\alpha_2 - 1) \|e_2\|^2 - k_a \|r\|^2 + \zeta_2 \|e_2\| \|e_z\| + \omega\tau \|\dot{u}\|^2 \qquad (5\text{–}28) \\
& + \varepsilon_1 \|r\| + \rho_1(\|z\|) \|z\| \|r\| - \left(\omega - \frac{\tau}{\gamma^2}\right) \int_{t-\tau}^{t} \|\dot{u}(\theta)\|^2 \, d\theta - \frac{\tau}{\gamma^2} \int_{t-\tau}^{t} \|\dot{u}(\theta)\|^2 \, d\theta.
\end{aligned}
$$

Utilizing (5–9) and the bounds given in (5–26) and (5–27), the inequality in (5–28) can be upper bounded as

$$
\begin{aligned}
\dot{V} \leq\ & -(2\alpha_1 - 1) \|e_1\|^2 - \left(\alpha_2 - 1 - \frac{\zeta_2^2 \gamma^2}{4}\right) \|e_2\|^2 - \left(1 - \omega k_a^2 \tau\right) \|r\|^2 - \frac{1}{\tau}\left(\omega - \frac{2\tau}{\gamma^2}\right) \|e_z\|^2 + \varepsilon_1 \|r\| \\
& + \rho_1(\|z\|) \|z\| \|r\| - k_{a_2} \|r\|^2 - k_{a_1} \|r\|^2 - \frac{\tau}{\gamma^2} \int_{t-\tau}^{t} \|\dot{u}(\theta)\|^2 \, d\theta. \qquad (5\text{–}29)
\end{aligned}
$$

After completing the squares, the inequality in (5–29) can be upper bounded as

$$
\dot{V} \leq -\beta_1 \|z\|^2 - \frac{\tau}{\gamma^2} \int_{t-\tau}^{t} \|\dot{u}(\theta)\|^2 \, d\theta + \frac{\rho_1^2(\|z\|)}{4k_{a_1}} \|z\|^2 + \frac{\varepsilon_1^2}{4k_{a_2}}, \qquad (5\text{–}30)
$$

where $\beta_1 \in \mathbb{R}^+$ is defined as

$$
\beta_1 = \min \left[\left(\alpha_2 - 1 - \frac{\zeta_2^2 \gamma^2}{4}\right), (2\alpha_1 - 1), \left(1 - \omega k_a^2 \tau\right), \frac{1}{\tau}\left(\omega - \frac{2\tau}{\gamma^2}\right) \right].
$$

Since

$$
\int_{t-\tau}^{t} \left(\int_{s}^{t} \|\dot{u}(\theta)\|^2 \, d\theta \right) ds \leq \tau \sup_{s \in [t, t-\tau]} \left[\int_{s}^{t} \|\dot{u}(\theta)\|^2 \, d\theta \right] = \tau \int_{t-\tau}^{t} \|\dot{u}(\theta)\|^2 \, d\theta,
$$

the expression in (5–30) can be rewritten as

$$
\dot{V} \leq -\left(\beta_1 - \frac{\rho_1^2(\|z\|)}{4k_{a_1}}\right) \|z\|^2 - \frac{1}{\gamma^2} \int_{t-\tau}^{t} \left(\int_{s}^{t} \|\dot{u}(\theta)\|^2 \, d\theta \right) + \frac{\varepsilon_1^2}{4k_{a_2}}. \qquad (5\text{–}31)
$$

Using the definition of $z(t)$ in (5–16) and $y(t)$ in (5–19), the expression in (5–31) can be expressed as

$$
\dot{V} \leq -\bar{\beta}_1 \|y\|^2 - \left(\beta_1 - \frac{\rho_1^2(\|z\|)}{4k_{a_1}}\right) \|e_z\|^2 + \frac{\varepsilon_1^2}{4k_{a_2}}, \qquad (5\text{–}32)
$$

where $\bar{\beta}_1(\|z\|) \in \mathbb{R}^+$ is defined as

$$
\bar{\beta}_1 = \min \left[\left(\beta_1 - \frac{\rho_1^2(\|z\|)}{4k_{a_1}}\right), \frac{1}{\omega\gamma^2} \right].
$$

By further utilizing (5–22), the inequality in (5–32) can be upper bounded as

$$\dot{V} \leq -\frac{\bar{\beta}_1}{\lambda_2}V + \frac{\varepsilon_1^2}{4k_{a_2}}. \tag{5–33}$$

Consider a set $\mathcal{S}$ defined as

$$\mathcal{S} \triangleq \left\{ z(t) \in \mathbb{R}^{4n} \mid \|z\| < \rho_1^{-1}\left(2\sqrt{\beta_1 k_{a_1}}\right) \right\}. \tag{5–34}$$

In $\mathcal{S}$, $\bar{\beta}_1(\|z\|)$ can be lower bounded by a constant $\delta_1 \in \mathbb{R}^+$ as

$$\delta_1 \leq \bar{\beta}_1(\|z\|). \tag{5–35}$$

Based on (5–35), the linear differential equation in (5–33) can be solved as

$$V(y,t) \leq V(0)e^{-\frac{\delta_1}{\lambda_2}t} + \frac{\varepsilon_1^2 \lambda_2}{4k_{a_2}\delta_1}\left[1 - e^{-\frac{\delta_1}{\lambda_2}t}\right], \tag{5–36}$$

provided $\|z\| \leq \rho_1^{-1}\left(2\sqrt{\beta_1 k_{a_1}}\right)$. From (5–36), if $z(0) \in \mathcal{S}$ then k_a can be chosen according to the sufficient conditions in (5–18) (i.e. a semi-global result) to yield the result in (5–17). Based on definition of $y(t)$, it can be concluded that $e_1(t)$, $e_2(t)$, $r(t) \in \mathcal{L}_\infty$ in $\mathcal{S}$. Given that $e_1(t)$, $e_2(t)$, $q_d(t)$, $\dot{q}_d(t) \in \mathcal{L}_\infty$ in $\mathcal{S}$, (5–4) and (5–5) indicate that $q(t)$, $\dot{q}(t) \in \mathcal{L}_\infty$ in $\mathcal{S}$. Since $r(t)$, $e_2(t)$, $q(t)$, $\dot{q}(t)$, $\dot{q}_d(t)$, $\ddot{q}_d(t) \in \mathcal{L}_\infty$ in $\mathcal{S}$, and $u(t) - u(t-\tau) = \int_{t-\tau}^{t} \dot{u}(\theta)d\theta = k_a \int_{t-\tau}^{t} r(\theta)d\theta$ (by Leibnitz-Newton formula)$\in \mathcal{L}_\infty$ in $\mathcal{S}$, then (5–6) and Assumption 3 indicate that $\ddot{q}(t) \in \mathcal{L}_\infty$ in $\mathcal{S}$. Given that $r(t)$, $e_2(t)$, $q(t)$, $\dot{q}(t)$, $\dot{q}_d(t)$ $\ddot{q}_d(t) \in \mathcal{L}_\infty$ in $\mathcal{S}$, (5–7) and Assumptions 3 and 4 indicate that $u(t) \in \mathcal{L}_\infty$ in $\mathcal{S}$.

5.3.3 Control development with an Unknown Inertia Matrix

To facilitate the subsequent control design and stability analysis for the uncertain inertia problem, the auxiliary signal, $e_2(t) \in \mathbb{R}^n$ is redefined as

$$e_2(t) = \dot{e}_1 + \alpha e_1 - B\int_{t-\tau}^{t} u(\theta)d\theta, \tag{5–37}$$

where $\alpha \in \mathbb{R}^+$ is a known constant, and $B \in \mathbb{R}^{n \times n}$ is a known symmetric, positive definite constant gain matrix that satisfies the following inequality

$$\|B\|_\infty \leq b \tag{5-38}$$

where $b \in \mathbb{R}^+$ is a known constant. To facilitate the subsequent stability analysis, the error between B and $M^{-1}(q)$ is defined by

$$\eta(q) = B - M^{-1}(q), \tag{5-39}$$

where $\eta(q) \in \mathbb{R}^{n \times n}$ satisfies the following inequality

$$\|\eta(q)\|_\infty \leq \bar{\eta}, \tag{5-40}$$

where $\bar{\eta} \in \mathbb{R}^+$ denotes a known constant. The open-loop tracking error system can be developed by multiplying the time derivative of (5–37) by $M(q)$ and utilizing the expressions in (5–1), (5–4), and (5–39) to obtain

$$M(q)\dot{e}_2 = M(q)\ddot{q}_d + V_m(q, \dot{q})\dot{q} + G(q) + F(\dot{q}) + d + \alpha M(q)\dot{e}_1 - u(t) - M(q)\eta \left[u - u_\tau \right]. \tag{5-41}$$

Based on (5–41) and the subsequent stability analysis, the control input $u(t) \in \mathbb{R}^n$ is designed as

$$u = k_b e_2, \tag{5-42}$$

where $k_b \in \mathbb{R}^+$ is a known control gain that can be expanded as

$$k_b = k_{b_1} + k_{b_2} + k_{b_3}, \tag{5-43}$$

to facilitate the subsequent analysis, where k_{b_1}, k_{b_2}, and $k_{b_3} \in \mathbb{R}^+$ are known constants. After adding and subtracting the auxiliary term $N_d(q_d, \dot{q}_d, \ddot{q}_d, t) \in \mathbb{R}^n$ defined as

$$N_d = M(q_d)\ddot{q}_d + V_m(q_d, \dot{q}_d)\dot{q}_d + G(q_d) + F(\dot{q}_d),$$

and using (5–37) and (5–42), the expression in (5–41) can be rewritten as

$$M(q)\dot{e}_2 = -\frac{1}{2}\dot{M}(q)e_2 + \tilde{N} + S - e_1 - k_b e_2 - k_b M(q)\eta\left[e_2 - e_{2\tau}\right], \qquad (5\text{–}44)$$

where the auxiliary terms $\tilde{N}(e_1, e_2, t)$, $N(e_1, e_2, t)$, $S(q_d, \dot{q}_d, \ddot{q}_d, t) \in \mathbb{R}^n$ are defined as

$$\tilde{N} = N - N_d, \qquad S = N_d + d, \qquad (5\text{–}45)$$

$$N = \frac{1}{2}\dot{M}(q)e_2 + M(q)\ddot{q}_d + V_m(q, \dot{q})\dot{q} + G(q) + F(q) + \alpha M(q)e_2 - \alpha^2 M(q)e_1 + e_1 + \alpha M(q)B\int_{t-\tau}^{t} u(\theta)d\theta,$$

where $\tilde{N}(e_1, e_2, t)$ and $S(q_d, \dot{q}_d, \ddot{q}_d, t)$ can be upper bounded as

$$\tilde{N} \leq \rho_2(\|z\|)\|z\|, \qquad \|S\| \leq \varepsilon_2. \qquad (5\text{–}46)$$

In (5–46), $\varepsilon_2 \in \mathbb{R}^+$ is a known constant, the bounding function $\rho_2(\|z\|) \in \mathbb{R}$ is a positive globally invertible nondecreasing function, and $z \in \mathbb{R}^{3n}$ is defined as

$$z = \begin{bmatrix} e_1^T & e_2^T & e_z^T \end{bmatrix}^T, \qquad (5\text{–}47)$$

where $e_z \in \mathbb{R}^n$ is defined as

$$e_z = \int_{t-\tau}^{t} u(\theta)d\theta.$$

Theorem 5. *The controller given in (5–42) ensures SUUB tracking in the sense that*

$$\|e_1(t)\| \leq \epsilon_0 \exp(-\epsilon_1 t) + \epsilon_2, \qquad (5\text{–}48)$$

where ϵ_0, ϵ_1, $\epsilon_2 \in \mathbb{R}^+$ denote constants, provided the control gains α and k_b introduced in (5–37) and (5–42), respectively are selected according to the sufficient conditions:

$$\alpha > \frac{b^2\gamma^2}{4}, \qquad k_{b_3} > \frac{2\bar{\eta}m_2\left(k_{b_1} + k_{b_2}\right) + \omega k_b^2\tau}{1 - 2\bar{\eta}m_2}, \qquad \omega\gamma^2 > 2\tau, \qquad (5\text{–}49)$$

where m_2, b, $\in \mathbb{R}^+$, $\bar{\eta} \in \mathbb{R}^+$ are defined in (5–2), (5–38), and (5–40), respectively, and γ, $\omega \in \mathbb{R}^+$ are subsequently defined constants.

Remark 1. *The second sufficient gain condition indicates that ω can be selected sufficiently small and k_{b_3} can be selected sufficiently large provided $1 - 2\bar{\eta}m_2 > 0$. The condition*

that $1 - 2\bar{\eta}m_2 > 0$ indicates that the constant approximation matrix B must be chosen sufficiently close to $M^{-1}(q)$ so that $\|B - M^{-1}(q)\|_\infty < \frac{1}{2m_2}$. Experimental results illustrate the performance/robustness of the developed controller with respect to the mismatch between B and $M^{-1}(q)$. Specifically, results indicate an insignificant amount of variation in the performance even when each element of $M^{-1}(q)$ is overestimated by as much as 100%. Different results may be obtained for different systems, but these results indicate that the gain condition is reasonable.

Proof: Let $y(t) \in \mathcal{D} \subset \mathbb{R}^{2n+2}$ be defined as

$$y(t) \triangleq \begin{bmatrix} e_1^T & e_2^T & \sqrt{P} & \sqrt{Q} \end{bmatrix}^T, \tag{5–50}$$

where $P(t), Q(t) \in \mathbb{R}$ denote LK functionals defined as [45]

$$P = \omega \int_{t-\tau}^t \left(\int_s^t \|u(\theta)\|^2 \, d\theta \right) ds, \quad Q = \frac{\bar{\eta}m_2 k_b}{2} \int_{t-\tau}^t \|e_2(\theta)\|^2 \, d\theta,$$

where $\omega \in \mathbb{R}^+$ is a known constant. A positive definite Lyapunov functional candidate $V(y,t) : \mathcal{D} \times [0 \quad \infty) \to \mathbb{R}$ is defined as

$$V(y,t) \triangleq \frac{1}{2}e_1^T e_1 + \frac{1}{2}e_2^T M(q)e_2 + P + Q, \tag{5–51}$$

and satisfies the following inequalities

$$\lambda_1 \|y\|^2 \leq V \leq \lambda_2 \|y\|^2, \tag{5–52}$$

where $\lambda_1, \lambda_2 \in \mathbb{R}^+$ are defined in (5–23).

Taking the time derivative of (5–51) and using (5–37) and (5–44) yields

$$\begin{aligned} \dot{V} &= -\alpha e_1^T e_1 + e_1^T B e_z + \omega\tau \|u\|^2 + e_2^T \left[S + \tilde{N} - k_b e_2 - k_b M(q)\eta (e_2 - e_{2\tau}) \right] \\ &\quad + \frac{\bar{\eta}m_2 k_b}{2} \left[\|e_2\|^2 - \|e_{2\tau}\|^2 \right] - \omega \int_{t-\tau}^t \|u(\theta)\|^2 \, d\theta, \end{aligned} \tag{5–53}$$

where the Leibniz integral rule was applied to determine the time derivative of $P(t)$ (see the Appendix 7.2) and $Q(t)$. Using (5–2), (5–38), and (5–46), the terms in (5–53) can be

upper bounded as

$$
\begin{aligned}
\dot{V} \leq\ & -\alpha\left\|e_1\right\|^2 - k_b\left\|e_2\right\|^2 + \bar{\eta}m_2 k_b\left\|e_2\right\|^2 + \omega\tau\left\|u\right\|^2 + \left\|e_2\right\|\varepsilon_2 + \left\|e_2\right\|\rho_2(\left\|z\right\|)\left\|z\right\| + b\left\|e_1\right\|\left\|e_z\right\| \\
& +\bar{\eta}m_2 k_b\left\|e_{2\tau}\right\|\left\|e_2\right\| + \frac{\bar{\eta}m_2 k_b}{2}\left[\left\|e_2\right\|^2 - \left\|e_{2\tau}\right\|^2\right] - \omega\int_{t-\tau}^{t}\left\|u(\theta)\right\|^2 d\theta.
\end{aligned}
\tag{5–54}
$$

The following terms in (5–54) can be upper bounded by utilizing Young's inequality:

$$
\begin{aligned}
b\left\|e_1\right\|\left\|e_z\right\| &\leq \frac{b^2\gamma^2}{4}\left\|e_1\right\|^2 + \frac{1}{\gamma^2}\left\|e_z\right\|^2, \\
\bar{\eta}m_2 k_b\left\|e_{2\tau}\right\|\left\|e_2\right\| &\leq \frac{\bar{\eta}m_2 k_b}{2}\left\|e_2\right\|^2 + \frac{\bar{\eta}m_2 k_b}{2}\left\|e_{2\tau}\right\|^2
\end{aligned}
\tag{5–55}
$$

where $\gamma \in \mathbb{R}^+$ is a known constant. Further, by using the Cauchy Schwarz inequality, the following term in (5–55) can be upper bounded as

$$
\left\|e_z\right\|^2 \leq \tau\int_{t-\tau}^{t}\left\|u(\theta)\right\|^2 d\theta.
\tag{5–56}
$$

After adding and subtracting $\frac{\tau}{\gamma^2}\int_{t-\tau}^{t}\left\|u(\theta)\right\|^2 d\theta$ to (5–54), and utilizing (5–42), (5–43), (5–55) and (5–56), the following expression is obtained:

$$
\begin{aligned}
\dot{V} \leq\ & -\left(\alpha - \frac{b^2\gamma^2}{4}\right)\left\|e_1\right\|^2 - \left(k_{b_3} - \omega k_b^2\tau - 2\bar{\eta}m_2 k_b\right)\left\|e_2\right\|^2 - \frac{1}{\tau}\left(\omega - \frac{2\tau}{\gamma^2}\right)\left\|e_z\right\|^2 \\
& -k_{b_1}\left\|e_2\right\|^2 + \rho_2(\left\|z\right\|)\left\|z\right\|\left\|e_2\right\| - k_{b_2}\left\|e_2\right\|^2 + \left\|e_2\right\|\varepsilon_2 - \frac{\tau}{\gamma^2}\int_{t-\tau}^{t}\left\|u(\theta)\right\|^2 d\theta.
\end{aligned}
\tag{5–57}
$$

By completing the squares, the inequality in (5–57) can be upper bounded as

$$
\dot{V} \leq -\left\{\beta_2 - \frac{\rho_2^2(\left\|z\right\|)}{4k_{b_1}}\right\}\left\|z\right\|^2 - \frac{\tau}{\gamma^2}\int_{t-\tau}^{t}\left\|u(\theta)\right\|^2 d\theta + \frac{\varepsilon_2^2}{4k_{b_2}},
\tag{5–58}
$$

where $\beta_2 \in \mathbb{R}^+$ is denoted as

$$
\beta_2 = \min\left[\left(\alpha - \frac{b^2\gamma^2}{4}\right),\quad \left(k_{b_3} - 2\bar{\eta}m_2 k_b - \omega k_b^2\tau\right),\quad \frac{1}{\tau}\left(\omega - \frac{2\tau}{\gamma^2}\right)\right].
$$

Since

$$
\int_{t-\tau}^{t}\left(\int_{s}^{t}\left\|u(\theta)\right\|^2 d\theta\right)ds \leq \tau\sup_{s\in[t,t-\tau]}\left[\int_{s}^{t}\left\|u(\theta)\right\|^2 d\theta\right] = \tau\int_{t-\tau}^{t}\left\|u(\theta)\right\|^2 d\theta,
$$

the expression in (5–58) can rewritten as

$$\dot{V} \leq -\left\{\beta_2 - \frac{\rho_2^2(\|z\|)}{4k_{b_1}}\right\} \|z\|^2 - \frac{\tau}{2\gamma^2} \int_{t-\tau}^t \|u(\theta)\|^2 \, d\theta - \frac{1}{2\gamma^2} \int_{t-\tau}^t \left(\int_s^t \|u(\theta)\|^2 \, d\theta\right) + \frac{\varepsilon_2^2}{4k_{b_2}}.$$
(5–59)

Using the definitions of $z(t)$ in (5–47), $y(t)$ in (5–50), and $u(t)$ in (5–42), the expression in (5–59) can be expressed as

$$\dot{V} \leq -\bar{\beta}_2 \|y\|^2 - \left\{\beta_2 - \frac{\rho_2^2(\|z\|)}{4k_{b_1}}\right\} \|e_z\|^2 + \frac{\varepsilon_2^2}{4k_{b_2}},$$
(5–60)

where $\bar{\beta}_2(\|z\|) \in \mathbb{R}^+$ is defined as

$$\bar{\beta}_2 = \min\left[\left(\beta_2 - \frac{\rho_2^2(\|z\|)}{4k_{b_1}}\right), \frac{k_b\tau}{\gamma^2\bar{\eta}m_2}, \frac{1}{2\omega\gamma^2}\right].$$

By further utilizing (5–52), the inequality in (5–60) can be written as

$$\dot{V} \leq -\frac{\bar{\beta}_2}{\lambda_2}V + \frac{\varepsilon_2^2}{4k_{b_2}}.$$
(5–61)

Consider a set $\mathcal{S}$ defined as

$$\mathcal{S} \triangleq \left\{z(t) \in \mathbb{R}^{3n} \mid \|z\| < \rho_2^{-1}\left(2\sqrt{\beta_2 k_{b_1}}\right)\right\}.$$
(5–62)

In $\mathcal{S}$, $\bar{\beta}_2(\|z\|)$ can be lower bounded by a constant $\delta_2 \in \mathbb{R}^+$ as

$$\delta_2 \leq \bar{\beta}_2(\|z\|).$$
(5–63)

Based on (5–63), the linear differential equation in (5–61) can be solved as

$$V \leq V(0)e^{-\frac{\delta_2}{\lambda_2}t} + \frac{\varepsilon_2^2\lambda_2}{4k_{b_2}\delta_2}\left[1 - e^{-\frac{\delta_2}{\lambda_2}t}\right],$$
(5–64)

provided $\|z\| < \rho_2^{-1}\left(2\sqrt{\beta_2 k_{b_1}}\right)$. From (5–64), if $z(0) \in \mathcal{S}$ then k_b can be chosen according to the sufficient conditions in (5–49) (i.e. a semi-global result) to yield result in (5–48). Based on the definition of $y(t)$, it can be concluded that $e_1(t), e_2(t) \in \mathcal{L}_\infty$ in $\mathcal{S}$. Given that $e_1(t), e_2(t), q_d(t), \dot{q}_d(t) \in \mathcal{L}_\infty$ in $\mathcal{S}$, (5–4), (5–42), and (5–37) indicate that $q(t), \dot{q}(t), u \in \mathcal{L}_\infty$ in $\mathcal{S}$.

5.4   Experimental Results and Discussion

Experiments for the developed controllers were conducted on a two-link robot
shown in Fig. 5-1. Each robot link is mounted on an NSK direct drive switched

Figure 5-1. Experimental testbed consiting of a 2-link robot. The input delay in the
system was artificially inserted in the control software.

reluctance motor (240.0 Nm Model YS5240-GN001, and 20.0 Nm Model YS2020-GN001,
respectively). The NSK motors are controlled through power electronics operating
in torque control mode. Rotor positions are measured through motor resolver with
a resolution of 614400 pulses/revolution. The control algorithms were executed on a
Pentium 2.8 GHz PC operating under QNX. Data acquisition and control implementation
were performed at a frequency of 1.0 kHz using the ServoToGo I/O board. Input delay
was artificially inserted in the system through the control software (i.e., the control
commands to the motors were delayed by a value set by the user). The developed
controllers were tested for various values of input delay ranging from 1 ms to 200 ms.
The desired link trajectories for link 1 $(q_{d_1}(t))$ and link 2 $(q_{d_2}(t))$ were selected as (in
degrees):

$$q_{d_1}(t) = q_{d_2}(t) = 20.0sin(1.5t)(1 - exp(-0.01t^3)).$$

The controller developed in (5–8) (*PID controller with delay compensation*) and the controller developed in (5–42) (*PD controller with delay compensation*) were compared with traditional PID and PD controllers, respectively, in the presence of input delay in the system. The input delayed two link robot dynamics are modeled as

$$
\begin{bmatrix} u_{1\tau} \\ u_{2\tau} \end{bmatrix} = \begin{bmatrix} p_1 + 2p_3 \cos(q_2) & p_2 + p_3 \cos(q_2) \\ p_2 + p_3 \cos(q_2) & p_2 \end{bmatrix} \begin{bmatrix} \ddot{q}_1 \\ \ddot{q}_2 \end{bmatrix} + \begin{bmatrix} -p_3 \sin(q_2)\dot{q}_2 & -p_3 \sin(q_2)(\dot{q}_1 + \dot{q}_2) \\ p_3 \sin(q_2)\dot{q}_1 & 0 \end{bmatrix}
$$
$$
\begin{bmatrix} \dot{q}_1 \\ \dot{q}_2 \end{bmatrix} + \begin{bmatrix} f_{d_1} & 0 \\ 0 & f_{d_2} \end{bmatrix} \begin{bmatrix} \dot{q}_1 \\ \dot{q}_2 \end{bmatrix} + \begin{bmatrix} f_{s_1} & 0 \\ 0 & f_{s_2} \end{bmatrix} \begin{bmatrix} \tanh(\dot{q}_1) \\ \tanh(\dot{q}_2) \end{bmatrix},
$$

where p_1, p_2, p_3, f_{d_1}, f_{d_2}, f_{s_1}, $f_{s_2} \in \mathbb{R}^+$ are unknown constants, and $\tau \in \mathbb{R}^+$ is the user-defined time delay value. However, the following values: $p_1 = 3.473 kg.m^2$, $p_2 = 0.196 kg.m^2$, and $p_3 = 0.242 kg.m^2$ were used to calculate the inverse inertia matrix for implementing the *PID controller with delay compensation* but were not used to implement the *PD controller with delay compensation*.

The control gains for the experiments were obtained by choosing gains and then adjusting based on performance (in particular, torque saturation). If the response exhibited a prolonged transient response (compared with the response obtained with other gains), the proportional gains were adjusted. If the response exhibited overshoot, derivative gains were adjusted. At a particular input delay value, the control gains were first tuned for the *PID/PD controllers with delay compensation* and then compared with traditional PID/PD controllers. Using the same control gains values as in the *PID/PD controllers with delay compensation*, the control torques for the traditional PID/PD controllers reached pre-set torque limits, leading to an incomplete experimental trial (e.g., if the control torque reaches 20 Nm, which is the set torque limit for the link-2 motor, the

control software aborts the experimental trial[2]). Therefore, for each case of input delay (except at 1 ms), control gains for the traditional PID/PD controllers were retuned (i.e., lowered) to avoid torque saturation. In contrast to the above approach, the control gains could potentially have been adjusted using more methodical approaches. For example, the nonlinear system in [124] was linearized at several operating points and a linear controller was designed for each point, and the gains were chosen by interpolating, or scheduling the linear controllers. In [125], a neural network is used to tune the gains of a PID controller. In [126] a genetic algorithm was used to fine tune the gains after initial guess were made by the controller designer. The authors in [127] provide an extensive discussion on the use of extremum seeking for tuning the gains of a PID controller. Additionally, in [128], the tuning of a PID controller for robot manipulators is discussed.

The experimental results are summarized in Table 5-1. The error and torque plots for the case when the input delay is 50 ms (as a representative example) are shown in Figs. 5-3-5-4. The *PD controller with delay compensation* was also tested to observe the sensitivity of the B gain matrix, defined in (5–37), where the input delay was selected as 100 ms. Each element of the B gain matrix was incremented/decremented by a certain percentage from the inverse inertia matrix (see Table 5-2). The purpose of this set of experiments was to show that the gain condition discussed in Remark 1 is a sufficient but not a necessary condition, and to explore the performance/robustness of the controller in (5–42) given inexact approximations of the inertia matrix. The controller exhibited no significant degradation, even when each element of the inertia matrix is over-approximated by 100%. However, underestimating the inverse inertia matrix (particularly when deviation from the inverse inertia matrix was 75 percent),

---

[2] Instead of aborting the experimental trial, the experiments could have also been performed by utilizing the saturation torque as the control torque in case the computed torque reaches or exceeds the torque limit; but for comparison purposes, the aforementioned criterion was chosen.

yielded increased tracking errors. Different results may be obtained for different systems. The third set of experiments, given in Table 5-3 were conducted to show that promising results can be obtained even when the input delay value is not exactly known; however, the tracking error performance degrades with increasing inaccuracy in delay value approximation (e.g., in the case of PD + compensator, the tracking error increases significantly when the delay value is overestimated by 80% or greater). For this set of experiments the input delay was chosen to be 100 ms.

The experimental results clearly show that the *PID/PD controllers with delay compensation* perform better than the traditional PID/PD controllers. Both controllers can be divided into respective PID/PD components and predictor (delay compensating) terms. The better performance shown by the controllers can be attributed to the predictor components in both the controllers. As an illustrative example, Fig. 5-2 shows the time plots of the *PD controller with delay compensation* and its control components. The two components: PD component and delay compensating term are plotted to show their behavior with respect to each other. The plot shows that the delay compensating component is always following the PD component but is opposite in sign (like an mirror image but less in magnitude). Thus, the net (actual) control torque is always less than the PD control component. This implies that the delay compensating term tends to correct the PD component (acts as a primary torque generator) which may have compiled extraneous torque due to the input delay. The delay compensating term predicts the correction term by finitely integrating control torque over the time interval ranging from current time minus the time delay to current time.

5.5   Delay compensation in NMES through Predictor-based Control

The primary goal of the input delay research was to compensate for Electromechanical delay (EMD) in NMES. EMD in muscle force generation is defined as the difference in time from the arrival of action potential at the neuromuscular junction to the development of tension in the muscle [8]. In NMES control, the EMD is modeled as an input delay
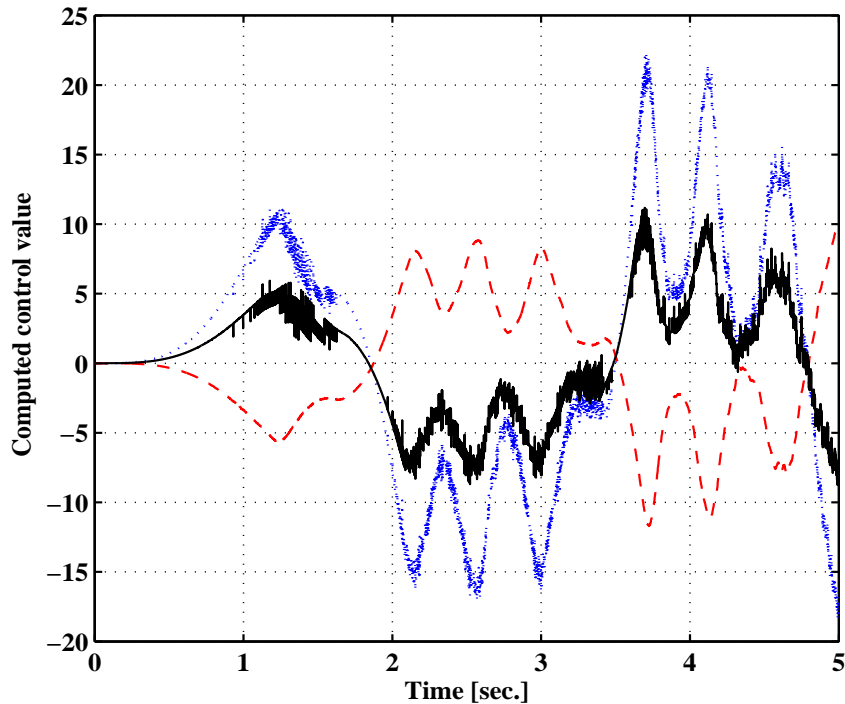
Figure 5-2. The plot shows three torque terms: PD component shown in dotted line, delay compensating term plotted in dashed line, and the net or actual control torque shown in solid line. The PD component and the delay compensating term (finite integral term of control values) are two components of the *PD controller with delay compensation* (actual control torque). Note that the delay compensating term is always opposite in sign to the PD component. Thus, the net control torque is always less than the PD controller. This implies that the delay compensating term tends to correct the PD component which may have compiled extraneous torque due to the input delay. The predictor term computes the correction term by finitely integrating control torque over the time interval ranging from current time minus the time delay to current time.

in the musculoskeletal dynamics [6] and occurs due to finite conduction velocities of the

chemical ions in the muscle in response to the external electrical input [36]. Input delay

can cause performance degradation as was observed during NMES experimental trials

on human subjects with RISE and NN+RISE controllers and has also been reported to

potentially cause instability during human stance experiments with NMES [40].

5.5.1 Experiments: Input Delay Characterization

Experiments were conducted to characterize input delay in healthy individuals during

NMES. The testbed consisted of LEM (detailed in Section 3.4.4.1). The delay in NMES

RMS Error								
Controller	PID		PID + CPTR		PD		PD + CPTR	
Time Delay	Link1	Link2	Link1	Link2	Link1	Link2	Link1	Link2
1 ms	0.106°	0.089°	0.109°	0.087°	0.077°	0.083°	0.077°	0.076°
2 ms	0.107°	0.125°	0.113°	0.092°	0.065°	0.151°	0.069°	0.065°
5 ms	0.129°	0.370°	0.115°	0.077°	0.061°	0.291°	0.076°	0.082°
10 ms	0.089°	0.285°	0.131°	0.091°	0.057°	0.505°	0.089°	0.088°
50 ms	1.954°	1.272°	0.370°	0.335°	1.037°	1.602°	0.407°	0.336°
100 ms	3.137°	6.605°	1.078°	0.726°	3.182°	5.595°	1.159°	0.729°
200 ms	7.629°	6.778°	3.118°	3.626°	14.532°	17.586°	3.625°	2.375°
Maximum Absolute Peak Error								
1 ms	0.164°	0.173°	0.169°	0.178°	0.124°	0.158°	0.127°	0.150°
2 ms	0.172°	0.230°	0.179°	0.18°	0.105°	0.275°	0.114°	0.125°
5 ms	0.204°	0.642°	0.179°	0.161°	0.108°	0.509°	0.127°	0.150°
10 ms	0.149°	0.512°	0.207°	0.211°	0.107°	0.707°	0.147°	0.200°
50 ms	3.430°	2.068°	0.671°	1.196°	1.776°	2.998°	0.774°	1.193°
100 ms	6.484°	11.603°	1.964°	2.415°	5.930°	11.551°	1.915°	2.333°
200 ms	14.960°	12.569°	6.600°	10.466°	24.629°	32.726°	5.520°	6.878°

Table 5-1. Summarized experimental results of traditional PID/PD controllers and the PID/PD controllers with delay compensation. The controllers were tested for different input delay values ranging from 1 ms to 200 ms. CPTR stands for compensator.

Elementwise percentage change in inverse inertia matrix	RMS Error	
	Link1	Link2
0	1.172°	1.005°
+10	1.246°	1.168°
−10	1.078°	0.955°
−50	1.583°	1.491°
+50	1.540°	1.249°
+100	1.191°	1.086°
−75	2.948°	1.331°

Table 5-2. Results compare performance of the PD controller with delay compensation, when the B gain matrix is varied from the known inverse inertia matrix. The input delay value was chosen to be 100 ms. The results indicate that large variations in the gain matrix may be possible.

was measured as the difference between the time when voltage is applied to the muscle and the time when the angle encoder detects the first leg movement. The input delay values were measured for ten healthy individuals (9 male and 1 female). The tests on each individual investigated the effect on input delay of three stimulation parameters: frequency, pulsewidth, and voltage. Three different set of tests including: frequency vs

Percent uncertainty in input delay	RMS Error			
	PD + Compensator		PID + Compensator	
	Link1	Link2	Link1	Link2
0%	1.159°	0.730°	1.078°	0.726°
(+)10%	1.234°	0.966°	0.937°	0.910°
(−)10%	1.079°	1.215°	0.756°	0.410°
(+)20%	1.338°	1.548°	1.304°	1.810°
(−)20%	1.192°	1.773°	0.782°	0.617°
(+)30%	1.451°	1.761°	1.498°	0.659°
(−)30%	1.452°	1.322°	0.768°	0.609°
(+)50%	1.629°	2.513°	2.242°	1.181°
(−)50%	1.186°	1.450°	0.987°	0.907°
(+)80%	3.528°	6.819°	3.092°	1.510°
(−)80%	1.229°	5.408°	0.915°	2.053°
(+)90%	4.099°	12.020°	3.322°	1.836°
(−)90%	3.260°	6.041°	0.874°	2.461°
(+)100%	4.331°	12.445°	4.219°	3.101°
(−)100%	3.182°	5.595°	3.137°	6.605°

Table 5-3. Experimental results when the input delay has uncertainty. The input delay value was selected as 100 ms.

input delay, voltage vs input delay, and pulsewidth vs input delay were performed on each individual. In each set of experiments, the other two stimulation parameters were kept constant. Before the start of experiments, the subject was instructed to relax to avoid voluntary leg motion. The threshold voltage was measured for each subject which can be defined as the minimum voltage applied to the subject's muscle that produces a movement large enough to be detected by the angle encoder. This measurement was performed by applying a constant input voltage, beginning at 10 V and increasing the voltage slightly until movement was detected. Once the threshold voltage was obtained, the aforementioned three sets of experiments were performed for each individual.

The first set of experiments constituted varying frequency while keeping voltage and pulsewidth constant. These tests consisted of measuring the input delay of the subject's muscle for three 0.2 second impulses, each 5 seconds apart. Each impulse imparted a constant voltage (threshold voltage + 10 V) to the muscle. The 5 second time separation between the impulses allowed the subjects to voluntarily bring their leg back to the

Figure 5-3. The top-left and bottom-left plots show the errors of Link 1 and Link 2, respectively, obtained from the PID controller with delay compensation and a traditional PID controller. The top-right and bottom-right plots show the errors of Link 1 and Link 2, respectively, obtained from the PD controller with delay compensation and a traditional PD controller. Errors obtained from the PID/PD + delay compensator are shown as solid lines and the errors obtained from the traditional PID/PD controller are shown as dash-dot lines. The input delay was chosen to be 50 ms.

rest position. Fig. 5-5 shows the typical EMD during NMES in a healthy individual.

Final input delay value was computed by averaging the measured delay values over three

impulses. Eight experiments were performed for different frequencies, where the frequency

was chosen randomly from the range of 30 Hz and 100 Hz (intra range interval of 10
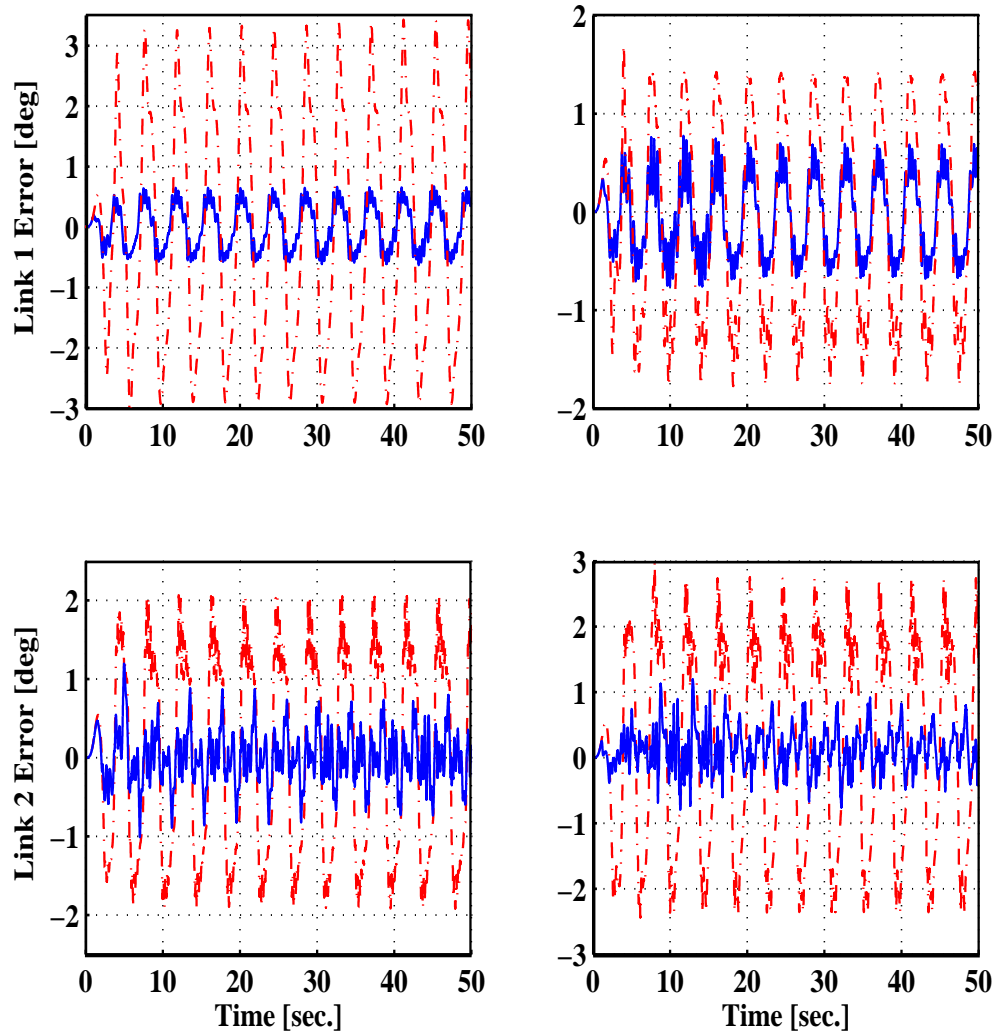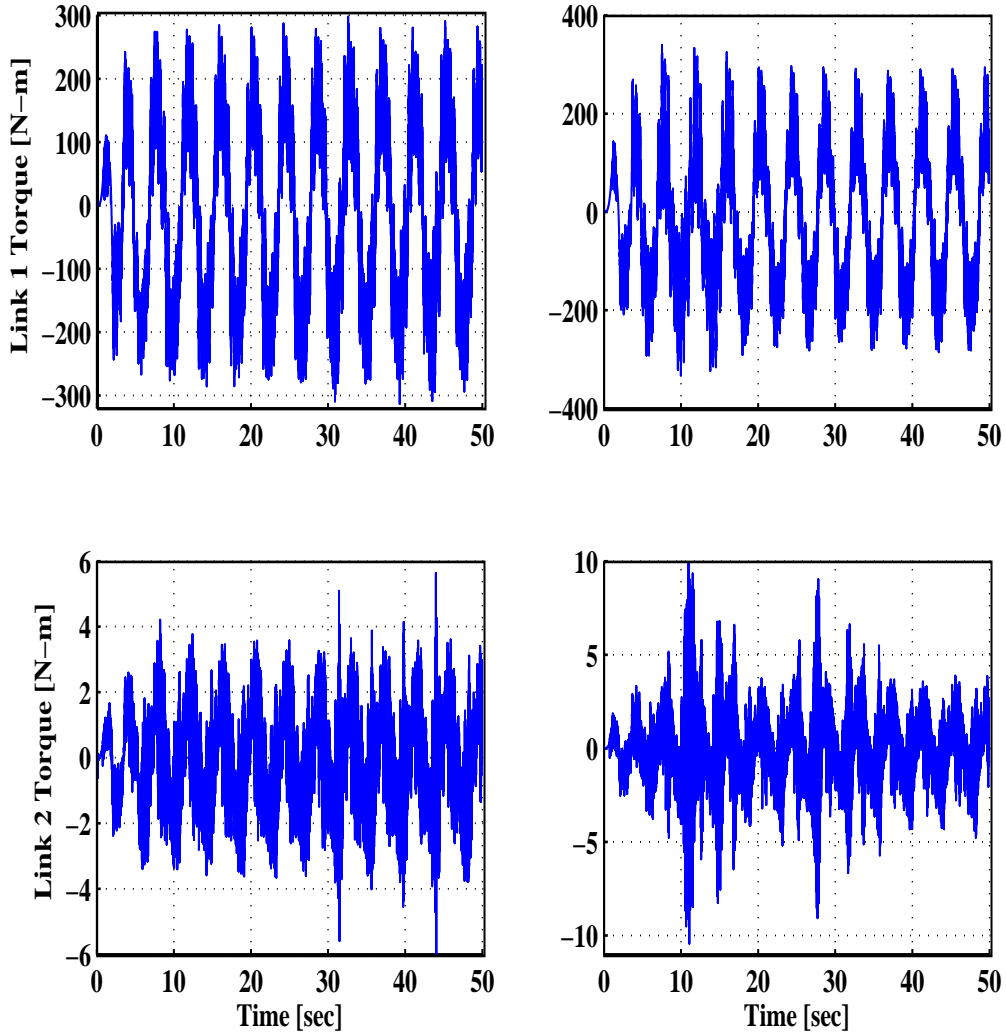
Figure 5-4. The top-left and bottom-left plots show the torques of Link 1 and Link 2, respectively, obtained from the PID controller with delay compensation. The top-right and bottom-right plots show the torques of Link 1 and Link 2, respectively, obtained from the PD controller with delay compensation. The input delay was chosen to be 50 ms.

Hz). The pulse width for this type of the experiments was kept at $100\mu s$. The second type of experiments consisted of varying pulsewidth while keeping voltage and frequency constant. Each experiment constituted three impulses as explained above for the frequency tests. Nine experiments were performed for different pulsewidths, where pulsewidth was randomly chosen from $100\mu s$. to $1000\mu s$ (intra range interval of $100\mu s$). For this set
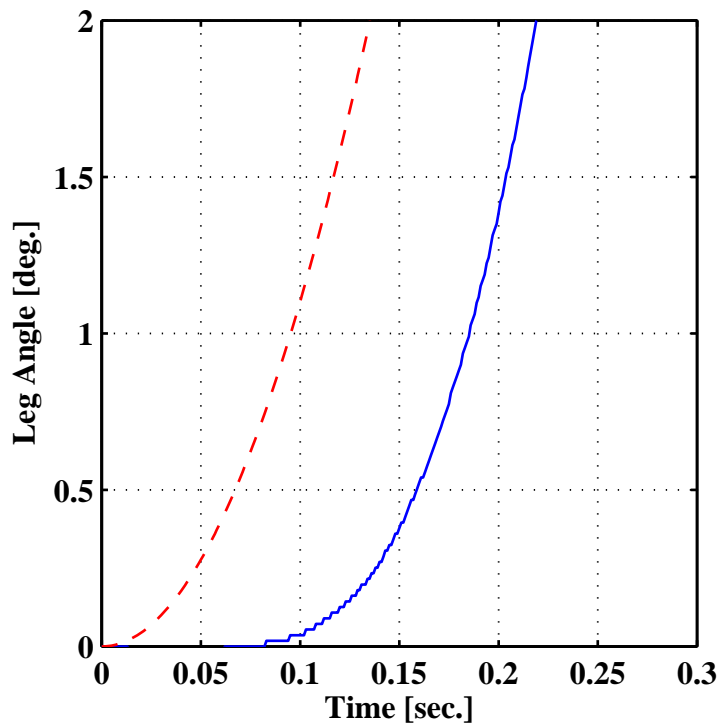
Figure 5-5. Typical input delay during NMES in a healthy individual. The desired trajectory is shown in dashed line and the actual leg angle is shown in solid line. Note that the actual leg angle starts rising around 70 ms.

of experiments, the frequency was kept constant at 30 Hz and the voltage consisted of minimum threshold voltage $+$ 10 V. The last set of experiments involved conducting experiments with varying voltages. Same impulse program as used in the earlier set of experiments was used, where pulsewidth and frequency were kept constant. The frequency was kept at 30 Hz and the pulse width was kept at 100 mus. Three experiments were performed for different voltages (threshold voltage $+$ additional voltage, where additional voltage was varied between 5 and 20 volts (intra range interval of 5 volts). Table 5-4 (as a representative example) shows the summarized input delay variations with respect to different stimulation parameters in a healthy individual.

ANOVA (Analysis of variance) tests were performed to determine the intraclass correlations. An ANOVA test is generally employed to determine the statistical significance between the means of data groups numbering more than two (using student t-test to

determine the statistical significance between more than two data groups can lead to Type-I error (i.e., rejection of null hypothesis which in reality is true)). The results of the stimulation frequency testing (see Fig. 5-6) showed that the difference in the means of EMD was statistically significant (P-$value = 1.50372E - 10$). Further, post-hoc test utilizing Tukey's method showed that the EMD was longer for the lower frequencies than for the higher frequencies. Particularly, the test showed that the average EMD of 76 ms at a frequency of 30 Hz is statistically different from the average EMD of 51 ms at a frequency of 100 Hz. However, the results of the stimulation pulse width (see Fig. 5-8) and voltage experiments (see Fig. 5-7) showed no significant correlation between either varying stimulation pulsewidth or stimulation voltage and electromechanical delay (P-$value = 0.6870$ and 0.072, respectively).
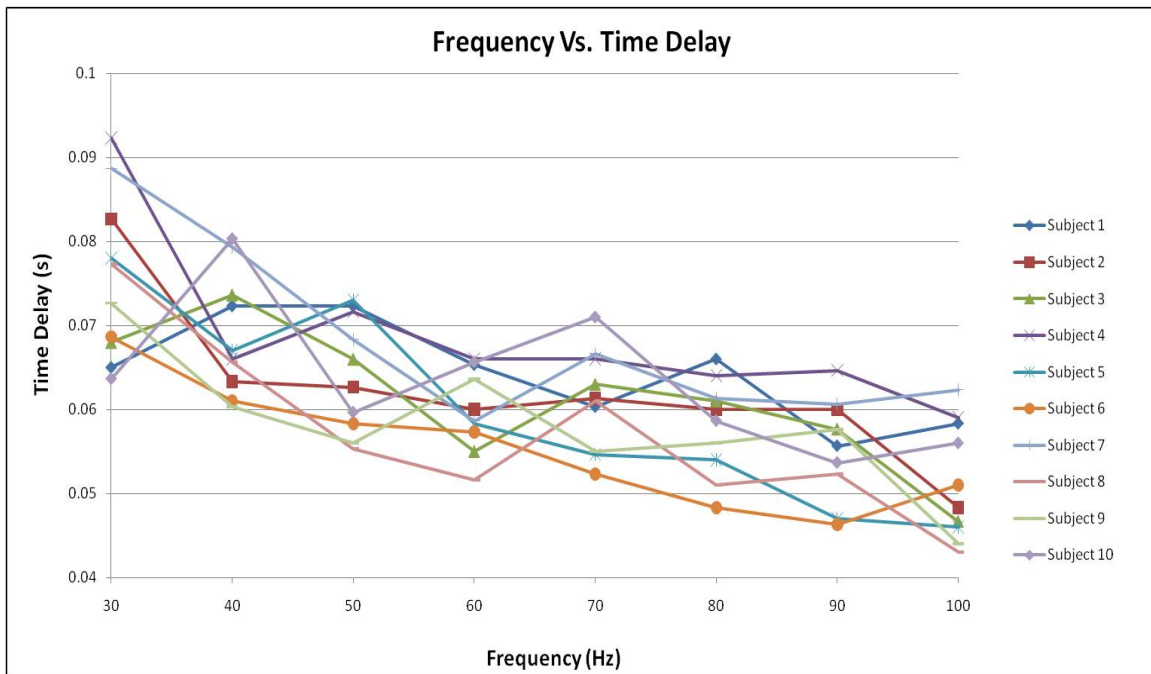
Figure 5-6. Average input delay values across different frequencies.

5.5.2 Experiments: PD Controller with Delay Compensation

The challenge in implementing the controllers in (5–8) and (5–42) is to measure inertia and input delay in the muscle dynamics. Implementing the controller in (5–8) becomes even more complicated due to the fact that it requires not only inertia of the
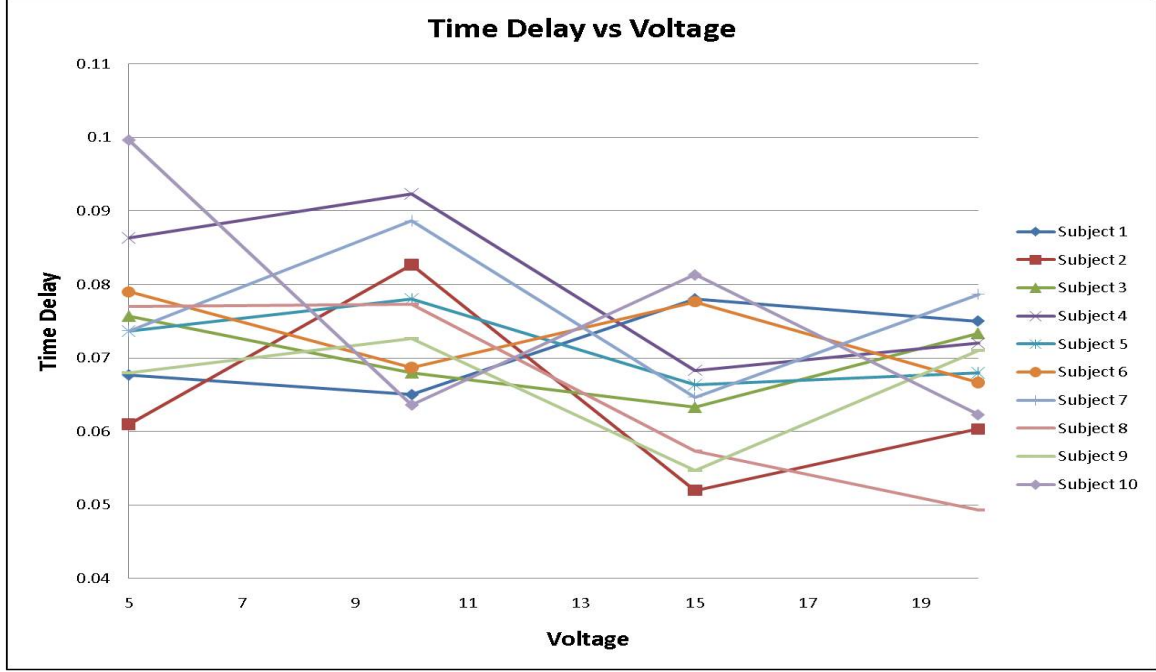
Figure 5-7. Average input delay values across different voltages.

musculoskeletal-LEM system to be measured but also the auxiliary function $\Omega(q, \dot{q}, t) \in \mathbb{R}$ defined in (2–8), which consists of unmeasurable muscle force-velocity and muscle force-length relationships to be known. However, the controller defined in (5–42) can be implemented provided the following assumptions are made.

Assumption 1: The input delay is measurable and is constant. Although the input delay for the NMES system is measurable but may not be constant due to variety of factors such as fatigue, non-isometric contractions, type of task, or stimulation parameters. However, these variations are likely to be minimal in the duration of a single trial, and the fact that the new controllers are shown to be robust to uncertainty in the input delay value (see Table 5-3).

Assumption 2: The function J_Ω introduced in (3.3) can be upper bounded as

$$a_1 \leq |J_\Omega| \leq a_2, \qquad \left| B - J_\Omega^{-1} \right| \leq a_3 \tag{5–65}$$

where a_1, a_2, $a_3 \in \mathbb{R}$ are some known positive constants, and B is the control gain introduced in (5–37).
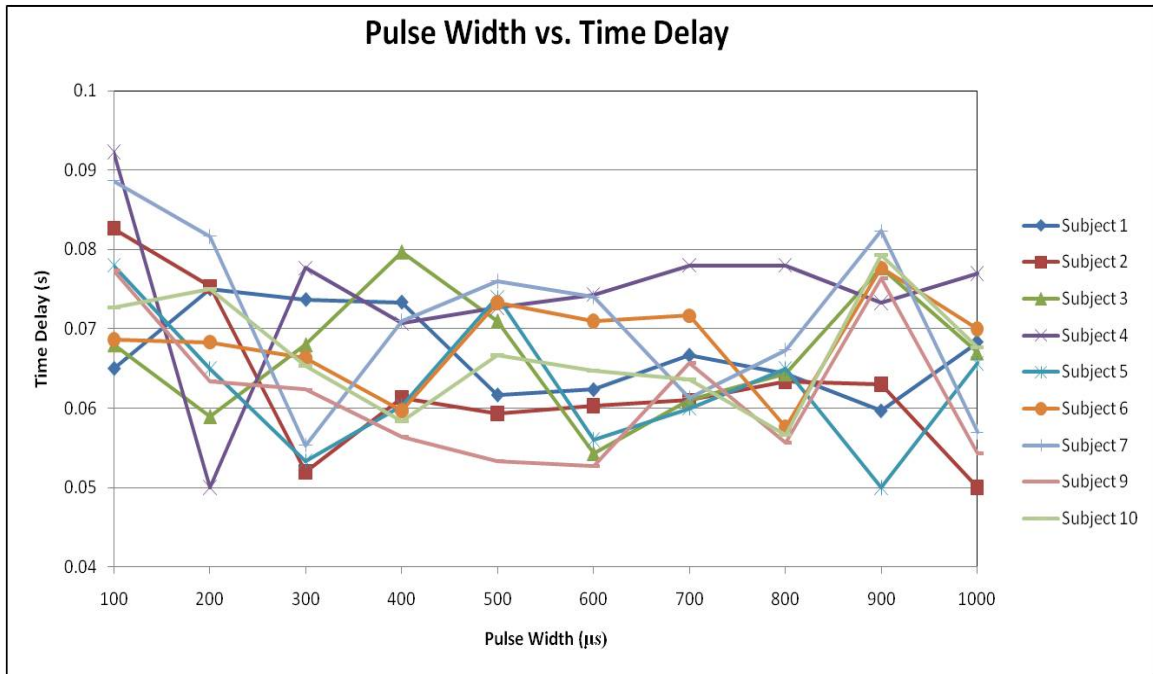
Figure 5-8. Average input delay values across different pulsewidths.

The testbed for experiments consisted of LEM (detailed in Section 3.4.4.1). The control objective was to track a continuous constant period (2 sec.) sinusoidal trajectory. Three healthy males (age: 21-28yrs) were chosen as the test subjects. After the protocol (see section 3.4.4.1), the input delay value was measured for each subject. The measured delay value was utilized for implementing the *PD controller with delay compensation* and throughout the duration of trials, the same respective measured delay value was used for each subject. The experiments compared the traditional PD controller with the *PD controller with delay compensation*. Each subject participated in two to four trials for each controller [3] The experimental results obtained for each controller are summarized in Table 5-5. The table shows best two results (results with minimum RMS errors out of all trials) obtained from each controller and subject.

---

[3] maximum number of trials are limited due to increasing discomfort that arises due to rapid muscle fatigue.

Frequency [Hz]	Pulsewidth [μ sec.]	Voltage [V]	τ_1	τ_2	τ_3	Avg. τ
30	100	10	0.069	0.053	0.073	0.065
40	100	10	0.076	0.064	0.077	0.072
50	100	10	0.073	0.069	0.075	0.072
60	100	10	0.062	0.074	0.06	0.065
70	100	10	0.064	0.066	0.051	0.060
80	100	10	0.062	0.059	0.077	0.066
90	100	10	0.062	0.057	0.048	0.056
100	100	10	0.055	0.061	0.059	0.058
30	200	10	0.065	0.066	0.094	0.075
30	300	10	0.07	0.072	0.079	0.074
30	400	10	0.065	0.065	0.09	0.073
30	500	10	0.058	0.056	0.071	0.062
30	600	10	0.05	0.073	0.064	0.062
30	700	10	0.065	0.077	0.058	0.067
30	800	10	0.065	0.067	0.061	0.064
30	900	10	0.071	0.053	0.055	0.060
30	1000	10	0.057	0.083	0.065	0.068
30	100	5	0.081	0.061	0.061	0.068
30	100	15	0.068	0.079	0.087	0.078
30	100	20	0.082	0.084	0.059	0.075

Table 5-4. Summarized input delay values of a healthy individual across different stimulation parameters. Delay values (τ) are shown in seconds. The voltages shown in column 3 are the added voltages to the threshold voltage.

A Student's t-test was also performed to confirm statistical significance in the mean differences of the RMS errors, maximum steady state errors (SSEs), RMS voltages, and the maximum voltages. The statistical comparison was conducted on the averages of the two best results obtained for each subject. The analysis shows that the mean differences in the RMS errors, maximum SSEs, and maximum voltages are statistically significant while the analysis shows no statistical difference in the RMS voltages. The mean RMS error of 4.43° obtained with the *PD controller with delay compensation* is lower than the RMS error of 6.03° obtained with the PD controller. Also, the mean maximum SSE and the mean maximum voltage obtained with the *PD controller with delay compensation* are lower than the mean maximum SSE and the mean maximum voltage obtained with the traditional PD controller. The respective p-values are given in the Table 5-5. The actual

leg angle, error, and voltage plots obtained from subject C (as a representative example) are shown in Figs. 5-9 and 5-10.

Figure 5-9. Top plot: Actual limb trajectory of a subject (solid line) versus the desired trajectory (dashed line) input obtained with the *PD controller with delay compensation.* Middle plot: The tracking error (desired angle minus actual angle) of a subject's leg, tracking a constant (2 sec.) period desired trajectory. Bottom plot: The computed voltage of the *PD controller with delay compensation* during knee joint tracking.

5.6   Conclusion

Control methods are developed for a class of an unknown Euler-Lagrange systems with input delay. The designed controllers have a predictor-based structure to compensate for delays in the input. LK functionals are constructed to aid the stability analysis which yields a semi global uniformly ultimately bounded result. The experimental results show that the developed controllers have improved performance when compared to
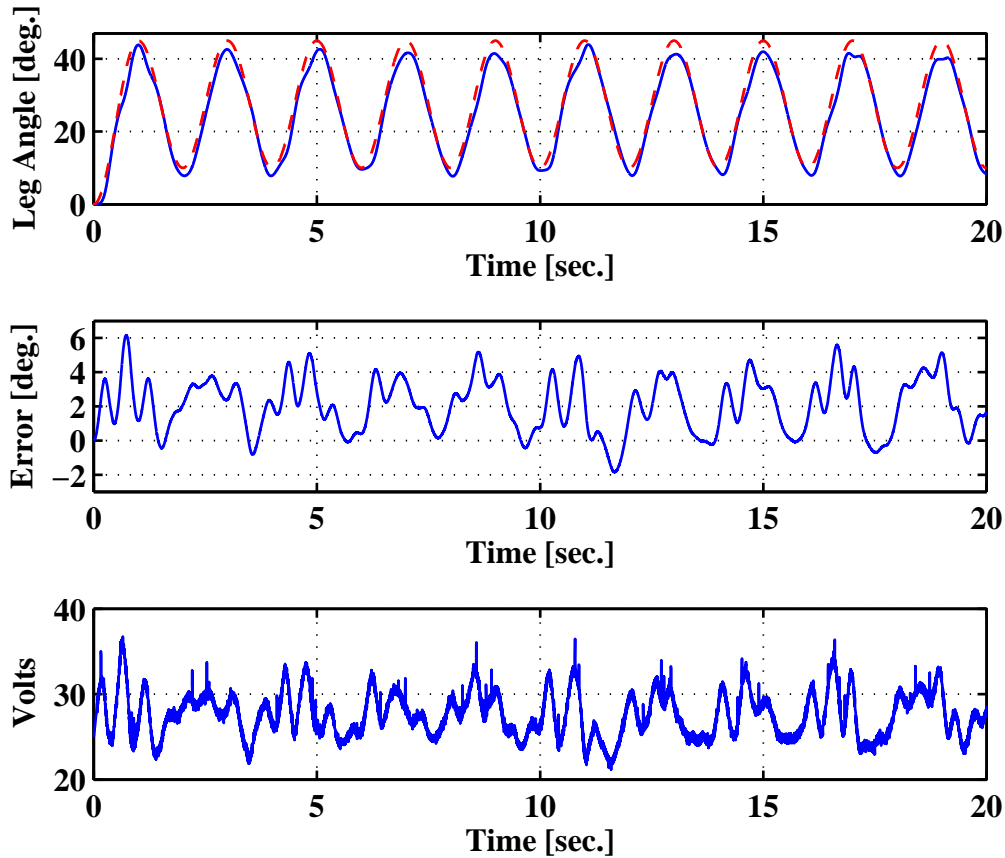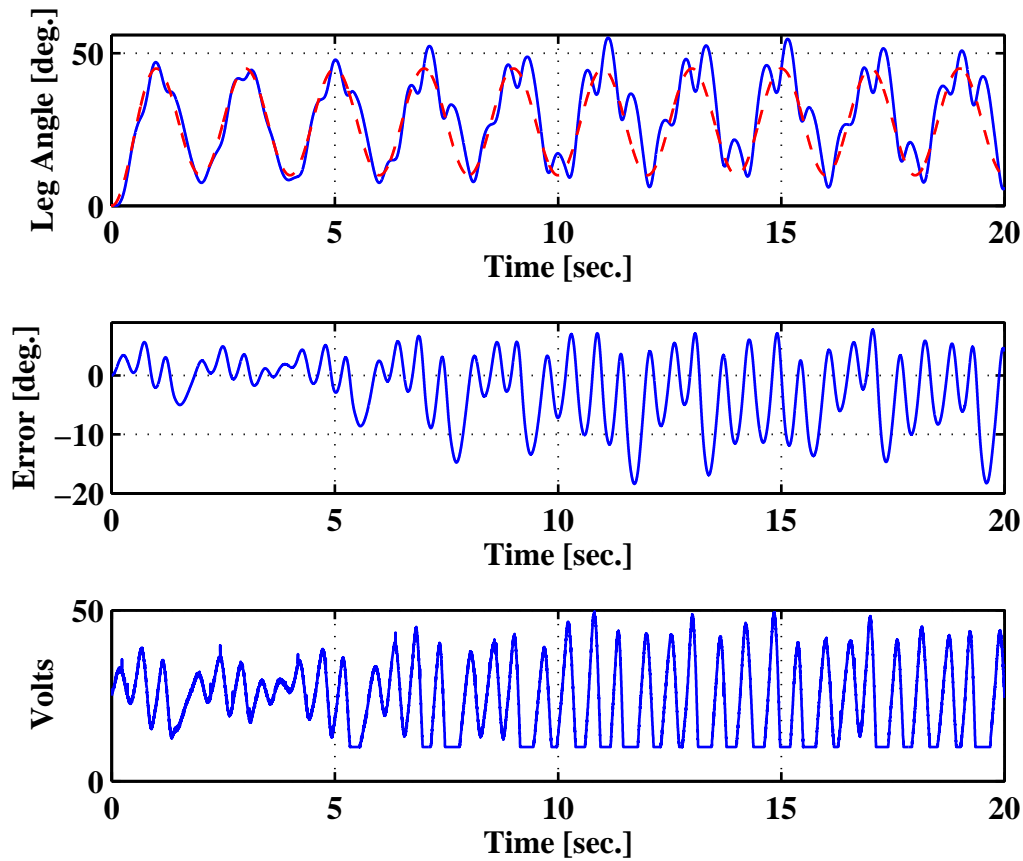
Figure 5-10. Top plot: Actual limb trajectory of a subject (solid line) versus the desired trajectory (dashed line) input, obtained with the traditional PD controller. Middle plot: The tracking error (desired angle minus actual angle) of a subject's leg, tracking a constant (2 sec.) period desired trajectory. Bottom plot: The computed PD voltage during knee joint tracking. Note that the voltage saturates at the user-defined set lower voltage threshold of 10 V

traditional PID/PD controllers in the presence of input delay. Additional experiments on healthy individuals showed that the PD controller with delay compensation is capable to compensate for input delay in NMES and also performs better than the traditional PD controller. A key contribution is the development of the first ever controllers to address delay in the input of an uncertain nonlinear system. The result has been heretofore an open challenge because of the need to develop a stabilizing predictor for the dynamic response of an uncertain nonlinear system. To develop the controllers, the time delay

Subject	RMS Error		RMS Voltage [V]		Max. SSE		Max. Voltage [V]	
	PD	PD +CTR	PD	PD +CTR	PD	PD +CTR	PD	PD +CTR
A	4.48°	5.26°	31.49	33.18	11.84°	11.51°	42.95	42.02
A	7.63°	3.52°	29.30	32.26	20.41°	9.04°	50	44.38
B	8.48°	6.35°	20.93	22.93	25.78°	9.611°	45.1	27.43
B	6.54°	5.96°	24.72	22.65	10.79°	10.72°	31.28	26.51
C	3.11°	2.85°	25.58	26.17	12.84°	5.68°	43.68	38.8
C	5.91°	2.61°	23.65	27.60	16.66°	5.6°	49.33	36.7
Mean	6.03°	4.43°	25.95	27.47	16.37°	8.69°	43.72	35.97
p value	0.003*		0.095		0.008*		0.040*	

Table 5-5. Table compares the experimental results obtained from the traditional PD controller and the *PD controller with delay compensation*. * indicates statistical significance and CTR stands for compensator.

was required to be a known constant. While some applications have known delays (e.g., teleoperation [129], some network delays [130], time constants in biological systems [6, 36]), the development of more generalized results (which have been developed for some linear systems) with unknown time delays remains an open challenge. However, the experimental results with two-link robot illustrated some robustness with regard to the uncertainty in the time delay.

CHAPTER 6
RISE-BASED ADAPTIVE CONTROL OF AN UNCERTAIN NONLINEAR SYSTEM WITH UNKNOWN STATE DELAYS

6.1 Introduction

The development in this chapter is motivated by the lack of continuous robust controllers that can achieve asymptotic stability for a class of uncertain time-delayed nonlinear systems with additive bounded disturbances. The approach described in the current effort uses a continuous implicit learning [96] based Robust Integral of the Sign of the Error (RISE) structure [11, 27]. Due to the added benefit of reduced control effort and improved control performance, an adaptive controller in conjunction with RISE feedback structure is designed. However, since the time delay value is not always known, it becomes challenging to design a delay free adaptive control law. Through the use of a desired compensation adaptive law (DCAL) based technique and segregating the appropriate terms in the open loop error system, the dependence of parameter estimate laws on the time delayed unknown regression matrix is removed. Contrary to previous results, there is no singularity in the developed controller. A Lyapunov-based stability analysis is provided that uses an LK functional along with Young's inequality to remove time delayed terms and achieves asymptotic tracking.

6.2 Problem Formulation

Consider a class of uncertain nonlinear systems with an unknown state delay as [87]

$$
\begin{aligned}
\dot{x}_1 &= x_2 \\
&\quad . \\
&\quad . \\
&\quad . \\
\dot{x}_{n-1}(t) &= x_n \\
\dot{x}_n(t) &= f(x(t)) + \delta_1(x(t)) + g(x(t-\tau)) + \delta_2(x(t-\tau)) + d(t) + bu(t) \\
y &= x_1
\end{aligned}
\tag{6–1}
$$

In (6–1), $f(x(t))$, $\delta_1(x(t)) \in \mathbb{R}^m$ are unknown functions, $g(x(t - \tau))$, $\delta_2(x(t - \tau)) \in \mathbb{R}^m$ are unknown time-delayed functions, $\tau \in \mathbb{R}^+$ is an unknown constant arbitrarily large time delay, $d(t) \in \mathbb{R}^m$ is a bounded disturbance, $b \in \mathbb{R}$ is an unknown positive constant, $u(t) \in \mathbb{R}^m$ is the control input, and $x(t) \triangleq \left[x_1^T \ x_2^T \ \ldots \ x_n^T \right]^T \in \mathbb{R}^{mn}$ denote system states, where $x(t)$ is assumed to be measurable. Also the following assumptions and notations will be exploited in the subsequent development.

Notation: Throughout the paper, a time dependent delayed function is denoted as $x(t - \tau)$ or x_τ, and a time dependent function (without time delay) is denoted as $x(t)$ or x.

Assumption 1: The unknown functions $b^{-1}f(x)$, $b^{-1}g(x)$ are linearly parameterizable, i.e., $b^{-1}f(x) = Y_1(x)\theta_1$, $b^{-1}g(x) = Y_2(x)\theta_2$, where $Y_1(x) \in \mathbb{R}^{m \times p_1}$, $Y_2(x) \in \mathbb{R}^{m \times p_2}$ are regression matrices of known functions, $\theta_1 \in \mathbb{R}^{p_1 \times 1}$, $\theta_2 \in \mathbb{R}^{p_2 \times 1}$ are constant unknown parameter vectors, and p_1, p_2 are positive integers. The regression matrix $Y_2(x_\tau)$ is not computable due to the unknown time delay present in the state

Assumption 2: If $x(t) \in \mathcal{L}_\infty$, then $g(x)$, $\delta_1(x)$, $\delta_2(x)$ are bounded. Moreover, the first and second partial derivatives of $g(x)$, $\delta_1(x)$, $\delta_2(x)$ with respect to $x(t)$ exist and are bounded (see [83, 87, 95]).

Assumption 3: The disturbance term and its first two time derivatives are bounded (i.e., $d(t)$, $\dot{d}(t)$, $\ddot{d}(t) \in \mathcal{L}_\infty$).

Assumption 4: The desired trajectory is designed such that $y_d(t)$, $y_d^i(t) \in \mathcal{L}_\infty$, where $y_d^{(i)}(t)$ denotes the ith time derivative for $i = 1, 2, ..., n + 2$.

6.3   Error System Development

The control objective is to ensure that the output $y(t) \in \mathbb{R}^m$ tracks a desired time-varying trajectory $y_d(t) \in \mathbb{R}^m$ despite uncertainties in the system and an unknown time delay in the state. To quantify the objective, a tracking error, denoted by $e_1(t) \in \mathbb{R}^m$, is defined as

$$e_1(t) \triangleq y(t) - y_d(t). \tag{6–2}$$

To facilitate the subsequent analysis, following filtered tracking errors are also defined as

$$e_2(t) \triangleq \dot{e}_1(t) + \alpha_1 e_1(t), \tag{6-3}$$

$$e_i(t) \triangleq \dot{e}_{i-1}(t) + \alpha_{i-1} e_{i-1}(t) + e_{i-2}, \tag{6-4}$$

$$r(t) \triangleq \dot{e}_n(t) + \alpha_n e_n(t), \tag{6-5}$$

where $\alpha_1, ..., \alpha_n \in \mathbb{R}$ denote positive constant control gains. As defined in (6–5), the filtered tracking error $r(t)$ is not measurable since the expression depends on $\dot{x}_n(t)$. However, $e_1(t), ..., e_n(t) \in \mathbb{R}^m$ are measurable because (6–4) can be expressed in terms of the tracking error $e_1(t)$ as

$$e_i(t) = \sum_{j=0}^{i-1} a_{ij} e_1^{(j)}, \qquad i = 2, ..., n, \tag{6-6}$$

where $a_{ij} \in \mathbb{R}$ are positive constants obtained from substituting (6–6) in (6–4) and comparing coefficients [114]. It can be easily shown that

$$a_{ij} = 1, \quad j = i - 1. \tag{6-7}$$

Using (6–2)-(6–7), the open loop error system can be written as

$$r = y^{(n)} - y_d^{(n)} + l, \tag{6-8}$$

where $l(e_1, \dot{e}_1, ..., e_1^{(n-1)}) \in \mathbb{R}^m$ is a function of known and measurable terms, defined as

$$l = \sum_{j=0}^{n-2} a_{nj} \left(e_1^{(j+1)} + \alpha_n e_1^{(j)} \right) + \alpha_n e_1^{(n-1)}.$$

The open-loop tracking error system can be developed by premultiplying (6–8) by b^{-1} and utilizing the expressions in (6–1) and Assumption 1 to obtain the following expression:

$$b^{-1}r = Y_1(x)\theta_1 + b^{-1}\delta_1(x) + Y_2(x_\tau)\theta_2 + b^{-1}\delta_2(x_\tau) + b^{-1}d + u - b^{-1}y_d^{(n)} + b^{-1}l. \tag{6-9}$$

In the subsequent development, a DCAL-based update law is developed in terms of $Y_2(\cdot)$ without a state delay. After some algebraic manipulation, the expression in (6–9) can be rewritten as

$$b^{-1}r \;=\; b^{-1}l + S_1 + S_2 + W + b^{-1}d + Y_1(x_d)\theta_1 + Y_2(x_d)\theta_2 + u,$$

where the auxiliary functions $S_1(x_d,\,x)$, $S_2(x_{d\tau},\,x_\tau)$, $W(x_d,\,x_{d\tau},\,y_d^{(n)}) \in \mathbb{R}^m$ are defined as

$$S_1 \;=\; Y_1(x)\theta_1 - Y_1(x_d)\theta_1 + b^{-1}\delta_1(x) - b^{-1}\delta_1(x_d), \tag{6–10}$$

$$S_2 \;=\; Y_2(x_\tau)\theta_2 - Y_2(x_{d\tau})\theta_2 + b^{-1}\delta_2(x_\tau) - b^{-1}\delta_2(x_{d\tau}), \tag{6–11}$$

$$W \;=\; b^{-1}\delta_1(x_d) + b^{-1}\delta_2(x_{d\tau}) - Y_2(x_d)\theta_2 + Y_2(x_{d\tau})\theta_2 - b^{-1}y_d^{(n)}, \tag{6–12}$$

where $x_d \triangleq \left[y_d^T \; \dot{y}_d^T \; \cdots \; \left(y_d^{(n-1)T}\right) \right]^T \in \mathbb{R}^{mn}$ denotes a column vector containing the desired trajectory and its derivatives. The grouping of terms and structure of (6–10) is motivated by the subsequent stability analysis and the need to develop an adaptive update law that is invariant to the unknown time delay. The auxiliary function $S_1(x_d, x)$ is defined because these terms are not functions of the time-delay. The auxiliary function $S_2(x_{d\tau}, x_\tau)$ is introduced because the time-delayed states are isolated in this term, and $W(x_d,\, x_{d\tau},\, \dot{x}_d)$ is isolated because it only contains functions of the desired trajectory.

Based on the open-loop error system in (6–10), the control input $u(t) \in \mathbb{R}^m$ is designed as

$$u = -Y_1(x_d)\hat{\theta}_1 - Y_2(x_d)\hat{\theta}_2 - \mu. \tag{6–13}$$

In (6–13), $\mu \in \mathbb{R}^m$ denotes the implicit learning-based [96] RISE term defined as the generalized solution to

$$\dot{\mu} = (k_s + 1)\,r + \beta sgn(e_n), \quad \mu(0) = 0, \tag{6–14}$$

where k_s, $\beta \in \mathbb{R}$ are known positive constant gains. In (6–13), $\hat{\theta}_1(t) \in \mathbb{R}^{p_1}$, $\hat{\theta}_2(t) \in \mathbb{R}^{p_2}$ denote parameter estimate vectors defined as

$$\dot{\hat{\theta}}_1 = \Gamma_1 \dot{Y}_1^T(x_d)r, \qquad \dot{\hat{\theta}}_2 = \Gamma_2 \dot{Y}_2^T(x_d)r, \tag{6–15a}$$

where $\Gamma_1 \in \mathbb{R}^{p_1 \times p_1}$, $\Gamma_2 \in \mathbb{R}^{p_2 \times p_2}$ are known, constant, diagonal, positive definite adaptation gain matrices. In (6–15a), $\dot{Y}_2^T(x_d)$ does not depend on the time delayed desired state. This delay free law is achieved by isolating the delayed term $Y_2(x_{d\tau})\theta_2$ in the auxiliary signal $W(x_d, x_{d\tau}, y_d^{(n)})$ in (6–12). The adaptation laws in (6–15a) depend on the unmeasurable signal $r(t)$, but by using the fact that $\dot{Y}_1(x_d)$, $\dot{Y}_2(x_d)$ are functions of the known time varying desired trajectory, integration by parts can be used to implement $\hat{\theta}_i(t)$ for $i = 1$, 2 where only $e_n(t)$ is required as

$$\hat{\theta}_i = \hat{\theta}_i(0) + \Gamma_i \dot{Y}_i^T(x_d)e_n(\sigma) \mid_0^t - \Gamma_i \int_0^t \left\{ \ddot{Y}_i^T(x_d)e_n(\sigma) - \alpha_n \dot{Y}_i^T(x_d)e_n(\sigma) \right\} d\sigma.$$

The closed-loop error system can be developed by substituting (6–13) into (6–10) as

$$b^{-1}r = b^{-1}l + S_1 + S_2 + W + b^{-1}d - \mu + Y_1(x_d)\tilde{\theta}_1 + Y_2(x_d)\tilde{\theta}_2, \tag{6–16}$$

where $\tilde{\theta}_i$ for $i = 1$, 2 are the parameter estimation error vectors defined as

$$\tilde{\theta}_i = \theta_i - \hat{\theta}_i. \tag{6–17}$$

To facilitate the subsequent stability analysis and to more clearly illustrate how the RISE structure in (6–14) is used to reject the disturbance terms, the time derivative of (6–16) is determined as

$$b^{-1}\dot{r} = \tilde{N} + N_d - e_n + \dot{Y}_1(x_d)\tilde{\theta}_1 + \dot{Y}_2(x_d)\tilde{\theta}_2 - (k_s + 1)r - \beta sgn(e_n), \tag{6–18}$$

where the auxiliary functions $\tilde{N}(e_1, ...e_n, r, e_{1\tau}, ..., e_{n\tau}, r_\tau)$, $N_d(\dot{x}_d, \ddot{x}_d, t) \in \mathbb{R}^m$ are defined as

$$
\begin{aligned}
\tilde{N} &= b^{-1}\dot{l} + \dot{S}_1 + \dot{S}_2 + e_n - Y_1(x_d)\Gamma_1\dot{Y}_1(x_d)r - Y_2(x_d)\Gamma_2\dot{Y}_2(x_d)r, \\
N_d &= \dot{W} + b^{-1}\dot{d}.
\end{aligned}
\tag{6-19}
$$

Using Assumptions 2, 3, and 4, $N_d(x_d, \dot{x}_d, \ddot{x}_d, t)$ and its time derivative can be upper bounded as

$$
\|N_d\| \leq \zeta_{N_d}, \qquad \left\|\dot{N}_d\right\| \leq \zeta_{\dot{N}_d},
\tag{6-20}
$$

where ζ_{N_d}, $\zeta_{\dot{N}_d} \in \mathbb{R}$ are known positive constants. The expression defined in (6-19) can be upper bounded using the Mean Value Theorem as [114]

$$
\left\|\tilde{N}\right\| \leq \rho_1(\|z\|)\|z\| + \rho_2(\|z_\tau\|)\|z_\tau\|,
\tag{6-21}
$$

where $z(t) \in \mathbb{R}^{(n+1)m}$ is defined as

$$
z = \begin{bmatrix} e_1^T & e_2^T & \cdot & \cdot & \cdot & e_n^T & r^T \end{bmatrix}^T,
\tag{6-22}
$$

and the known bounding functions $\rho_1(\|z\|)$, $\rho_2(\|z\|) \in \mathbb{R}$ are positive, globally invertible, and nondecreasing functions. Note that the upper bound for the auxiliary function $\tilde{N}(e_1, e_2, e_{1\tau}, e_{2\tau})$ in (6-21) is segregated into delay free and delayed upper bound functions. Motivation for this segregation of terms is to eliminate the delay dependent term through the use of an LK functional in the stability analysis. Specifically, let $Q(t) \in \mathbb{R}$ denote an LK functional defined as

$$
Q = \frac{1}{2k_s} \int_{t-\tau}^{t} \rho_2^2(\|z(\sigma)\|)\|z(\sigma)\|^2 \, d\sigma,
\tag{6-23}
$$

where $k_s \in \mathbb{R}$ and $\rho_2(\cdot)$ are introduced in (6-14) and (6-21), respectively.

6.4 Stability Analysis

Theorem 6. *The controller given in (6-13), (6-14), and (6-15a) ensures that all system signals are bounded under closed-loop operation. The tracking error is regulated in the*

sense that

$$\|e_1(t)\| \to 0 \qquad as\ t \to \infty,$$

provided the control gain k_s introduced in (6–14) is selected sufficiently large, and α_{n-1}, α_n, and β are selected according to the following sufficient conditions:

$$\beta > \left(\zeta_{N_d} + \frac{1}{\alpha} \zeta_{\dot{N}_d} \right), \qquad \alpha_{n-1},\ \alpha_n > \frac{1}{2} \tag{6–24}$$

where α_{n-1}, α_n are introduced in (6–4) and (6–5), respectively; β is introduced in (6–14); and ζ_{N_d} and $\zeta_{\dot{N}_d}$ are introduced in (6–20).

Proof: Let $\mathcal{D} \subset \mathbb{R}^{(n+1)m+p_1+p_2+2}$ be a domain containing $y(t) = 0$, where $y(t) \in \mathbb{R}^{(n+1)m+p_1+p_2+2}$ is defined as

$$y(t) \triangleq \begin{bmatrix} z^T & \sqrt{P(t)} & \sqrt{Q(t)} & \tilde{\theta}_1^T & \tilde{\theta}_2^T \end{bmatrix}^T, \tag{6–25}$$

where $\tilde{\theta}_i(t)$ are defined in (6–17), $z(t)$ and $Q(t)$ are defined in (6–22) and (6–23), respectively, and the auxiliary function $P(t) \in \mathbb{R}$ is the generalized solution to the differential equation

$$\dot{P}(t) = -L(t), \quad P(0) = \beta \sum_{i=1}^{n} |e_{ni}(0)| - e_n(0)^T N_d(0) \tag{6–26}$$

The auxiliary function $L(t) \in \mathbb{R}$ in (6–26) is defined as

$$L(t) \triangleq r^T (N_d(t) - \beta sgn(e_n)). \tag{6–27}$$

Provided the sufficient conditions stated in Theorem 6 are satisfied, then $P(t) \geq 0$ (see the Appendix B).

Let $V_L(y,t) : \mathcal{D} \times [0, \infty) \to \mathbb{R}$ denote a Lipschitz continuous regular positive definite functional defined as

$$V(y,t) \triangleq \frac{1}{2} e_1^T e_1 + \frac{1}{2} e_2^T e_2 + \ldots + \frac{1}{2} e_n^T e_n + \frac{1}{2} r^T b^{-1} r + P + Q + \frac{1}{2} \tilde{\theta}_1^T \Gamma_1^{-1} \tilde{\theta}_1 \tag{6–28}$$
$$+ \frac{1}{2} \tilde{\theta}_2^T \Gamma_2^{-1} \tilde{\theta}_2,$$

which satisfies the following inequalities

$$U_1(y) \leq V(y,t) \leq U_2(y),\tag{6-29}$$

provided the sufficient conditions introduced in Theorem 6 are satisfied. In (6–29), $U_1(y), U_2(y) \in \mathbb{R}$ are continuous, positive definite functions defined as

$$U_1(y) = \gamma_1 \|y\|^2 \quad U_2(y) = \gamma_2 \|y\|^2,\tag{6-30}$$

where $\gamma_1,\ \gamma_2 \in \mathbb{R}$ are defined as

$$\begin{aligned}
\gamma_1 &= \frac{1}{2}\min(1, b^{-1}, \gamma_{\min}\{\Gamma_1^{-1}\}, \gamma_{\min}\{\Gamma_2^{-1}\}),\\
\gamma_2 &= \max(\frac{1}{2}b^{-1}, 1, \gamma_{\max}\{\Gamma_1^{-1}\}, \gamma_{\max}\{\Gamma_2^{-1}\}),
\end{aligned}\tag{6-31}$$

and $\gamma_{\min}\{\cdot\}$, $\gamma_{\max}\{\cdot\}$ denote the minimum and maximum Eigenvalues, respectively. After taking the time derivative of (6–28), $\dot{V}_L(y,t)$ can be expressed as

$$\dot{V}_L(y,t) \triangleq e_1^T \dot{e}_1 + e_2^T \dot{e}_2 + \ldots + e_n^T \dot{e}_n + r^T b^{-1} \dot{r} + \dot{P} + \dot{Q} + \tilde{\theta}_1^T \Gamma_1^{-1} \dot{\tilde{\theta}}_1 + \tilde{\theta}_2^T \Gamma_2^{-1} \dot{\tilde{\theta}}_2.$$

From (6–3), (6–4), (6–18), (6–26), (6–27), adaptation laws in (6–15a), and the time derivative of $Q(t)$ in (6–23), some of the differential equations describing the closed-loop system for which the stability analysis is being performed have discontinuous right-hand

sides as

$$\dot{e}_1 = e_2 - \alpha_1 e_1, \tag{6–32a}$$

$$\dot{e}_2 = e_3 - \alpha_2 e_2 - e_1, \tag{6–32b}$$

$$. \tag{6–32c}$$

$$. \tag{6–32d}$$

$$. \tag{6–32e}$$

$$\dot{e}_n = r - \alpha_n e_n \tag{6–32f}$$

$$b^{-1}\dot{r} = \tilde{N} + N_d - e_n + \dot{Y}_1(x_d)\tilde{\theta}_1 + \dot{Y}_2(x_d)\tilde{\theta}_2 - (k_s + 1)\, r - \beta sgn(e_n), \tag{6–32g}$$

$$\dot{P}(t) = -r^T\left(N_d(t) - \beta sgn(e_n)\right), \tag{6–32h}$$

$$\dot{Q}(t) = \frac{1}{2k_s}\left(\rho_2^2(\|z(t)\|)\,\|z(t)\|^2 - \rho_2^2(\|z(t-\tau)\|)\,\|z(t-\tau)\|^2\right), \tag{6–32i}$$

$$\tilde{\theta}_1^T \Gamma_1^{-1} \dot{\tilde{\theta}}_1 = -\tilde{\theta}_1^T \dot{Y}_1^T(x_d) r, \tag{6–32j}$$

$$\tilde{\theta}_2^T \Gamma_2^{-1} \dot{\tilde{\theta}}_2 = -\tilde{\theta}_2^T \dot{Y}_2^T(x_d) r. \tag{6–32k}$$

Let $f(y,t) \in \mathbb{R}^{(n+1)m+p_1+p_2+2}$ denote the right hand side of (6–32). $f(y,t)$ is continuous except in the set $\{(y,t)|e_2 = 0\}$. From [103–106], an absolute continuous Filippov solution $y(t)$ exists almost everywhere (a.e.) so that

$$\dot{y} \in K[f](y,t) \quad a.e.$$

The generalized time derivative of (6–28) exists a.e., and $\dot{V}_L(y,t) \in^{a.e.} \dot{\tilde{V}}_L(y,t)$ where

$$\dot{\tilde{V}}_L(y,t) = \bigcap_{\xi \in \partial V_L(y,t)} \xi^T K \left[\begin{array}{ccccccccc} \dot{e}_1 & \dot{e}_2 & \cdot & \cdot & \cdot & \dot{e}_n & \frac{1}{2}P^{-\frac{1}{2}}\dot{P} & \frac{1}{2}Q^{-\frac{1}{2}}\dot{Q} & \dot{\tilde{\theta}}_1 & \dot{\tilde{\theta}}_2 \end{array} \right]^T, \tag{6–33}$$

$$= \nabla V_L^T K \left[\begin{array}{ccccccccc} \dot{e}_1 & \dot{e}_2 & \cdot & \cdot & \cdot & \dot{e}_n & \dot{r} & \frac{1}{2}P^{-\frac{1}{2}}\dot{P} & \frac{1}{2}Q^{-\frac{1}{2}}\dot{Q} & \dot{\tilde{\theta}}_1 & \dot{\tilde{\theta}}_2 \end{array} \right]^T,$$

$$\subset \left[\begin{array}{ccccccc} e_1^T & e_2^T & \cdot & \cdot & \cdot & e_n^T & r^T b^{-1} & 2P^{\frac{1}{2}} & 2Q^{\frac{1}{2}} & \tilde{\theta}_1^T \Gamma_1^{-1} & \tilde{\theta}_2^T \Gamma_2^{-1} \end{array} \right] K \left[\begin{array}{ccccc} \dot{e}_1 & \dot{e}_2 & \cdot & \cdot & \cdot & \dot{e}_n & \dot{r} \end{array} \right.$$

$$\left. \begin{array}{cccc} \frac{1}{2}P^{-\frac{1}{2}}\dot{P} & \frac{1}{2}Q^{-\frac{1}{2}}\dot{Q} & \dot{\tilde{\theta}}_1 & \dot{\tilde{\theta}}_2 \end{array} \right]^T.$$

For more details of the notations used in 6–32 to 6–33 and discussion, see Section 3.3.1. After utilizing (6–3), (6–4), (6–18), (6–26), (6–27), adaptation laws in (6–15a) and the time derivative of $Q(t)$ in (6–23), the expression in (6–33) can be rewritten as

$$
\begin{aligned}
\dot{\tilde{V}}_L(y,t) \subset\ & -\alpha_1 e_1^T e_1 - \ldots - \alpha_n e_n^T e_n + e_n^T e_{n-1} + e_n^T r + r^T \tilde{N} + r^T N_d - r^T e_n + r^T \dot{Y}_1(x_d)\tilde{\theta}_1 \\
& + r^T \dot{Y}_2(x_d)\tilde{\theta}_2 - (k_s+1)\|r\|^2 - \beta r^T K[sgn(e_n)] - r^T N_d(t) + \beta r^T K[sgn(e_n)] \\
& - \tilde{\theta}_1^T \dot{Y}_1^T(x_d)r - \tilde{\theta}_2 \dot{Y}_2^T(x_d)r + \frac{1}{2k_s}\left(\rho_2^2(\|z\|)\|z\|^2 - \rho_2^2(\|z_\tau\|)\|z_\tau\|^2\right).
\end{aligned} \tag{6–34}
$$

Cancelling common terms yields and using (6–21)

$$
\begin{aligned}
\dot{\tilde{V}}_L(y,t) \subset\ & -\sum_{i=1}^{n}\alpha_i\|e_i\|^2 + e_{n-1}^T e_n - \|r\|^2 - k_s\|r\|^2 + \rho_2(\|z_\tau\|)\|z_\tau\|\|r\| + \rho_1(\|z\|)\|z\|\|r\| \\
& + \frac{\rho_2^2(\|z\|)\|z\|^2}{2k_s} - \frac{\rho_2^2(\|z_\tau\|)\|z_\tau\|^2}{2k_s}.
\end{aligned} \tag{6–35}
$$

After applying following Young's inequality to determine that

$$
\rho_2(\|z_\tau\|)\|z_\tau\|\|r\| \le \frac{\rho_2^2(\|z_\tau\|)\|z_\tau\|^2}{2k_s} + \frac{k_s}{2}\|r\|^2, \quad e_{n-1}^T e_n \le \frac{1}{2}\left(\|e_{n-1}\|^2 + \|e_n\|^2\right), \tag{6–36}
$$

the expression in (6–35) can be written as

$$
\begin{aligned}
\dot{\tilde{V}}_L(y,t) \subset\ & -\sum_{i=1}^{n-2}\alpha_i\|e_i\|^2 - \left(\alpha_{n-1} - \frac{1}{2}\right)\|e_{n-1}\|^2 - \left(\alpha_n - \frac{1}{2}\right)\|e_n\|^2 - \|r\|^2 - \frac{k_s}{2}\|r\|^2 \\
& + \rho_1(\|z\|)\|z\|\|r\| + \frac{\rho_2^2(\|z\|)\|z\|^2}{2k_s}.
\end{aligned}
$$

After completing the squares, the expression in (6–37) can be written as

$$
\dot{\tilde{V}}_L(y,t) \subset -\left[\gamma_3 - \frac{\rho^2(\|z\|)}{2k_s}\right]\|z\|^2 \tag{6–37}
$$

where $\rho^2(\|z\|) \in \mathbb{R}$ is defined as

$$
\rho^2(\|z(t)\|) = \rho_1^2(\|z(t)\|) + \rho_2^2(\|z(t)\|), \tag{6–38}
$$

and $\gamma_3 \triangleq \min\left[\alpha_1,\ \alpha_2,\ \ldots,\ \alpha_{n-2},\ \alpha_{n-1} - \frac{1}{2},\ \alpha_n - \frac{1}{2},\ 1\right]$. The bounding function $\rho(\|z\|)$ is a positive, globally invertible, and nondecreasing function that does not depend on

the time-delay. The expression in (6–37) can be further upper bounded by a continuous, positive semi-definite function

$$\dot{\tilde{V}}_L(y,t) \subset -U(y) = -c\,\|z\|^2 \qquad \forall y \subset \mathcal{D} \tag{6–39}$$

for some positive constant c, where

$$\mathcal{D} \triangleq \left\{ y(t) \in \mathbb{R}^{(n+1)m+p_1+p_2+2} \mid \|y\| \leq \rho^{-1}\left(\sqrt{2\gamma_3 k_s}\right) \right\}.$$

Larger values of k_s will expand the size of the domain $\mathcal{D}$. The inequalities in (6–29) and (6–39) can be used to show that $V(y,t) \in \mathcal{L}_\infty$ in $\mathcal{D}$; hence, $e_1, e_2, ..., e_n, \tilde{\theta}_1, \tilde{\theta}_2 \in \mathcal{L}_\infty$ in $\mathcal{D}$. The closed-loop error systems can now be used to conclude all remaining signals are bounded in $\mathcal{D}$, and the definitions for $U(y)$ and $z(t)$ can be used to prove that $U(y)$ is uniformly continuous in $\mathcal{D}$. Let $\mathcal{S} \subset \mathcal{D}$ denote a set defined as

$$\mathcal{S} \triangleq \left\{ y(t) \in \mathcal{D} \mid U_2(y(t)) < \gamma_1 \left(\rho^{-1}\left(\sqrt{2\gamma_3 k_s}\right) \right)^2 \right\}. \tag{6–40}$$

The region of attraction in (6–40) can be made arbitrarily large to include any initial conditions by increasing the control gain k_s (i.e., a semi-global stability result), and hence

$$c\,\|z\|^2 \to 0 \qquad \text{as} \qquad t \to \infty \qquad \forall y(0) \in \mathcal{S}. \tag{6–41}$$

Based on the definition of $z(t)$, (6–41) can be used to show that

$$\|e_1(t)\| \to 0 \qquad \text{as} \qquad t \to \infty \qquad \forall y(0) \in \mathcal{S}. \tag{6–42}$$

6.5   Simulations

To illustrate the performance of the RISE-based adaptive controller, we consider the following first order scalar nonlinear plant [87]:

$$\dot{x}_1 = x_2 \tag{6–43}$$
$$\dot{x}_2 = f(x) + g(x_\tau) + \delta_1(x) + \delta_2(x_\tau) + d + bu,$$

where $f(x)$, $g(x_\tau)$ are linearly parameterizable functions, $\delta_1(x)$ is an unknown function, $\delta_2(x_\tau)$ is an unknown delayed function, $d(t)$ is a disturbance term, $u(t)$ is the control input, and b is an unknown coefficient. Since the time delay is unknown, the regression matrix for $g(x_\tau)$ is unknown to the controller. However, the adaptive estimate laws in the controller do not require the time delay value to be known. For the simulation purposes, these functions and parameters are chosen: $f(x) = 0.5\sin(x_1(t))$; $g(x_\tau) = 0.2x_1^2(t - \tau) + 2\cos(x_2(t))$; $\delta_1(x_\tau) = \sin(5x_2(t))$; $\delta_2(x_\tau) = 0.5x^2(t - \tau)\sin(2x_1(t - \tau))$; $d = 0.1sin(t)$; $b = 1$. The simulations are performed for the two cases of unknown time delays, namely, $\tau = 3$ s; $\tau = 10$ s. The desired trajectory is chosen as

$$x_d(t) = 0.5\left[\sin(t) + \sin(0.5t)\right]. \tag{6–44}$$

The following gains are chosen for $\tau = 3$ s and $\tau = 10$ s

$$k_s = 10, \quad \alpha_1 = 7, \quad \alpha_2 = 6, \quad \beta = 5, \quad \Gamma_1 = 0.5,$$
$$\Gamma_2 = [2, 0; 0, 10].$$

From the results shown in Figs. 6-1-6-5, it is clear that the controller tracks the time varying desired trajectory effectively. In both the cases, the steady state errors stay between ± 0.003 radians and the control inputs are bounded. Also it can be seen that there is a little variation in the control performances for time delays $\tau = 3$ s and $\tau = 10$ s.

6.6   Conclusion

A robust continuous RISE-based structure is utilized in conjunction with an adaptive controller for stabilizing a class of uncertain nonlinear systems with unknown state delays and bounded disturbances. By properly utilizing a DCAL-based method and segregating the necessary terms, the controller and the adaptive estimate law do not depend on the unknown time delay in the state. Appropriate LK functional is constructed to cancel the time delayed terms in the stability analysis. Simulations are provided to show the
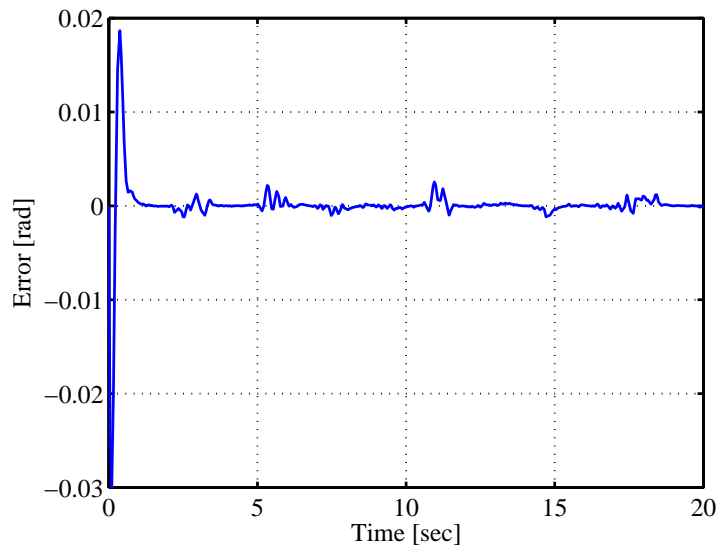
Figure 6-1. Tracking error for the case $\tau = 3\ s$.
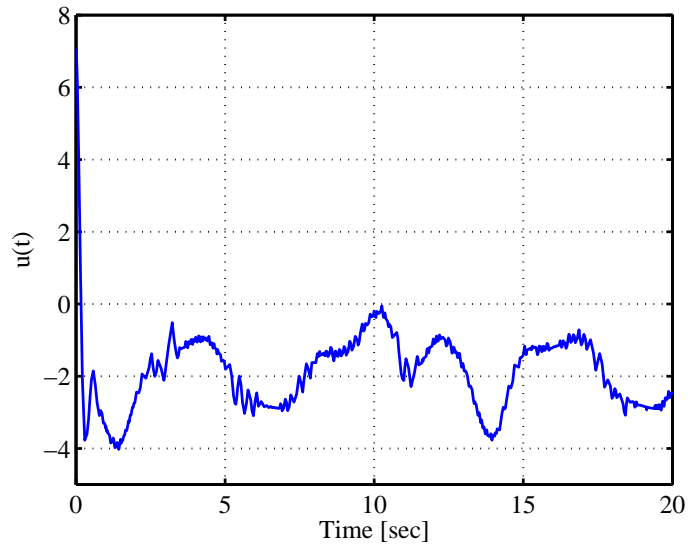
Figure 6-2. Control input for the case $\tau = 3\ s$.

performance of the controller. A Lyapunov-based stability analysis proves asymptotic stability for the closed loop nonlinear system.
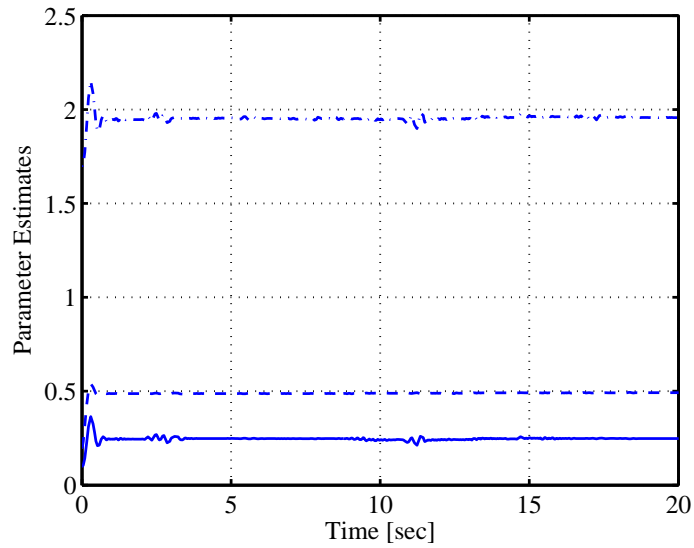
Figure 6-3. Parameter estimates for the case $\tau = 3$ s. Dashed line shows the parameter estimate of θ_1. Solid line shows the parameter estimate of $\theta_2(1)$. Dash-dot line shows the parameter estimate of $\theta_2(2)$.

Figure 6-4. Tracking error for the case $\tau = 10$ s.

Figure 6-5. Control input for the case $\tau = 10$ s.

Figure 6-6. Parameter estimates for the case $\tau = 10$ s. Dashed line shows the parameter estimate of θ_1. Solid line shows the parameter estimate of $\theta_2(1)$. Dash-dot line shows the parameter estimate of $\theta_2(2)$.
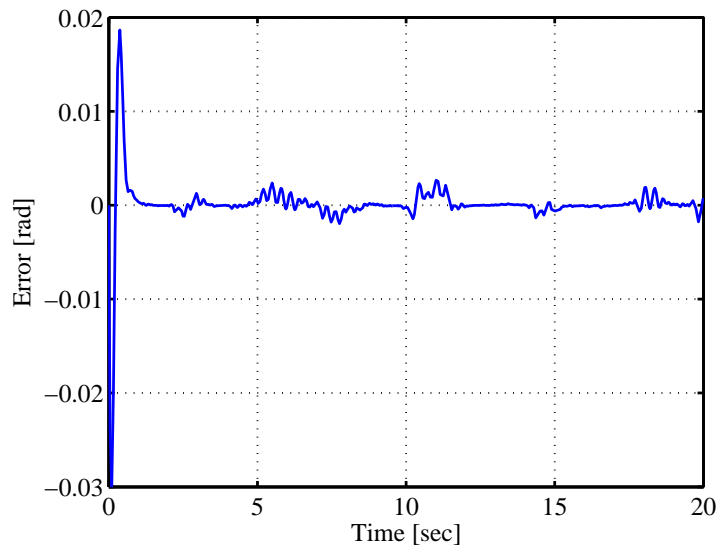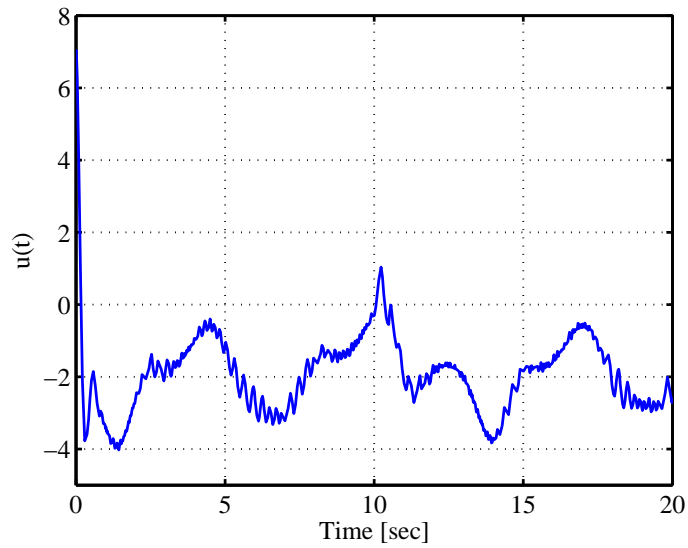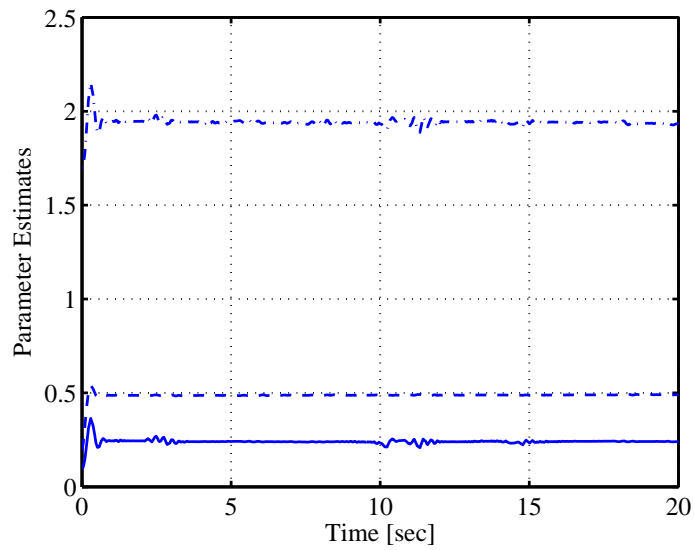
CHAPTER 7
CONCLUSION AND FUTURE WORK

7.1   Conclusion

New nonlinear controllers are developed to tackle various technical challenges in implementing NMES. These difficulties include unknown nonlinear mapping between the applied voltage to the muscle and the force generated in the muscle, bounded disturbances, muscle fatigue, and time delay. The first two controllers developed in Chapter 3 deal with unknown nonlinear mapping, bounded disturbances, and other unknown nonlinearities and uncertainties. The Lyapunov-based stability analysis is utilized to prove semi-global asymptotic stability for the controllers. Extensive experiments on healthy volunteers were conducted for both RISE and NN+RISE controllers. Particularly, it was shown that the inclusion of neural network based feedforward component in the RISE controller improves performance during NMES. Also, preliminary experimental trials demonstrating sit-to-stand task depicted the feasibility of the NN+RISE controller in a clinical-type scenario.

In Chapter 4, a NN-based controller is developed to compensate for fatigue. The benefit of the controller is that it incorporates more muscle dynamics knowledge namely, calcium and fatigue dynamics. The effectiveness of the controller to compensate fatigue is shown through simulation results. Further simulations show that the controller performs better than the RISE controller.

An important technical difficulty in NMES is input delay which becomes more challenging due to the presence of unknown nonlinearities and disturbances. Lack of input delay compensating controllers for uncertain nonlinear systems motivated to develop predictor-based controllers for general Euler Lagrange system in Chapter 5. The Lyapunov-based stability analysis utilizes LK functionals to prove semi-global UUB tracking. Extensive experimental results show better performance of the controller in comparison to the traditional PD/PID controller as well as their robustness to uncertainty

in input delay value and inertia matrix. Further, the feasibility of the predictor-based controller for NMES is shown through experimental trials on healthy individuals. Also, a study to characterize input delay in NMES is included in the chapter which shows that the input delay is dependent on frequency.

The last chapter in the dissertation covers the development of RISE-based adaptive controller for a class of nonlinear system with state delays. The significance of the result is that a robust and continuous controller is developed for a nonlinear system with unknown state delays and additive disturbances. Lyapunov-based stability analysis aided with LK functionals is utilized to show a semi-global asymptotic tracking.

7.2   Future Work

The following points discuss future work that can be built on the current research described in the dissertation.

- Current experiments focussed extensively on testing controllers on healthy volunteers. These experiments showed that the controllers hold potential for clinical tasks. Also, a preliminary test with the NN+RISE controller showed a promising sit-to-stand task performance. Therefore, extensive experiments can be performed where controllers should be tested on patients for functional tasks such as walking and sit-to-stand maneuvers.

- Efforts in Chapter 3 showed that the RMS error difference (for both RISE and NN+RISE controllers) between the flexion and extension phase of the leg movement is statistically significant. These results suggest that the role of switching controllers (hybrid control approach) can be investigated. Specifically, two different controllers can be utilized where each controller is dedicated for a particular phase of the leg movement.

- The result developed in Chapter 4 has three main limitations: unmeasurable calcium and fatigue dynamics, dependence on acceleration, and uniformly ultimately bounded stability result. Efforts can be made to develop an observer-based controller to remove the dependence on mathematical fatigue and calcium dynamics models. Specifically, recurrent neural network based observer can be designed to identify system states. Further, improvement in stability analysis can be achieved by developing a controller with asymptotic tracking. An extensive investigation is required to observe the effect of the controller in Chapter 4 on reducing fatigue. Experiments should not only compare the result with an existing controller for improved performance but should specifically study the effectiveness of the included fatigue model for fatigue compensation. The results may (or may not)

136

point to a need for improved fatigue models that are more suitable for non-isometric contractions and account for multiple factors affecting the fatigue onset in NMES. Also, additional information can be gathered to predict fatigue onset through incorporating Electromyogram (EMG) signals. Measuring surface EMG signals can be used as an indicator or can be utilized to quantify the fatigue onset which can be further incorporated in NMES control design.

- Currently most of the NMES control implementation utilize single modulation methods (e.g., the experiments were performed with amplitude modulation technique, where the frequency and pulsewidth were kept constant while voltage is varied). Methods can be developed to modulate multiple stimulation parameters simultaneously. However, more efforts will be required first to investigate the effects of multiple modulation during NMES control. The benefits of this research may manifest as improved control performance during fatigue onset (e.g., frequency plays an important role in the fatigue onset. Modulating frequency along with amplitude may delay the onset of fatigue during NMES.)

- One of the most important technical issue in NMES is the rapid onset of fatigue. Numerous factors influence the early onset of fatigue during NMES control. Overstimulation due to high gain controller is one of the factors that affects the fatigue onset. Feedforward methods or using low gain control are always suggested to avoid early onset of fatigue. However, high gain controllers are required to obtain minimal tracking errors during functional tasks. A solution to optimize these two conflicting strategies can be obtained by designing optimal controllers. Proper mechanisms can be built into these controllers to provide a choice between better error performance or delaying the fatigue onset.

- The focus of the current research was mainly on developing control techniques for non-invasive surface electrical stimulation. The main disadvantage of surface electrical stimulation is repetitive and non-selective recruitment of muscle fibres which lie in the path of applied current. This type of muscle recruitment is the main cause of rapid fatigue onset and is in contrast to the recruitment employed by the brain and central nervous system during voluntary contractions. In context to this disadvantage, researchers have used invasive electrodes to stimulate specific muscles or nerves in the paralyzed patients to produce desired functional movements. The main benefit of these methods is selective and non-repetitive recruitment of muscle fibres, thereby avoiding muscle fatigue. However, wires protruding out from the skin and chances of infection have made this option unattractive. With the advancement of technology, some researchers have developed micro-stimulators called BIONs [131], which can be surgically implanted at specific sites in the muscle. These microelectrodes which do not require wires are powered externally through an inductive coil and a battery. Multiple BIONs to stimulate specific muscle sites can not only be used to produce desired functional movements but also can be used to eliminate muscle fatigue through utilizing non-repetitive and selective muscle recruitment. In order to produce NMES control via BIONs, studies will be required

to imitate the strategies used by brain and central nervous system during voluntary contractions. The real challenge will be to maintain stability and coordination of multiple implanted BIONs in order to extract desired movements. Approaches from hybrid control theory and co-operative control should be investigated to develop NMES control via BIONs.

- Development focussed on input delay measurement in the Chapter 5 showed that the input delay in NMES depends only on varying frequency. However, further investigations are required to study the effect of fatigue and non-isometric contractions on input delay. Also, results in Chapter 5 are only applicable with known constant input delay values. Therefore, controllers need to be developed to account for time-varying or unknown input delay. Other delay compensating techniques such as model predictive control (MPC) can also be investigated for NMES. One of the advantages of MPC is that it inherently compensates for input delays. Although the technique would require muscle dynamics to be known, advantages such as performance and control optimization in addition to delay compensation makes MPC a worthy candidate for investigation.

APPENDIX A
(CHAPTER 5) PREDICTOR-BASED CONTROL FOR AN UNCERTAIN EULER-LAGRANGE SYSTEM WITH INPUT DELAY

Lemma 1. *Define $Q(t) \in \mathbb{R}$ as*

$$Q(t) = \omega \int_{t-\tau}^{t} \left(\int_{s}^{t} \|\dot{u}(\theta)\|^2 \, d\theta \right) ds. \tag{1-1}$$

The time derivative of $Q(t)$ is

$$\dot{Q}(t) = \omega\tau \|\dot{u}(t)\|^2 - \omega \int_{t-\tau}^{t} \|\dot{u}(\theta)\|^2 \, d\theta. \tag{1-2}$$

Proof: The time derivative of $Q(t)$

$$\dot{Q}(t) = \omega \frac{d}{dt} \left[\int_{t-\tau}^{t} \left(\int_{s}^{t} \|\dot{u}(\theta)\|^2 \, d\theta \right) ds \right],$$

on applying Leibniz integral rule can be written as

$$\dot{Q}(t) = \omega \left(\int_{t}^{t} \|\dot{u}(\theta)\|^2 \, d\theta \right) \frac{dt}{dt} - \omega \left(\int_{t-\tau}^{t} \|\dot{u}(\theta)\|^2 \, d\theta \right) \frac{d(t-\tau)}{dt} + \omega \int_{t-\tau}^{t} \left(\frac{\partial}{\partial t} \int_{s}^{t} \|\dot{u}(\theta)\|^2 \, d\theta \right) ds. \tag{1-3}$$

The expression in (1–3) can be simplified as

$$- \omega \int_{t-\tau}^{t} \|\dot{u}(\theta)\|^2 \, d\theta + \omega \int_{t-\tau}^{t} \left(\frac{\partial}{\partial t} \int_{s}^{t} \|\dot{u}(\theta)\|^2 \, d\theta \right) ds. \tag{1-4}$$

Again applying Leibniz integral rule on second integral in (1–4)

$$- \omega \int_{t-\tau}^{t} \|\dot{u}(\theta)\|^2 \, d\theta + \omega \int_{t-\tau}^{t} \left(\|\dot{u}(t)\|^2 \frac{dt}{dt} - \|\dot{u}(s)\|^2 \frac{ds}{dt} + \int_{s}^{t} \frac{\partial}{\partial t} \|\dot{u}(\theta)\|^2 \, d\theta \right) ds. \tag{1-5}$$

The expression in (1–5) can be simplified as

$$- \omega \int_{t-\tau}^{t} \|\dot{u}(\theta)\|^2 \, d\theta + \omega \|\dot{u}(t)\|^2 \int_{t-\tau}^{t} ds. \tag{1-6}$$

Further integrating the second integral in (1–6)

$$\omega\tau \|\dot{u}(t)\|^2 - \omega \int_{t-\tau}^{t} \|\dot{u}(\theta)\|^2 \, d\theta.$$

Lemma 2. *Define $P(t) \in \mathbb{R}$ as*

$$P(t) = \omega \int_{t-\tau}^{t} \left(\int_{s}^{t} \|u(\theta)\|^2 \, d\theta \right) ds. \tag{1–7}$$

The time derivative of $P(t)$ is

$$\dot{P}(t) = \omega\tau \|u(t)\|^2 - \omega \int_{t-\tau}^{t} \|u(\theta)\|^2 \, d\theta. \tag{1–8}$$

Proof: The proof is similar to the proof given for Lemma 1

APPENDIX B
(CHAPTER 6) RISE-BASED ADAPTIVE CONTROL OF AN UNCERTAIN
NONLINEAR SYSTEM WITH UNKNOWN STATE DELAYS

Lemma 3. *Define $L(t) \in \mathbb{R}$ as*

$$L \triangleq r^T(N_d - \beta sgn(e_n)). \tag{2–9}$$

Then, if β satisfies

$$\beta > \zeta_{N_d} + \frac{\zeta_{\dot{N}_d}}{\alpha}, \tag{2–10}$$

then

$$\int_0^t L(\tau) \, d\tau \leq \beta \sum_{i=1}^n |e_{ni}(0)| - e_n(0)^T N_d(0), \tag{2–11}$$

where $e_{ni}(0) \in \mathbb{R}$ denotes the ith element of the vector $e_n(0)$.

Proof: Integrating both sides of (2–9)

$$\int_0^t L(\sigma)d\sigma = \int_0^t \left[r^T(N_d - \beta sgn(e_n)) \right] d\sigma. \tag{2–12}$$

On substituting (6–5) in (2–12) yields

$$\int_0^t L(\sigma)d\sigma = \int_0^t \dot{e}_n^T N_d d\sigma - \int_0^t \dot{e}_n^T \beta sgn(e_n) d\sigma + \int_0^t \alpha e_n^T(N_d - \beta sgn(e_n))d\sigma. \tag{2–13}$$

After utilizing integration by parts for the first integral and integrating the second integral in (2–13), the following expression is obtained:

$$\int_0^t L(\sigma)d\sigma = e_n^T N_d - e_n^T(0) N_d(0) + \beta \sum_{i=1}^n |e_{ni}(0)| - \beta \sum_{i=1}^n |e_{ni}(t)| +$$

$$\int_0^t \left[\alpha e_n^T(N_d - \frac{1}{\alpha}\frac{\partial N_d}{d\sigma} - \beta sgn(e_n)) \right] d\sigma, \tag{2–14}$$

where the fact that $sgn(e_n)$ can be denoted as

$$sgn(e_n) = [sgn(e_{n1}) \quad sgn(e_{n2}) \quad --- \quad sgn(e_{nn})]^T, \tag{2–15}$$

is utilized in the second integral. Using the bounds given in (6–20) and the fact that

$$\|e_n(t)\| \leq \sum_{i=1}^{n} |e_{ni}(t)|,$$ (2–16)

the expression in (2–14) can be upper bounded as

$$\int_0^t L(\sigma)d\sigma \leq \beta \sum_{i=1}^{n} |e_{ni}(0)| - e_n^T(0) N_d(0) + (\zeta_{N_d} - \beta \|e_n\|) + \int_0^t \alpha \|e_n\| \left(\zeta_{N_d} + \frac{\zeta_{\dot{N}_d}}{\alpha} - \beta \right) d\sigma.$$ (2–17)

It is clear from (2–17) that if the following sufficient condition

$$\beta > \zeta_{N_d} + \frac{\zeta_{\dot{N}_d}}{\alpha}$$ (2–18)

is satisfied, then the following inequality holds

$$\int_0^t L(\sigma)d\tau \leq \beta \sum_{i=1}^{n} |e_{ni}(0)| - e_n(0)^T N_d(0).$$ (2–19)

REFERENCES

[1] P. H. Peckham and D. B. Gray, "Functional neuromuscular stimulation," *J. Rehabil. Res. Dev.*, vol. 33, pp. 9–11, 1996.

[2] P. H. Peckham and J. S. Knutson, "Functional electrical stimulation for neuromuscular applications," *Annu. Rev. Biomed. Eng.*, vol. 7, pp. 327–360, 2005.

[3] J. J. Abbas and H. J. Chizeck, "Feedback control of coronal plane hip angle in paraplegic subjects using functional neuromuscular stimulation," *IEEE Trans. Biomed. Eng.*, vol. 38, no. 7, pp. 687–698, 1991.

[4] N. Lan, P. E. Crago, and H. J. Chizeck, "Control of end-point forces of a multijoint limb by functional neuromuscular stimulation," *IEEE Trans. Biomed. Eng.*, vol. 38, no. 10, pp. 953–965, 1991.

[5] ——, "Feedback control methods for task regulation by electrical stimulation of muscles," *IEEE Trans. Biomed. Eng.*, vol. 38, no. 12, pp. 1213–1223, 1991.

[6] T. Schauer, N. O. Negard, F. Previdi, K. J. Hunt, M. H. Fraser, E. Ferchland, and J. Raisch, "Online identification and nonlinear control of the electrically stimulated quadriceps muscle," *Control Eng. Pract.*, vol. 13, pp. 1207–1219, 2005.

[7] K. Stegath, N. Sharma, C. M. Gregory, and W. E. Dixon, "An extremum seeking method for non-isometric neuromuscular electrical stimulation," in *Proc. IEEE Int. Conf. Syst. Man. Cybern.*, 2007, pp. 2528–2532.

[8] A. H. Vette, K. Masani, and M. R. Popovic, "Implementation of a physiologically identified PD feedback controller for regulating the active ankle torque during quiet stance," *IEEE Trans. Neural Syst. Rehabil. Eng.*, vol. 15, no. 2, pp. 235–243, June 2007.

[9] G. Khang and F. E. Zajac, "Paraplegic standing controlled by functional neuromuscular stimulation: Part I - computer model and control-system design," *IEEE Trans. Biomed. Eng.*, vol. 36, no. 9, pp. 873–884, 1989.

[10] F. Previdi, M. Ferrarin, S. Savaresi, and S. Bittanti, "Gain scheduling control of functional electrical stimulation for assisted standing up and sitting down in paraplegia: a simulation study," *Int. J. Adapt Control Signal Process.*, vol. 19, pp. 327–338, 2005.

[11] P. M. Patre, W. MacKunis, C. Makkar, and W. E. Dixon, "Asymptotic tracking for systems with structured and unstructured uncertainties," *IEEE Trans. Control Syst. Technol.*, vol. 16, no. 2, pp. 373–379, 2008.

[12] ——, "Asymptotic tracking for systems with structured and unstructured uncertainties," in *Proc. IEEE Conf. Decis. Control*, San Diego, CA, Dec. 2006, pp. 441–446.

[13] N. Lan, H. Feng, and E. Crago, "Neural network generation of muscle stimulation patterns for control of arm movements," *IEEE Trans. Rehabil. Eng.*, vol. 2, no. 4, pp. 213–224, 1994.

[14] J. J. Abbas and H. J. Chizeck, "Neural network control of functional neuromuscular stimulation systems: computer simulation studies," *IEEE Trans. Biomed. Eng.*, vol. 42, no. 11, pp. 1117–1127, Nov. 1995.

[15] D. Graupe and H. Kordylewski, "Artificial neural network control of FES in paraplegics for patient responsive ambulation," *IEEE Trans. Biomed. Eng.*, vol. 42, no. 7, pp. 699–707, July 1995.

[16] G.-C. Chang, J.-J. Lub, G.-D. Liao, J.-S. Lai, C.-K. Cheng, B.-L. Kuo, and T.-S. Kuo, "A neuro-control system for the knee joint position control with quadriceps stimulation," *IEEE Trans. Rehabil. Eng.*, vol. 5, no. 1, pp. 2–11, Mar. 1997.

[17] J. A. Riess and J. J. Abbas, "Adaptive neural network control of cyclic movements using functional neuromuscular stimulation," *IEEE Trans. Neural Syst. Rehabil. Eng.*, vol. 8, pp. 42–52, 2000.

[18] H. Kordylewski and D. Graupe, "Control of neuromuscular stimulation for ambulation by complete paraplegics via artificial neural networks," *Neurol. Res.*, vol. 23, no. 5, pp. 472–481, 2001.

[19] D. G. Zhang and K. Y. Zhu, "Simulation study of FES-assisted standing up with neural network control," in *Proc. Annu. Int. Conf. IEEE Eng. Med. Biol. Soc.*, vol. 6, 2004, pp. 4118–4121.

[20] J. P. Giuffrida and P. E. Crago, "Functional restoration of elbow extension after spinal-cord injury using a neural network-based synergistic FES controller," *IEEE Trans. Neural Syst. Rehabil. Eng.*, vol. 13, no. 2, pp. 147–152, 2005.

[21] Y.-L. Chen, W.-L. Chen, C.-C. Hsiao, T.-S. Kuo, and J.-S. Lai, "Development of the FES system with neural network + PID controller for the stroke," in *Proc. IEEE Int. Symp. Circuits Syst.*, May 23–26, 2005, pp. 5119–5121.

[22] K. Kurosawa, R. Futami, T. Watanabe, and N. Hoshimiya, "Joint angle control by FES using a feedback error learning controller," *IEEE Trans. Neural Syst. Rehabil. Eng.*, vol. 13, pp. 359–371, 2005.

[23] A. Pedrocchi, S. Ferrante, E. De Momi, and G. Ferrigno, "Error mapping controller: a closed loop neuroprosthesis controlled by artificial neural networks," *J. Neuroeng. Rehabil.*, vol. 3, no. 1, p. 25, 2006.

[24] S. Kim, M. Fairchild, A. Iarkov, J. Abbas, and R. Jung, "Adaptive control for neuromuscular stimulation-assisted movement therapy in a rodent model," *IEEE Trans. Biomed. Eng.*, vol. 56, pp. 452–461, 2008.

[25] A. Ajoudani and A. Erfanian, "A neuro-sliding-mode control with adaptive modeling of uncertainty for control of movement in paralyzed limbs using functional electrical stimulation," *IEEE Trans. Biomed. Eng.*, vol. 56, no. 7, pp. 1771–1780, Jul. 2009.

[26] J. Lujan and P. Crago, "Automated optimal coordination of multiple-DOF neuromuscular actions in feedforward neuroprostheses," *IEEE Trans. Biomed. Eng.*, vol. 56, no. 1, pp. 179–187, Jan. 2009.

[27] P. M. Patre, W. MacKunis, K. Kaiser, and W. E. Dixon, "Asymptotic tracking for uncertain dynamic systems via a multilayer neural network feedforward and RISE feedback control structure," *IEEE Trans. Autom. Control*, vol. 53, no. 9, pp. 2180–2185, 2008.

[28] M. J. Levy, M. and Z. Susak, "Recruitment, force and fatigue characteristics of quadriceps muscles of paraplegics, isometrically activated by surface FES," *J. Biomed. Eng.*, vol. 12, pp. 150–156, 1990.

[29] D. Russ, K. Vandenborne, and S. Binder-Macleod, "Factors in fatigue during intermittent electrical stimulation of human skeletal muscle," *J. Appl. Physiol.*, vol. 93, no. 2, pp. 469–478, 2002.

[30] J. Mizmhi, "Fatigue in muscles activated by functional electrical stimulation," *Crit. Rev. Phys. Rehabil. Med.*, vol. 9, no. 2, pp. 93–129, 1997.

[31] E. Asmussen, "Muscle fatigue," *Med. Sci. Sports. Exerc.*, vol. 11, no. 4, pp. 313–321, 1979.

[32] R. Maladen, R. Perumal, A. Wexler, and S. Binder-Macleod, "Effects of activation pattern on nonisometric human skeletal muscle performance," *J. Appl. Physiol.*, vol. 102, no. 5, pp. 1985–91, 2007.

[33] S. Binder-Macleod, J. Dean, and J. Ding, "Electrical stimulation factors in potentiation of human quadriceps femoris," *Muscle Nerve*, vol. 25, no. 2, pp. 271–9, 2002.

[34] Y. Giat, J. Mizrahi, and M. Levy, "A musculotendon model of the fatigue profiles of paralyzed quadriceps muscle under FES," *IEEE Trans. Biomed. Eng.*, vol. 40, no. 7, pp. 664–674, 1993.

[35] R. Riener, J. Quintern, and G. Schmidt, "Biomechanical model of the human knee evaluated by neuromuscular stimulation," *J. Biomech.*, vol. 29, pp. 1157–1167, 1996.

[36] R. Riener and T. Fuhr, "Patient-driven control of FES-supported standing up: A simulation study," *IEEE Trans. Rehabil. Eng.*, vol. 6, pp. 113–124, 1998.

[37] J. Ding, A. Wexler, and S. Binder-Macleod, "A predictive fatigue model. I. predicting the effect of stimulation frequency and pattern on fatigue," *IEEE Trans. Rehabil. Eng.*, vol. 10, no. 1, pp. 48–58, 2002.

[38] ——, "A predictive fatigue model. II. predicting the effect of resting times on fatigue," *IEEE Trans. Rehabil. Eng.*, vol. 10, no. 1, pp. 59–67, 2002.

[39] S. Jezernik, R. Wassink, and T. Keller, "Sliding mode closed-loop control of FES: Controlling the shank movement," *IEEE Trans. Biomed. Eng.*, vol. 51, pp. 263–272, 2004.

[40] K. Masani, A. Vette, N. Kawashima, and M. Popovic, "Neuromusculoskeletal torque-generation process has a large destabilizing effect on the control mechanism of quiet standing," *J. Neurophysiol.*, vol. 100, no. 3, p. 1465, 2008.

[41] S. Evesque, A. Annaswamy, S. Niculescu, and A. Dowling, "Adaptive control of a class of time delay systems," *J. Dyn. Syst. Meas. Contr.*, vol. 125 (2), pp. 186–193, 2003.

[42] J. Huang and F. Lewis, "Neural-network predictive control for nonlinear dynamic systems with time-delay," *IEEE Trans. Neural Networks*, vol. 14, no. 2, pp. 377–389, 2003.

[43] D. Yanakiev and I. Kanellakopoulos, "Longitudinal control of automated CHVs with significant actuatordelays," *IEEE Trans. Veh. Technol.*, vol. 50, no. 5, pp. 1289–1297, 2001.

[44] B. Bequette, "Nonlinear control of chemical processes: A review," *Ind. Eng. Chem. Res.*, vol. 30, no. 7, pp. 1391–1413, 1991.

[45] J.-P. Richard, "Time-delay systems: an overview of some recent advances and open problems," *Automatica*, vol. 39, no. 10, pp. 1667 – 1694, 2003.

[46] K. Gu, V. L. Kharitonov, and J. Chen, *Stability of Time-delay systems.* Birkhauser, 2003.

[47] W. Kwon and A. Pearson, "Feedback stabilization of linear systems with delayed control," *IEEE Trans. Autom. Control*, vol. 25, no. 2, pp. 266–269, 1980.

[48] Z. Artstein, "Linear systems with delayed controls: A reduction," *IEEE Trans. Autom. Control*, vol. 27, no. 4, pp. 869–879, 1982.

[49] Y. Fiagbedzi and A. Pearson, "Feedback stabilization of linear autonomous time lag systems," *IEEE Trans. Autom. Control*, vol. 31, no. 9, pp. 847–855, 1986.

[50] M. Jankovic, "Recursive predictor design for linear systems with time delay," in *Proc. IEEE Am. Control Conf.*, June 2008, pp. 4904–4909.

[51] A. Manitius and A. Olbrot, "Finite spectrum assignment problem for systems with delays," *IEEE Trans. Autom. Control*, vol. 24, no. 4, pp. 541–552, 1979.

[52] S. Mondié and W. Michiels, "Finite spectrum assignment of unstable time-delay systems with a safe implementation," *IEEE Trans. Autom. Control*, vol. 48, no. 12, pp. 2207–2212, 2003.

[53] Y. Roh and J. Oh, "Robust stabilization of uncertain input-delay systems by sliding mode control with delay compensation," *Automatica*, vol. 35, pp. 1861–1865, 1999.

[54] M. Krstic, "Lyapunov tools for predictor feedbacks for delay systems: Inverse optimality and robustness to delay mismatch," *Automatica*, vol. 44, no. 11, pp. 2930–2935, 2008.

[55] M. Krstic and D. Bresch-Pietri, "Delay-adaptive full-state predictor feedback for systems with unknown long actuator delay," in *Proc. IEEE Am. Control Conf.*, 2009, pp. 4500–4505.

[56] D. Bresch-Pietri and M. Krstic, "Adaptive trajectory tracking despite unknown input delay and plant parameters," *Automatica*, vol. 45, no. 9, pp. 2074–2081, 2009.

[57] M. Krstic and A. Smyshlyaev, "Backstepping boundary control for first-order hyperbolic PDEs and application to systems with actuator and sensor delays," *Syst. Contr. Lett.*, vol. 57, no. 9, pp. 750–758, 2008.

[58] W. Michiels, K. Engelborghs, P. Vansevenant, and D. Roose, "Continuous pole placement for delay equations," *Automatica*, vol. 38, no. 5, pp. 747–761, 2002.

[59] O. M. Smith, "A controller to overcome deadtime," *ISA J.*, vol. 6, pp. 28–33, 1959.

[60] M. Matausek and A. Micic, "A modified smith predictor for controlling a process with an integrator and long dead-time," *IEEE Trans. Autom. Control*, vol. 41, no. 8, pp. 1199–1203, Aug 1996.

[61] S. Majhi and D. Atherton, "Modified smith predictor and controller for processes with timedelay," *IEE Proc. Contr. Theor. Appl.*, vol. 146, no. 5, pp. 359–366, 1999.

[62] W. Zhang and Y. Sun, "Modified smith predictor for controlling integrator/time delay processes," *Ind. Eng. Chem. Res.*, vol. 35, no. 8, pp. 2769–2772, 1996.

[63] A. Nortcliffe and J. Love, "Varying time delay smith predictor process controller," *ISA Trans.*, vol. 43, no. 1, pp. 61–71, 2004.

[64] P. Garcia and P. Albertos, "A new dead-time compensator to control stable and integrating processes with long dead-time," *Automatica*, vol. 44, no. 4, pp. 1062 – 1071, 2008.

[65] S. Majhi and D. Atherton, "Obtaining controller parameters for a new smith predictor using autotuning," *Automatica*, vol. 36, no. 11, pp. 1651–1658, Nov 2000.

[66] I. Chien, S. Peng, and J. Liu, "Simple control method for integrating processes with long deadtime," *J. Process Control*, vol. 12, no. 3, pp. 391–404, 2002.

[67] L. Roca, J. Luis Guzman, J. E. Normey-Rico, M. Berenguel, and L. Yebra, "Robust constrained predictive feedback linearization controller in a solar desalination plant collector field," *Control Eng. Pract.*, vol. 17, no. 9, pp. 1076–1088, Sep. 2009.

[68] C. Xiang, L. Cao, Q. Wang, and T. Lee, "Design of predictor-based controllers for input-delay systems," in *Proc. IEEE Int. Symp. Ind. Electron.*, 30 2008-July 2 2008, pp. 1009–1014.

[69] H.-H. Wang, "Optimal vibration control for offshore structures subjected to wave loading with input delay," in *Int. Conf. Meas. Technol. Mechatron. Autom.*, vol. 2, April 2009, pp. 853–856.

[70] ——, "Optimal tracking for discrete-time systems with input delays," in *Proc. Chin. Control Decis. Conf.*, July 2008, pp. 4033–4037.

[71] H.-H. Wang, N.-P. Hu, and B.-L. Zhang, "An optimal control regulator for nonlinear discrete-time systems with input delays," in *World Congr. Intell. Control Autom.*, June 2008, pp. 5540–5544.

[72] M. Krstic and A. Smyshlyaev, *Boundary control of PDEs: A course on Backstepping Designs.* SIAM, 2008.

[73] S. Niculescu and A. Annaswamy, "An adaptive smith-controller for time-delay systems with relative degree n*<2," *Syst. Contr. Lett.*, vol. 49, no. 5, pp. 347–358, 2003.

[74] C. Kravaris and R. Wright, "Deadtime compensation for nonlinear processes," *AIChE J.*, vol. 35, no. 9, pp. 1535–1542, 1989.

[75] M. Henson and D. Seborg, "Time delay compensation for nonlinear processes," *Ind. Eng. Chem. Res.*, vol. 33, no. 6, pp. 1493–1500, 1994.

[76] F. Mazenc and P. Bliman, "Backstepping design for time-delay nonlinear systems," *IEEE Trans. Autom. Control*, vol. 51, no. 1, pp. 149–154, 2006.

[77] M. Jankovic, "Control of cascade systems with time delay - the integral cross-term approach," in *Proc. IEEE Conf. Decis. Control*, Dec. 2006, pp. 2547–2552.

[78] A. Teel, "Connections between Razumikhin-type theorems and the ISS nonlinearsmall gain theorem," *IEEE Trans. Autom. Control*, vol. 43, no. 7, pp. 960–964, 1998.

[79] M. Krstic, "On compensating long actuator delays in nonlinear control," *IEEE Trans. Autom. Control*, vol. 53, no. 7, pp. 1684–1688, 2008.

[80] Y. Xia and Y. Jia, "Robust sliding-mode control for uncertain time-delay systems: an LMI approach," *IEEE Trans. Autom. Control*, vol. 48, no. 6, pp. 1086–1091, June 2003.

[81] X.-J. Jing, D.-L. Tan, and Y.-C. Wang, "An LMI approach to stability of systems with severe time-delay," *IEEE Trans. Autom. Control*, vol. 49, no. 7, pp. 1192–1195, July 2004.

[82] S. Nguang, "Robust stabilization of a class of time-delay nonlinear systems," *IEEE Trans. Autom. Control*, vol. 45, no. 4, pp. 756–762, 2000.

[83] S. Ge, F. Hong, and T. H. Lee, "Adaptive neural network control of nonlinear systems with unknown time delays," *IEEE Trans. Autom. Control*, vol. 48, no. 11, pp. 2004–2010, Nov. 2003.

[84] S. Mondie and V. Kharitonov, "Exponential estimates for retarded time-delay systems: an LMI approach," *IEEE Trans. Autom. Control*, vol. 50, no. 2, pp. 268–273, Feb. 2005.

[85] D. Ho, L. Junmin, and Y. Niu, "Adaptive neural control for a class of nonlinearly parametric time-delay systems," *IEEE Trans. Neural Networks*, vol. 16, pp. 625–635, 2005.

[86] X. Li and C. de Souza, "Delay-dependent robust stability and stabilization of uncertain linear delay systems: a linear matrix inequality approach," *IEEE Trans. Autom. Control*, vol. 42, no. 8, pp. 1144–1148, Aug 1997.

[87] S. Ge, F. Hong, and T. Lee, "Robust adaptive control of nonlinear systems with unknown time delays," *Automatica*, vol. 41, no. 7, pp. 1181–1190, Jul. 2005.

[88] S. Zhou, G. Feng, and S. Nguang, "Comments on "robust stabilization of a class of time-delay nonlinear systems," *IEEE Trans. Autom. Control*, vol. 47, no. 9, 2002.

[89] S. J. Yoo, J. B. Park, and Y. H. Choi, "Comments on "adaptive neural control for a class of nonlinearly parametric time-delay systems"," *IEEE Trans. Neural Networks*, vol. 19, no. 8, pp. 1496–1498, Aug. 2008.

[90] D. Ho, J. Li, and Y. Niu, "Reply to "comments on "adaptive neural control for a class of nonlinearly parametric time-delay systems""," *IEEE Trans. Neural Networks*, vol. 19, no. 8, pp. 1498–1498, Aug. 2008.

[91] K. Shyu and J. Yan, "Robust stability of uncertain time-delay systems and its stabilization by variable structure control," *Int. J. Control*, vol. 57, no. 1, pp. 237–246, 1993.

[92] F. Gouaisbaut, W. Perruquetti, and J. P. Richard, "A sliding mode control for linear systems with input and state delays," in *Proc. IEEE Conf. Decis. Control*, vol. 4, Dec. 1999, pp. 4234–4239.

[93] F. Gouaisbaut, M. Dambrine, and J. P. Richard, "Sliding mode control of TDS via functional surfaces," in *Proc. IEEE Conf. Decis. Control*, vol. 5, Dec. 2001, pp. 4630–4634.

[94] F. Gouaisbaut, M. Dambrine, and J. Richard, "Robust control of delay systems: a sliding mode control design via LMI," *Syst. Contr. Lett.*, vol. 46, no. 4, pp. 219–230, 2002.

[95] B. Mirkin, P. Gutman, and Y. Shtessel, "Continuous model reference adaptive control with sliding mode for a class of nonlinear plants with unknown state delay," in *Proc. IEEE Am. Control Conf.*, 2009, pp. 574–579.

[96] Z. Qu and J. X. Xu, "Model-based learning controls and their comparisons using Lyapunov direct method," *Asian J. Control*, vol. 4(1), pp. 99–110, 2002.

[97] M. Ferrarin and A. Pedotti, "The relationship between electrical stimulus and joint torque: A dynamic model," *IEEE Trans. Rehabil. Eng.*, vol. 8, no. 3, pp. 342–352, 2000.

[98] J. L. Krevolin, M. G. Pandy, and J. C. Pearce, "Moment arm of the patellar tendon in the human knee," *J. Biomech.*, vol. 37, pp. 785–788, 2004.

[99] W. L. Buford, Jr., F. M. Ivey, Jr., J. D. Malone, R. M. Patterson, G. L. Peare, D. K. Nguyen, and A. A. Stewart, "Muscle balance at the knee - moment arms for the normal knee and the ACL - minus knee," *IEEE Trans. Rehabil. Eng.*, vol. 5, no. 4, pp. 367–379, 1997.

[100] O. M. Rutherford and D. A. Jones, "Measurement of fibre pennation using ultrasound in the human quadriceps in vivo," *Eur. J. Appl. Physiol.*, vol. 65, pp. 433–437, 1992.

[101] R. Nathan and M. Tavi, "The influence of stimulation pulse frequency on the generation of joint moments in the upper limb," *IEEE Trans. Biomed. Eng.*, vol. 37, pp. 317–322, 1990.

[102] T. Watanabe, R. Futami, N. Hoshimiya, and Y. Handa, "An approach to a muscle model with a stimulus frequency-force relationship for FES applications," *IEEE Trans. Rehabil. Eng.*, vol. 7, no. 1, pp. 12–17, 1999.

[103] A. Filippov, "Differential equations with discontinuous right-hand side," *Am. Math. Soc. Transl.*, vol. 42, pp. 199–231, 1964.

[104] ——, *Differential equations with discontinuous right-hand side.* Netherlands: Kluwer Academic Publishers, 1988.

[105] G. V. Smirnov, *Introduction to the theory of differential inclusions.* American Mathematical Society, 2002.

[106] J. P. Aubin and H. Frankowska, *Set-valued analysis.* Birkhuser, 2008.

[107] F. H. Clarke, *Optimization and nonsmooth analysis.* SIAM, 1990.

[108] B. Paden and S. Sastry, "A calculus for computing Filippov's differential inclusion with application to the variable structure control of robot manipulators," *IEEE Trans. Circuits Syst.*, vol. 34, pp. 73–82, 1987.

[109] D. Shevitz and B. Paden, "Lyapunov stability theory of nonsmooth systems," *IEEE Trans. Autom. Control*, vol. 39, pp. 1910–1914, 1994.

[110] R. Riener and J. Quintern, *Biomechanics and Neural Control of Posture and movement*, J. Winters and P. E. Crago, Eds. Springer-Verlag New York, Inc, 2000.

[111] J. Hausdorff and W. Durfee, "Open-loop position control of the knee joint using electrical stimulation of the quadriceps and hamstrings," *Med. Biol. Eng. Comput.*, vol. 29, pp. 269–280, 1991.

[112] F. L. Lewis, R. Selmic, and J. Campos, *Neuro-Fuzzy Control of Industrial Systems with Actuator Nonlinearities.* Philadelphia, PA, USA: Society for Industrial and Applied Mathematics, 2002.

[113] F. L. Lewis, D. M. Dawson, and C. Abdallah, *Robot Manipulator Control Theory and Practice.* CRC, 2003.

[114] B. Xian, M. de Queiroz, and D. Dawson, "A continuous control mechanism for uncertain nonlinear systems," in *Optimal Control, Stabilization and Nonsmooth Analysis*, ser. Lecture Notes in Control and Information Sciences. Heidelberg, Germany: Springer, 2004, vol. 301, pp. 251–264.

[115] C. Makkar, G. Hu, W. G. Sawyer, and W. E. Dixon, "Lyapunov-based tracking control in the presence of uncertain nonlinear parameterizable friction," *IEEE Trans. Autom. Control*, vol. 52, no. 10, pp. 1988–1994, 2007.

[116] N. Sharma, K. Stegath, C. M. Gregory, and W. E. Dixon, "Nonlinear neuromuscular electrical stimulation tracking control of a human limb," *IEEE Trans. Neural Syst. Rehabil. Eng.*, vol. 17, no. 6, pp. 576–584, Dec. 2009.

[117] N. Sharma, C. M. Gregory, M. Johnson, and W. E. Dixon, "Modified neural network-based electrical stimulation for human limb tracking," in *Proc. IEEE Int. Symp. Intell. Control*, Sep. 2008, pp. 1320–1325.

[118] C. M. Gregory, W. Dixon, and C. S. Bickel, "Impact of varying pulse frequency and duration on muscle torque production and fatigue," *Muscle and Nerve*, vol. 35, no. 4, pp. 504–509, 2007.

[119] F. Zajac, "Muscle and tendon: properties, models, scaling, and application to biomechanics and motor control," *Crit. Rev. Biomed. Eng.*, vol. 17, no. 4, pp. 359–411, 1989.

[120] H. Hatze, "A myocybernetic control model of skeletal muscle," *Biological Cybernetics*, vol. 25, no. 2, pp. 103–119, 1977.

[121] R. Happee, "Inverse dynamic optimization includin muscular dynamics, a new simulation method applied to goal directed movements," *J. Biomech.*, vol. 27, no. 7, pp. 953–960, 1994.

[122] F. L. Lewis, "Neural network control of robot manipulators," *IEEE Expert*, vol. 11, no. 3, pp. 64–75, 1996.

[123] M. Ferrarin, F. Palazzo, R. Riener, and J. Quintern, "Model-based control of FES-induced single joint movements," *IEEE Trans. Neural Syst. Rehabil. Eng.*, vol. 9, no. 3, pp. 245–257, Sep. 2001.

[124] N. Stefanovic, M. Ding, and L. Pavel, "An application of L2 nonlinear control and gain scheduling to erbium doped fiber amplifiers," *Control Eng. Pract.*, vol. 15, pp. 1107–1117, 2007.

[125] T. Fujinaka, Y. Kishida, M. Yoshioka, and S. Omatu, "Stabilization of double inverted pendulum with self-tuning neuro-PID," in *Proc. IEEE-INNS-ENNS Int. Joint Conf. Neural Netw.*, vol. 4, 24–27 July 2000, pp. 345–348.

[126] F. Nagata, K. Kuribayashi, K. Kiguchi, and K. Watanabe, "Simulation of fine gain tuning using genetic algorithms for model-based robotic servo controllers," in *Proc. Int. Sym. Comput. Intell. Robot. Autom.*, 20-23 June 2007, pp. 196–201.

[127] N. J. Killingsworth and M. Krstic, "PID tuning using extremum seeking: online, model-free performance optimization," *IEEE Contr. Syst. Mag.*, vol. 26, no. 1, pp. 70–79, 2006.

[128] R. Kelly, V. Santibanez, and A. Loria, *Control of Robot Manipulators in Joint Space.* Springer, 2005.

[129] R. Anderson, M. Spong, and N. Sandia National Labs., Albuquerque, "Bilateral control of teleoperators with time delay," *IEEE Trans. Autom. Control*, vol. 34, no. 5, pp. 494–501, 1989.

[130] G. Liu, J. Mu, D. Rees, and S. Chai, "Design and stability analysis of networked control systems with random communication time delay using the modified MPC," *Int. J. Control*, vol. 79, no. 4, pp. 288–297, 2006.

[131] T. Cameron, G. Loeb, R. Peck, J. Schulman, P. Strojnik, and P. Troyk, "Micromodular implants to provide electrical stimulation of paralyzed muscles and limbs," *IEEE Trans. on Biomed. Eng.*, vol. 44, no. 9, pp. 781–790, 1997.

BIOGRAPHICAL SKETCH

Nitin Sharma was born in November 1981 in Amritsar, India. He received his Bachelor of Engineering degree in industrial engineering from Thapar University, India. After his graduation in 2004, he was hired as a graduate engineer trainee from 2004 to 2005 and worked as an executive engineer from 2005 to 2006 in Maruti Suzuki India Ltd. He then joined the Nonlinear Controls and Robotics (NCR) research group to pursue his doctoral research under the advisement of Dr. Warren E. Dixon. He will be joining as a postdoctoral fellow in Dr. Richard Stein's laboratory at the University of Alberta, Edmonton, Canada.